Modeling Duchenne muscular dystrophy to unravel the complex mechanisms of disease progression: from biomechanics to cell physiology

---

A Dissertation

Presented to

the faculty of the School of Engineering and Applied Science

University of Virginia

In partial fulfillment

of the requirements for the degree

Doctor of Philosophy

By

Kelley Mitchell Virgilio

December

2018

Modeling Duchenne muscular dystrophy to unravel the complex mechanisms of disease progression: from biomechanics to cell physiology

By Kelley Mitchell Virgilio

Acknowledgements

The decision to return to graduate school after spending four year in industry was one of the most impactful, life-changing, and ultimately best decisions in my life. Although I was excited about the transition, I could not have imagined how equally challenging and rewarding it would be to complete my PhD. However, I would not have been successful without such a tremendous network of mentors, colleagues, friends, and family.

First, I must acknowledge my mentor Silvia Blemker. When I applied to UVA I had a background in civil engineering and construction management, a long jump to the biomechanics and physiology research in my PhD. Yet, she saw the potential and welcomed me into the lab. Silvia has been an insightful visionary and tireless supporter throughout the last five years of my research. She has allowed me the creative freedom to extend my work to model the cell physiology driving DMD in a complex ABM of muscle regeneration. Then when it came time to test my model predictions, she trusted me to carry out these experiments, as “Science Kelley”. There is no one I would rather send exciting results to, and judging by the time it takes for her to open any emails with “plots” in the subject line, she is equally as excited about the results of our studies.

I was lucky to have another mentor at UVA in Shayn Peirce-Cottler. Shayn has been a constant supportive force and is an exceptional scientist who always offers great insight into my research. As a mother and scientist myself, it has been inspiring to be mentored by two incredible female researchers in Shayn and Silvia. I hope that I am able to inspire the next generation of female scientists in the same way that they have inspired me.

I feel very fortunate to have such an incredible network of scientists in the BME department here at UVA. My BME committee members, Jeff Holmes, George Christ, Tom Barker are all exceptional researchers and luminaries in their own field, and I am truly grateful for their time and guidance throughout the dissertation process. Outside of BME, I have had the opportunity to work with the clinician, Rebecca Scharf. Rebecca has always been a knowledgeable resource and positive voice for our research. She has graciously invited us to take part in the DMD clinics so that we can connect with and better understand the patients we are trying to help. This experience has been both illuminating and motivating and I am so thankful for that experience. Finally, Zhen Yan’s passion for skeletal muscle and science is both palpable and contagious. I have always left meetings with Zhen more excited about my research.

Research is certainly not an individual pursuit and I am truly grateful for the support and insight from all my current and former members of the Multiscale Muscle Mechanophysiology Lab: Katie K, Katie P, Xiao, Brian, Kyle, Amanda, Evan, Vi, Adrienne, Hunter, Geoff, Emily, Elnaz, and Katherine. I have learned so much from each of you and will miss the support (and crafting) in our lab. One of the greatest scientific contributors to my research was Kyle Martin. Kyle’s constant energy and enthusiasm, and our endless white-board sessions was pivotal in my successful development of an ABM to study DMD. Even after Kyle left for Stockholm, he has been a continuous contributor and consultant for my research, and I am forever grateful for his ongoing help, and more importantly, his friendship.

When it came time to test my model predictions experimentally, I was lucky to have a village of incredible scientific peers to answer my endless questions, especially the Holmes, Peirce-Cottler, Christ, and Munson labs. I can’t possibly list all those who have been helpful contributors to my work, but I am grateful for the guidance and insight from Ellen, Juliana,

Laura, Bruce, Anthony, Molly, Kathryn, Ali, and Sadegh. I am extremely grateful for Brian's ability to build anything and his endless help with my experiments over the past 6 months.

The final months of graduate school have been a challenging time and I feel so lucky that I was able to go through this process alongside Ali and Kathryn. Especially Ali who also added "Mom" to her many talents this year. Outside of graduate school, I am also fortunate to have the greatest network of smart, successful women who I have the privilege of calling my best friends, Julie, Farah, and Kaye. I cannot imagine having to navigate life, and new motherhood without you three, and I am forever grateful for your constant support and love.

I have the most supportive parents and brothers and am so thankful for their ongoing encouragement over the past five years, and throughout my life. Thank you for letting me talk through all my stresses and being the best uncles and grandparents to Riley. I cannot wait to celebrate this milestone with you all at the Mitchell family vacation/training camp this month.

While a village of people have significantly contributed to this work over the past five years, there is no one I could thank more than my husband, best friend, cycling/running partner, and father to our daughter, Chris. Five years ago, Chris jumped on board and believed in me when I decided to leave California to go to graduate school, and we haven't looked back since. Over the past years there have been countless late nights, early mornings, and long work-weekends, and Chris has always been there for an encouraging word, delicious dinner, cup of coffee, and most recently, to take care of Riley while I worked. I truly couldn't have done this without you, and I couldn't ask for a better partner. I am so happy that I get to do life with you.

Finally, I have to thank my daughter, Riley. Most people know that having a baby in graduate school is not easy. But what they don't tell you, is that sometimes when everything feels like it is falling apart, a simple smile from your child can immediately put all that back into perspective. Riley, I dedicate this work to you and hope that I can inspire you to fearlessly conquer all your dreams.

Abstract

Duchenne muscular dystrophy is a devastating muscle wasting disease affecting 1 in 3500 boys. It is caused by the lack of the dystrophin protein, which serves as a structural link to the muscle fiber membrane. Boys are typically diagnosed around age three to five as they exhibit changes in walking patterns, begin using a wheel-chair in their teens, and die due to respiratory or cardiac malfunction in their third decade of life. Despite extensive experimental research, there remains no cure for DMD. We hypothesize that one of the reasons DMD is so difficult to treat is that multiple mechanisms contribute to disease progression. Without the dystrophin protein the muscle is more susceptible to contraction-induced damage, resulting in chronic inflammation and fibrosis. Coupled with altered satellite stem cell (SSC) dynamics, these disease mechanisms lead to impaired muscle regeneration and progressive muscle wasting.

We believe this is an ideal opportunity to use computational models to help unravel the complex, multifaceted nature of DMD. My dissertation developed two computational models to investigate disease mechanisms in DMD. First, I developed a micromechanical finite element (FE) model that predicted that fibrosis would impair function by increasing the stiffness of the muscle, but protect the muscle from contraction-induced damage. This effect was dependent on whether the ECM was stiffer or more compliant than the skeletal muscle fibers. Then I developed an agent-based model (ABM) to study the cellular physiology driving disease progression. The model predicted muscle regeneration from injury, based on the autonomous actions of the different cell types in the model. The cell types included SSCs, fibroblasts, neutrophils, macrophages, ECM, and muscle cells. We simulated injury and regeneration in healthy and mdx mice (the most common animal model used in DMD). The simulations

predicted that suppressed SSC counts at the later stages of disease impaired regeneration. However, no individual factor in the model was able to predict the decreased SSC counts. Finally, we used the model to design an experiment to test the effect of fibrosis on muscle regeneration in mdx mice. While our intervention increased the area fraction of collagen in the muscle, the stiffness of the muscle was decreased. Given this baseline condition, both our model and the experiment showed no effect on regeneration. However, our model predicted that if the fibrosis resulted in an increased ECM stiffness, then regeneration would be impaired.

Ultimately, the models developed in this dissertation were used to investigate the role of DMD disease mechanisms, both in isolation and combined in our model representations of dystrophic muscle. Both models predicted that the fibrotic microenvironment was a key regulator of function, damage susceptibility, and muscle regeneration in dystrophic muscle. Further, this work highlighted a key utility of this modeling framework for designing experiments, making predictions, and understanding the complex results of these experiments. Future development of the models in this dissertation could provide a platform for predicting chronic, long-term disease progression in DMD, and *in silico* therapeutic testing.

Contents

Acknowledgements **iii**
Abstract **v**

Chapter 1: Introduction

1.1 Overview **1**
1.2 Background **4**

Chapter 2: Multiscale models of skeletal muscle predict the complex effects of tissue function and damage susceptibility in Duchenne muscular dystrophy

2.1 Abstract **16**
2.2 Introduction **16**
2.3 Materials and Methods **18**
2.4 Results **27**
2.5 Discussion **30**

Chapter 3: Agent-based model illustrates the role of the microenvironment in regeneration in healthy and mdx skeletal muscle

3.1 Abstract **36**
3.2 Introduction **36**
3.3 Methods **39**
3.4 Results **53**
3.5 Discussion **62**

Chapter 4:

4.1 Abstract **69**
4.2 Introduction **69**
4.3 Methods **71**
4.4 Results **75**
4.5 Discussion **83**

Chapter 5: Discussion and future directions

5.1 Overview **88**
5.2 Contributions **92**
5.3 Current and Future Applications **94**
5.4 Final Remarks **105**

Appendix: Converting the inflammatory cell ABM into a system of ODEs **107**

References **112**

List of Figures, Tables, and Equation

Figures

1.1: Hierarchical structure of skeletal muscle 1
1.2: DMD disease progression 7
1.3: Skeletal muscle regeneration overview 10
1.4: Skeletal muscle constitutive model 12
2.1: Histological images of DMD muscle 19
2.2: Method of generating FE cross-sections with ABM 20
2.3: Components of FE micromechanical model of muscle 21
2.4: Finite element micromechanical model in shear 24
2.5: Effect of disease properties on shear modulus 27
2.6: Effect of disease properties on membrane strain 28
2.7: Case study of fascicle changes during DMD progression 29
3.1: ABM spatial representation following injury 40
3.2: Overview of ABM rules 42
3.3: ABM predictions of healthy regeneration 53
3.4: ABM predictions of damage, fibroblasts, and inflammatory cell perturbations 55
3.5: ABM predictions of SSC perturbations 57
3.6: Comparison of model predictions to the literature 59
3.7: Model predictions of regeneration in mdx mice 61
3.8: Correlation between impaired regeneration and model parameters 62
4.1: Baseline experimental measurements from mdx experiment 77
4.2: Fiber CSA and ECM following injury 78
4.3: Distribution of fiber sizes in *mdx*, *mdx*+TGFβ, and WT muscle 79
4.4: Fibroblast and macrophage counts following injury 80
4.5: *In silico* analysis of TGFβ injections 81
4.6: Model fiber CSA predictions compared to experiment 82
4.7: Model predictions of the effect of increased ECM stiffness 83
5.1: ABM-FE framework for chronic damage 96
5.2: Simulations of repetitive damage 98
5.3: Simulations of potential therapies 99
5.4: Representative images of ABM simulating VML 100
5.5: Model predictions of microtears leading to acute injury 102
5.6: Schematic of mouse diaphragm for passive mechanical testing 104
5.7: Proposed biaxial testing protocol 105
A.1: Growth factor secretions and cell responses from previous ABM 108
A.2: Calculated effects of cell relationships for ODEs 109
A.3: Inflammatory cell counts predicted from ODEs 110

Tables

3.1: SSC agent behaviors 45
3.2: Fibroblast agent behaviors 46
3.3: Unknown model parameters 49
3.4: Input parameters for model verification simulations 50
3.5: Model input parameters for mdx simulations 51

Equations

2.1: Deformation gradient and tensor 22
2.2: 2nd Piola-Kirchoff Stress 22
2.3: Skeletal muscle strain energy density function 22
2.4: Along-fiber and cross-fiber shear modulus 23
2.5: Rules of mixtures to define boundary material properties 24
2.6: Macroscopic along-fiber shear modulus 25
A.1: ODE for resident macrophages 109
A.2: ODE for neutrophils 109
A.3: ODE for apoptotic neutrophils 109
A.4: ODE for M1 macrophages 110
A.5: ODE for apoptotic-neutrophil-phagocytosing M1 macrophages 110
A.6: ODE for phagocytosing M1 macrophages 110
A.7: ODE for M2 macrophages 110

Chapter 1

1.1 Overview

Skeletal muscle is the driving force behind all aspects of daily life, from walking to talking to breathing. Therefore, neuromuscular diseases that disrupt healthy muscle function can severely debilitate quality of life. In one of its most severe cases, Duchenne muscular dystrophy (DMD), the lack of a skeletal muscle protein (dystrophin) leads to devastating muscle wasting and premature death. Extensive experimental research is aimed at studying the healthy and pathological functions of skeletal muscle; however there remains no cure for the myriad of muscle diseases, including DMD. With experimental tools alone it is often difficult to discern primary disease mechanisms and causal relationships. These mechanisms are particularly hard to elucidate with the heterogeneity between muscles, between people, and throughout disease progression. As the foundation of this thesis, I posit that computational modeling is a powerful tool for investigating muscle function in healthy and disease populations. I believe that computational models can unravel the complexities of disease and reveal new hypotheses and avenues for research that may be difficult to discern with experimental tools alone.

The inherent structure of skeletal muscle lends itself to multiscale modeling. It allows us to build models across many scales, from whole muscle, to fascicles, to fibers, down to individual proteins. The protein that we are most interested in within this work is the dystrophin protein, which connects the interior of the muscle to the muscle fiber membrane (68). This protein is so important that its absence alone leads to Duchenne muscular dystrophy, or DMD (68, 79, 80, 108, 122).

DMD is the most common neuromuscular disease of childhood, affecting 1 in 3500 boys. It is caused by the incomplete translation of the dystrophin protein, and results in progressive muscle wasting (68, 79, 80, 108, 127). The boys are typically first diagnosed around age three

to five when they have trouble rising from the floor (26). Since they are missing the dystrophin protein, their muscle is more susceptible to contraction induced damage (17, 52, 153, 177). Therefore, everyday movements, such as walking, results in cycles of degeneration and regeneration. This leads to a state of chronic inflammation in the muscle (28, 132, 168). As the disease progresses, healthy contractile muscle tissue is replaced by fibrosis and fatty infiltration, and the boys have changes in their walking patterns around age six to eight. The boys typically begin to use a wheel chair in their teens, and ultimately die due to respiratory or cardiac malfunction in their twenties to thirties (110). The current standard of care is corticosteroids; however it is merely palliative to prolong ambulation (9, 76, 96). While therapies to replace the missing dystrophin protein are promising, many barriers preventing successful use of this treatment remain. Therefore, it is critical that we develop effective therapies to treat boys living with DMD today.

We hypothesize that one of the reasons DMD is so difficult to treat is that multiple mechanisms contribute to the disease pathophysiology, including: an increased susceptibility to contraction-induced damage, chronic inflammation, fibrosis, impaired regeneration, and altered satellite stem cell (SSC) dynamics (41, 52, 121, 150). Since all these mechanisms and others likely play a role in disease progression, it is difficult to discern what the primary drivers of disease are, and subsequently, which would be the best targets for therapies. We believe this is an ideal opportunity to use computational models.

We can use the decades of experimental work to build and validate our computational models. Once developed, these models can be used to reveal causal relationships, ask “what if” questions, and generate new hypotheses. We can then use experiments to inform our new model hypotheses and test our model predictions. In this work, we have developed two models to probe disease mechanisms in DMD. First, in Chapter 2, we developed finite element (FE) micromechanical models of skeletal muscle. These models revealed the complex effects of disease progression on damage susceptibility and tissue function. We predicted that fibrosis

would impair function by increasing the stiffness of the muscle fiber, but protect the dystrophic muscle from contraction-induced damage. The effect of fibrosis is dependent on whether the ECM is stiffer or more compliant than the skeletal muscle fibers. However, it is unclear in the literature if the ECM or fibers are stiffer.

In Chapter 3, we developed an agent-based model (ABM) to study the cellular physiology driving disease progression in DMD. In dystrophic muscle, regeneration from injury is affected by all of the disease mechanisms that we are investigating in this body of work - damage susceptibility, fibrosis, chronic inflammation, and altered SSC dynamics. Therefore, we believe regeneration from injury is an ideal platform for investigating how these mechanisms contribute to disease pathophysiology. We developed a new ABM that predicts muscle regeneration from injury, based on the autonomous actions of the different cell types in the model. We included spatial rules for SSCs, fibroblasts, ECM, and muscle cells, and simplified the inflammatory cell dynamics from a previous ABM into a system of ODEs. We used the ABM to probe the effect of isolated mechanisms of disease on muscle regeneration in otherwise healthy muscle. Then we extended the model to study dystrophic muscle by generating models of the *mdx* mouse, the most commonly utilized animal model for DMD, at three ages. The simulations predicted that the pro-fibrotic microenvironment at the later stages of disease suppressed peak SSC counts, ultimately leading to impaired regeneration.

In Chapter 4, we used these model hypotheses to design an experiment to test the effect of fibrosis on muscle regeneration in *mdx* mice. We injected the tibialis anterior (TA) muscle of 3 month *mdx* mice with TGFβ, which resulted in an increase in the area fraction of collagen. However, passive mechanical testing revealed that the stiffness of the muscle decreased significantly. Assuming that the fiber mechanical properties have not been altered, this suggests that the ECM stiffness was decreased with our intervention. The freeze injury and regeneration experiment found no significant difference in recovery between control (WT), *mdx*, and *mdx*+ TGFβ groups. Then we simulated the experiment with the ABM in Chapter 3 to predict the effect

of these injections, and the model similarly predicted no effect on regeneration. However, our model predicted that if the injections lead to a stiffer fibrotic microenvironment then regeneration would be impaired in the *mdx*+TGFβ group. This suggests that area fraction of collagen alone does not predict the regeneration in dystrophic muscle.

Ultimately, we developed a set of models to study disease mechanisms in DMD. Both our mechanical and physiology models predicted that fibrosis is a key regulator of disease progression in dystrophic muscle. However, the effect is dependent on the stiffness of the fibrosis. We hypothesize that in DMD stiff fibrosis protects the muscle from contraction-induced damage, but impairs the function and regenerative capacity of the muscle. This body of work also highlighted the utility of the modeling framework for designing experiments, making predictions, and understanding the complex results of these experiments.

1.2 Background

Skeletal muscle microstructure

Skeletal muscle has a hierarchical structure, where at each scale the contractile muscle tissue is surrounded by a network of extracellular matrix (ECM). Whole muscle is comprised of fascicles, fascicles are comprised of fibers, and fibers are multinucleated cells comprised of the fundamental force generating unit, the sarcomere. The structural link between the contractile muscle tissue and the muscle fiber membrane is the dystrophin glycoprotein complex, where the dystrophin protein resides (52, 80). Together, these microstructural properties give rise to muscle's ability to generate force. Sarcomere overlap gives rise to the force-length and force-velocity relationships that define the force-generating capacity of the muscle (67, 70, 184). The muscle length determines the range of motion of the muscle, and the cross-sectional area (CSA) and pennation angle define the active force generating capacity (Figure 1.1).

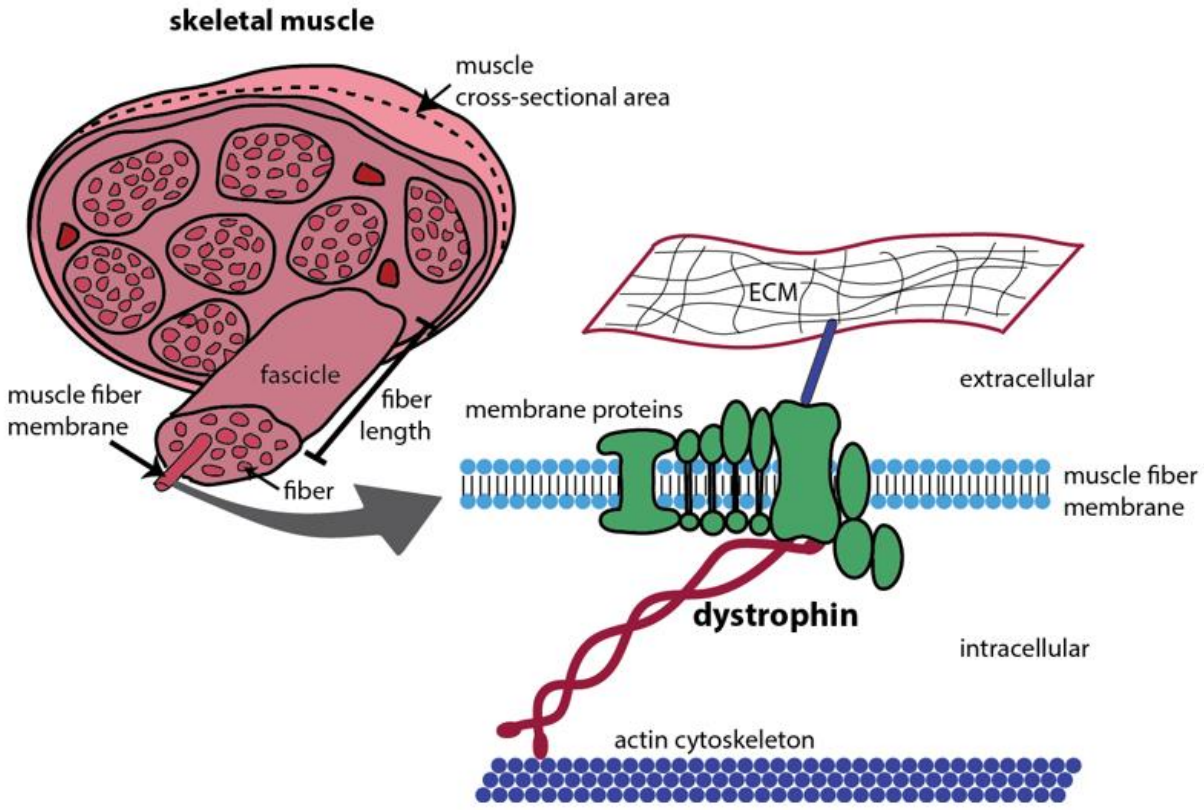

Figure 1.1. The hierarchical structure of skeletal muscle, from whole muscle to individual proteins.

The main resident cell types within skeletal muscle are the satellite stem cells (SSCs), connective tissue fibroblasts, and resident macrophages. SSCs are the resident skeletal muscle progenitor cells that are responsible for repair and maintenance of skeletal muscle. When quiescent the SSCs reside at the fiber membrane. Once activated from damage they divide, differentiate, and fuse with the myofiber to repair it. Connective tissue fibroblasts reside in the ECM surrounding muscle fibers and are the primary cells responsible for maintaining the ECM. During homeostasis, muscle remodeling is low, and these resident cell types have a decreased role; however, during muscle regeneration these cell type counts increase significantly and are critical for muscle regeneration, as described in later sections.

Duchenne muscular dystrophy

Duchenne muscular dystrophy (DMD) is an X-linked recessive disorder caused by a mutation in the dystrophin gene, resulting in incomplete translation of the transmembrane protein dystrophin (68, 80, 108). It affects 1 in 3500. Over time, DMD results in dramatically impaired muscle function and progressive muscle wasting (Figure 1.2). Boys are often first diagnosed around age three to five when they have trouble rising from the floor (26). They begin to exhibit changes in walking patterns around age six to eight and often use a wheelchair in their early to mid-teens. The boys typically die of cardiac or pulmonary malfunction by the third decade of life (110). Despite extensive experimental research, there remains no cure for DMD. The current standard of care is corticosteroids; however it is merely palliative to prolong ambulation (9, 76, 96). While new therapies to replace the missing dystrophin protein are promising, many barriers preventing successful use of this treatment remain. For instance, the drug eteplirsen has been granted approval by the FDA; however it has yet to show significant improvement in muscle function in treated boys (81, 104). Until therapies to replace the dystrophin proteins are successful, it is critical to develop therapies to treat boys living with DMD today. However, DMD is a complex, multifaceted disease in which multiple mechanisms are known to contribute to the pathophysiology. In this work, we hypothesize that the multiple disease mechanisms make it difficult to discern the primary drivers of DMD, and subsequently make it challenging to design effective therapies.

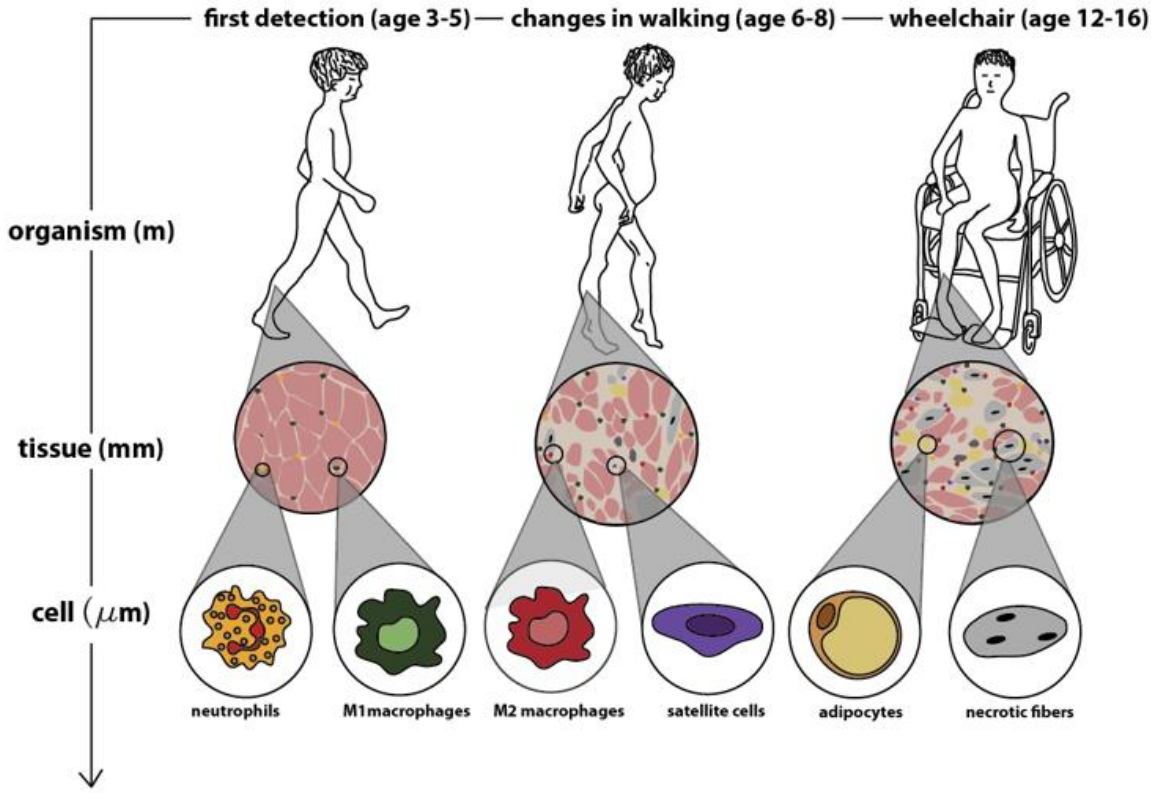

Figure 1.2. DMD is a degenerative, muscle-wasting disease in which increased susceptibility to damage, chronic inflammation, fibrosis, and fatty infiltration lead to impaired muscle function and loss of mobility.

The multiple disease mechanisms are initiated by the lack of the dystrophin protein which makes the muscle more susceptible to contraction-induced damage (17, 52, 153, 177). Therefore, muscle contractions incurred during everyday movements can lead to muscle injury in dystrophic muscle. These constant cycles of degeneration and regeneration, coupled with altered cell signaling, lead to a state of chronic inflammation in the muscle (28, 132, 168). As the disease progresses, the contractile muscle tissue is replaced by fibrotic tissue and fatty infiltrate. Fibrosis not only affects mechanical function, but is also hypothesized to decrease the effectiveness of treatments (9, 95, 118). Further, recent experiments have revealed the role of dystrophin in regulating cell polarity during asymmetric divisions (41, 42). Without dystrophin,

SSCs undergo impaired asymmetric division resulting in either senescent cells or decreased differentiated myocytes.

Failure to translate therapies from animal models, such as the *mdx* mouse, to humans is one of the critical barriers to developing effective treatments for DMD (61, 178). The *mdx* mouse is the most commonly used animal model to study DMD. However, the *mdx* mouse phenotype is significantly less severe than humans. The *mdx* mouse undergoes less fibrosis and muscle degeneration as compared to boys with DMD (33, 111). Additionally, there are temporal variations in disease phenotype as the dystrophic mouse ages, and these variations differ from age-associated changes in DMD patients (118, 151). Very young *mdx* mice (4 weeks) have a substantial pro-inflammatory response, with little fibrosis and markers of necrosis and degeneration (centrally nucleated fibers, necrotic fibers) (46, 118, 166, 167, 176). Young *mdx* mice (3 months) have a more stable inflammatory response as the inflammation shifts to a more regenerative phenotype (63, 166, 167, 176). Adult *mdx* mice (9 months +) exhibit fibrosis and some impaired muscle regeneration (63, 95, 103, 118).

Since most pre-clinical testing is still completed in mice, a number of new mouse models have been developed to address the milder phenotype. For instance, the dystrophin-utrophin double knock out mice eliminate the compensatory increases in the transmembrane protein utrophin, leading to more substantial muscle damage and degeneration (33). The *mdx*/mTR model addresses stem cell exhaustion and telomere shortening that is not captured in the standard *mdx* mouse model (135). Despite the limitations of the *mdx* mouse, and recent advances in new mouse models, the *mdx* mouse remains the most commonly used animal model for studying DMD.

Skeletal muscle regeneration from injury

Skeletal muscle regeneration following injury is a complex, dynamic process involving numerous cell types (Figure 1.3). Immediately following injury, neutrophils are recruited to the muscle, reaching maximum cell numbers approximately 24 hours after injury (43, 160). Neutrophils begin the process of necrosis removal by recruiting inflammatory (M1) macrophages, which peak approximately two days after injury. Inflammatory macrophages phagocytose debris and apoptotic neutrophils (24, 25, 44, 136, 140, 149, 154). This process of phagocytosis causes some of the inflammatory macrophages to transition into anti-inflammatory (M2) macrophages, while new anti-inflammatory macrophages are recruited to the muscle. Anti-inflammatory macrophage populations peak approximately four days after injury and remain in the muscle for at least ten days (24, 25, 37, 44, 136, 149, 166).

While neutrophils and inflammatory macrophages are working to clear the damage, SSCs are the stem cells responsible for repair and maintenance of skeletal muscle fibers. SSCs typically reside at the muscle fiber membrane, and remain mostly quiescent prior to injury (130). Following injury, SSCs are activated by damage and the presence of HGF (3, 107, 156). SSCs are also recruited to the site of damage by growth factors, including: HGF, IGF, FGF, MMPs, and deterred by TGF-B (27, 57, 74, 144). SSCs divide, both symmetrically (into two SSCs) and asymmetrically (into one SSC, one committed myogenic progenitor), based on growth factors, such as TNF-α, IL6, VEGF, and PDGF (additional details including in Chapter 3) (2, 4, 7, 51, 105, 136, 138, 152, 181). Through this division, the SSCs reach peak cell counts approximately three to seven days post injury (112). Then the fibers terminally differentiate and fuse with the fiber to repair the muscle (2, 4, 7). Approximately 10% of the SSCs do not terminally differentiate and help to restore the SSC pool until returning to quiescence (54, 85).The SSCs also secrete growth factors such as VEGF, TNF- α, and IL-6 during regeneration (11, 20, 25, 147).

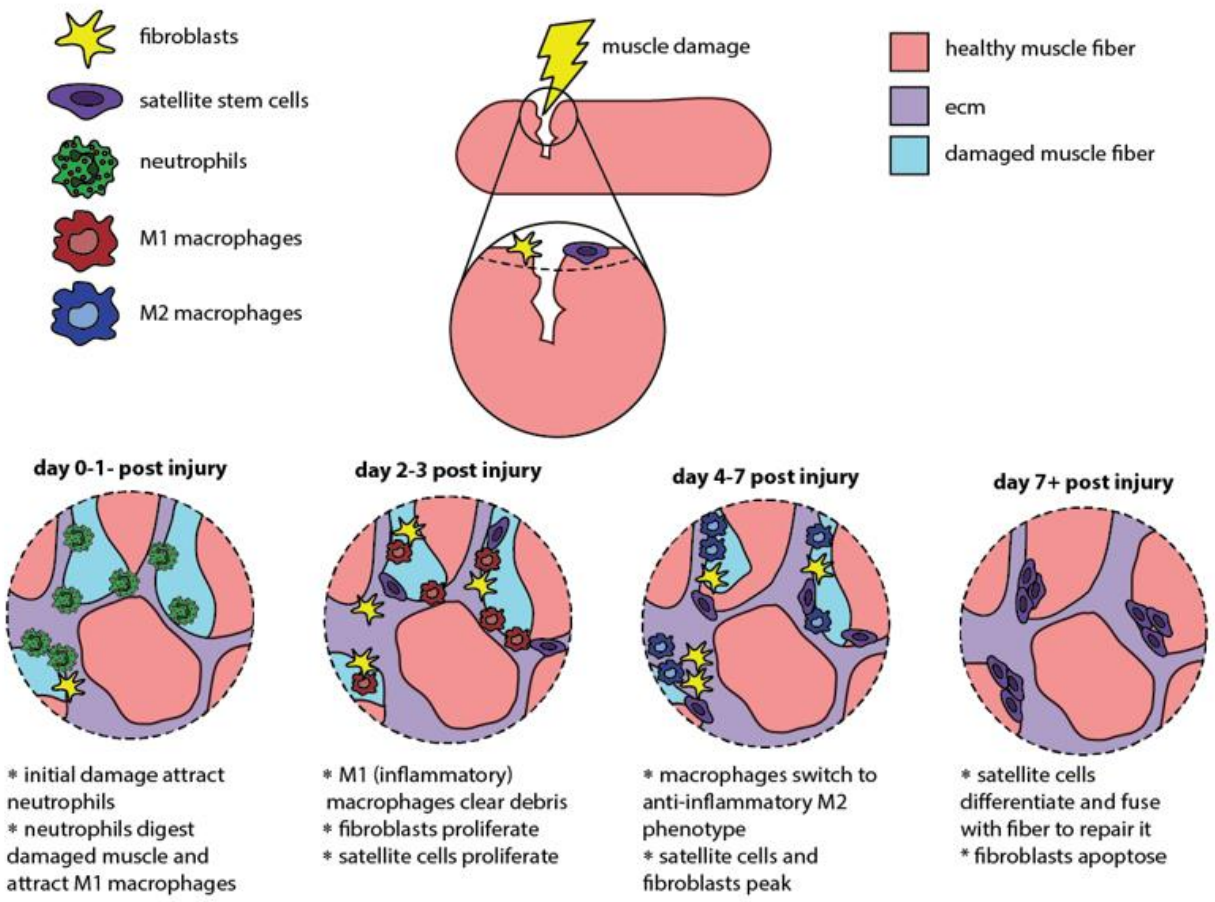

Figure 1.3. Skeletal muscle regeneration from injury is a complex process involving numerous cell types, including fibroblasts, SSCs, neutrophils, M1 macrophages, and M2 macrophages.

Connective tissue fibroblasts are also an integral part of muscle regeneration. Recent studies have shown that without fibroblasts, SSCs undergo premature differentiation resulting in impaired regeneration from injury (112). Following injury, fibroblasts are recruited to the site of damage based on IL-4 secreted from eosinophils (66). Population counts reach a maximum approximately three to seven days after injury (66, 72, 112, 162, 163). Although the mechanism is unclear, recent experiments with a SSC knockout mouse have shown that fibroblasts proliferate in the presence of SSCs (112). TNF-α induces fibroblast apoptosis, while active TGF-β blocks the apoptosis (86). Extended exposure to TGF-β has been shown to induce fibroblast differentiation into myofibroblasts (30, 86). During this process, the fibroblasts secrete collagen to repair the ECM (137, 188). They also secrete a number of growth factors that contribute to

the regenerative, or pro-fibrotic microenvironment, depending on the state of the muscle, such as TGF- β, IGF1, and MMPs (10, 72, 98, 117, 120, 133, 146, 185).

Skeletal muscle modeling

Computational modeling is a powerful tool for simulating the complex behaviors of biological tissues. The models can be used to reveal cause-effect relationships, ask “what-if” questions, and develop new hypotheses. Computational models of skeletal muscle have advanced significantly over the past two decades. Initially, these models were used to represent the cross-bridge mechanics that gives rise to muscle contraction. The earliest models simplified the architecture into Hill-type, lumped, one-dimensional parameter models to probe effects such as the force-length and force-velocity relationships (184). Lumped parameter models assume all fibers generate the same amount of force and change length uniformly. This can provide a great deal of insight into human movement (36); however, these models do not allow us to investigate deformations of complex muscle geometries to gain insight into injury, disease, and muscle adaptations.

More recently, a new phenomenological skeletal muscle constitutive model was developed that represents the muscle as a fiber-reinforced composite (15, 16). This three-dimensional FE model was used throughout this thesis to represent the behavior of skeletal muscle. The model assumes the tissue is hyperelastic, transversely isotropic, and nearly incompressible. FE simulations are quasi-static and do not account for viscoelasticity. The constitutive model uses an uncoupled form of the strain energy density function that separates the dilatational and deviatoric portions. Physically based strain invariants were used to relate material parameters to experimentally quantifiable measurements (32), as shown in Figure 1.4. Where λ is the along fiber stretch, ψ is along-fiber shear, β is cross-fiber shear, and J is the relative change in volume of the tissue. The fiber direction is assumed to run along the path of

the muscle for both the ECM and the muscle fibers. The along-fiber stretch parameter determines both the active and passive force-length properties of the muscle. $W_\lambda, W_\psi, W_\beta, W_J$, were defined as shown in Figure 1.4, where G_ψ is the along-fiber shear modulus, G_β is cross-fiber shear modulus, and K is the bulk modulus (16).

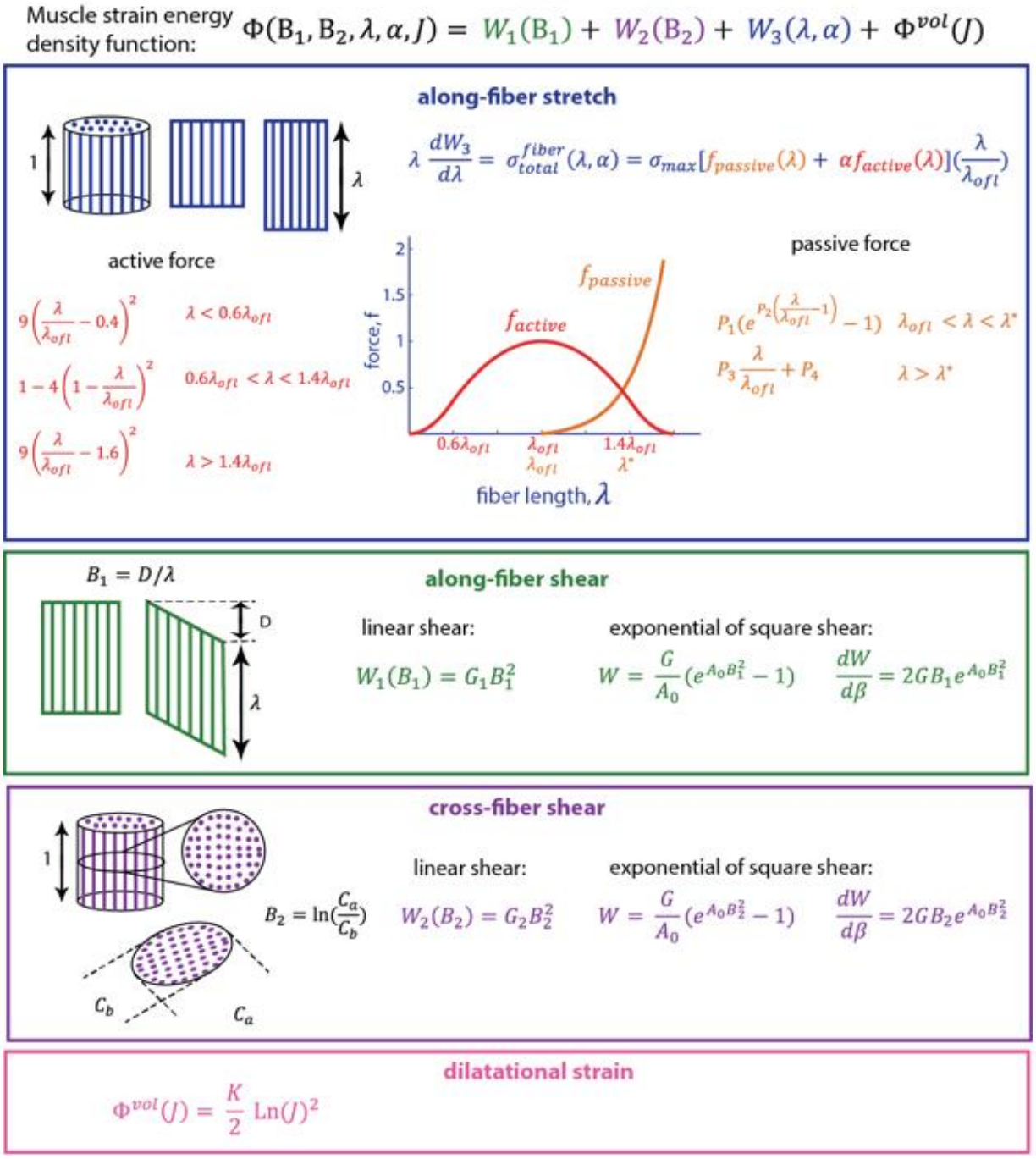

Figure 1.4. Skeletal muscle constitutive model uses physically based strain invariants to relate material properties to experimentally quantifiable measurements.

This continuum model of skeletal muscle has illustrated the heterogeneity in muscle deformations across many scales. Models of whole muscle have been used to investigate how strains in the biceps femoris longhead may contribute to injury (49, 129). At the fascicle level, micromechanical models that separate the muscle fibers and ECM have investigated how changes in the microstructure affect tissue level material properties (141). While these micromechanical models allowed Sharafi et al. to understand how microstructural changes altered the fascicle and fiber level properties, they were not designed to probe how changes associated with disease (such as DMD) would alter the tissue level properties. Therefore, we used the work by Sharafi et al. to develop micromechanical models of skeletal muscle fascicles to probe how changes associated with DMD alter tissue level properties and damage susceptibility (Chapter 2).

Agent-Based Modeling

Agent-based modeling is a computational modeling approach that simulates the actions of autonomous agents to analyze their effect on the system as a whole. ABMs stochastically simulate behaviors based on rule sets for each agent. Historically, ABMs have been used to represent ecological or social phenomenon (18, 21). More recently this computational approach has been extended to represent biological processes, such as microvasculature networks, atherogenesis, and surgical site infections (6, 13, 58). The stochastic, rules-based approach in agent-based modeling is a powerful tool for modeling biological processes. The agent actions are typically defined based on literature-derived rules that depend on the agent environment. This method mirrors the interactions between biological cells and the microenvironment.

Previous work in our lab has developed ABMs to represent muscle adaptation from disuse-induced muscle atrophy and regeneration from injury (98, 99, 101). Both of these models spatially represented a cross-section of skeletal muscle and analyzed how the interactions of various growth factors and inflammatory cells contributed to muscle adaptation. The muscle atrophy model found that no individual parameter could predict the differential atrophy response across muscles (98). The acute injury and regeneration model explored how the interactions of skeletal muscle neutrophils and macrophages gives rise to muscle regeneration (99, 102). The model was then used to investigate the effect of priming the inflammatory response with a macrophage recruitment factor (MCSF). Ultimately, this *in silico* analysis was used to design and test the hypothesis experimentally in an *in vivo* rodent model. The injury and regeneration ABM by Martin et al. served as the foundation of the ABM in this dissertation; where additional complexity for the SSCs and fibroblasts was incorporated in order to study how regeneration is impaired in DMD.

Chapter 2

Multiscale models of skeletal muscle predict the complex effects of tissue function and damage susceptibility in Duchenne muscular dystrophy

Acknowledgements: Kyle S. Martin, Shayn Peirce, Silvia Blemker

"The Standard ... is the standard." - Mike Tomlin

2.1 Abstract

Computational models have been increasingly used to study the tissue-level constitutive properties of muscle microstructure; however, these models were not created to study or incorporate the influence of disease-associated modifications in muscle. The purpose of this paper was to develop a novel multiscale muscle modelling framework to elucidate the relationship between microstructural disease adaptations and modifications in both mechanical properties of muscle and strain in the cell membrane. We used an agent-based model to randomly generate new muscle fiber geometries and mapped them into a finite-element model representing a cross section of a muscle fascicle. The framework enabled us to explore variability in the shape and arrangement of fibers, as well as to incorporate disease-related changes. We applied this method to reveal the trade-offs between mechanical properties and damage susceptibility in Duchenne muscular dystrophy (DMD). DMD is a fatal genetic disease caused by a lack of the transmembrane protein dystrophin, leading to muscle wasting and death due to cardiac or pulmonary complications. The most prevalent microstructural variations in DMD include: lack of transmembrane proteins, fibrosis, fatty infiltration and variation in fiber cross-sectional area. A parameter analysis of these variations and case study of DMD revealed that the nature of fibrosis and density of transmembrane proteins strongly affected the stiffness of the muscle and susceptibility to membrane damage.

2.2 Introduction

Skeletal muscle has a complex hierarchical structure consisting of long contractile muscle cells (fibers) embedded within a connective tissue matrix. The importance of the interaction between contractile muscle cells and the extracellular matrix (ECM) has received significant attention over the past two decades (69, 77, 83, 90, 124). In particular, the ECM is thought to

play a critical role in enabling force transmission from fibers to tendons and in the protection of muscle cells from excessive damage during muscle contractions.

Muscle cells, ECM, and their transmembrane connections have all been implicated in muscle disease. For example, Duchenne muscular dystrophy (DMD) is an x-linked recessive disorder caused by a mutation in the DMD gene, resulting in the incomplete translation of the transmembrane protein dystrophin (68, 79, 80, 108, 127). It is the most common neuromuscular disease of childhood and is responsible for dramatically impaired muscle function and progressive muscle wasting (45, 68). Boys born with DMD become very weak at an early age, need wheelchairs by their teens, and die of respiratory or cardiac failure by their third decade of life (26, 110). There is no cure for DMD, despite extensive experimental research regarding the pathophysiology of the disease. While the current standard treatment is corticosteroids, it is merely palliative to prolong ambulation (9, 76, 96). Several animal models of the disease have been developed – including zebrafish (8, 62), mouse (38, 118), and canine (19, 164); however, there are still unanswered questions regarding the role of dystrophin in muscle function and how this leads to progressive muscle wasting in DMD. How does the protein protect the cell membrane from mechanical damage? How does the protein affect muscle properties? How do secondary changes in the muscle – such as fibrosis and fatty infiltration – influence the function of the muscle? In this chapter, we posit that multi-scale computational models can provide a quantitative, mechanistic approach to investigate the influence of muscle diseases, like DMD, on muscle function. These scientific underpinnings provide a new framework to generate hypotheses regarding treatment targets moving forward.

Computational models of skeletal muscle have advanced significantly over the last two decades. While historically models of muscle have simplified the architecture of muscle into a lumped-parameter representation (184), there has been a movement towards tissue-level models that represent muscle tissue as a fiber-reinforced composite. These tissue-level models make

use of “phenomenological” constitutive models that do an excellent job of accounting for the underlying structure of muscle (16, 73). However, muscle cells and connective tissue are not explicitly defined in these models, which limits their capacity to relate molecular and cellular underpinnings and reveal insights into disease-related muscle changes. Recently, micromechanical models of muscle have been developed to derive tissue-level constitutive properties from the muscle microstructure (141). This work provided a framework for multi-scale analysis of muscle; however, the models were not created to study or incorporate the influences of disease-associated modifications in muscle.

The overall goal of this chapter is to develop a multi-scale muscle modeling framework to elucidate the relationship between microstructural disease adaptations and modifications in both mechanical properties of muscle and strain in the cell membrane. To achieve this goal we developed a novel approach for randomly generating muscle fascicle geometries, enabling us to explore disease related changes by altering muscle fiber and ECM volume fractions, variance in fiber cross-sectional area, amount of fat infiltration, and fiber-ECM transmembrane protein density. We used the models to reveal the tradeoffs between mechanical properties and damage susceptibility in the context of DMD-associated changes in muscle.

2.3 Materials and Methods

2.3.1 Random generation of fascicle cross sections from an agent-based model

We utilized an agent-based model of muscle to generate new fascicle cross sections with the agent-based modeling platform Netlogo (http://ccl.northwestern.edu/netlogo/). A unique cross-section of one muscle fascicle was generated from fourteen “seed” fibers within a two-dimensional discretized grid. The grid dimensions were: 130 by 130 elements, with each element 3 by 3 microns. Fibers were grown in a stepwise function according to their defined mean and

variance of the fiber cross sectional area (CSA). The unused elements were prescribed as boundary elements.

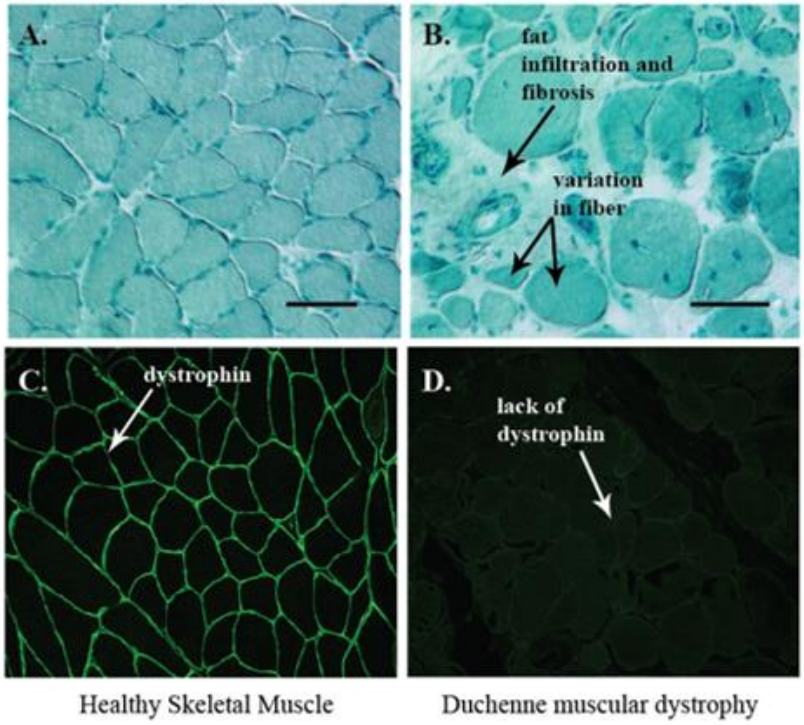

Figure 2.1 Histological comparison of healthy (a) and DMD (b) muscle reveals common pathological variations seen in musculoskeletal disease, including increased variation in fiber CSA, fibrosis and fat infiltration. Scale bar, 60 mm. (Adapted from Leiber et al. 2013) Immunofluorescence staining of healthy (c) and DMD (d) muscle samples show a lack of dystrophin expression in the DMD muscle compared with the healthy muscle. (Adapted from Beekman et al. 2014).

In order to determine the input parameters necessary to model structural changes in musculoskeletal disease, we determined the most prevalent pathological variations seen in DMD (Fig. 2.1). These variations include: density of transmembrane proteins, variation of fiber CSA, and pseudohypertrophy which manifests as an increase of fibrosis and fat infiltration within the muscle (45, 78). To enable the agent-based model to simulate these pathological variations, we modified the mean and variance of the fiber CSA, and added additional capabilities to increase the amount of fibrosis or change muscle fiber into fat tissue. In addition, by defining the variance of fiber CSA, we utilized the agent-based model to randomly create new fascicle cross-sections.

Each simulation had a unique set of muscle fiber shapes and sizes, accounting for physiologic variability. Through manipulation of these input parameters we generated fascicle geometries that account for both structural changes seen in disease and variability inherent in muscle tissue (Fig. 2.2). The generation of new fascicle geometries were completed under the assumption of constant physiological conditions (e.g. pH, temperature, and electrolyte-composition).

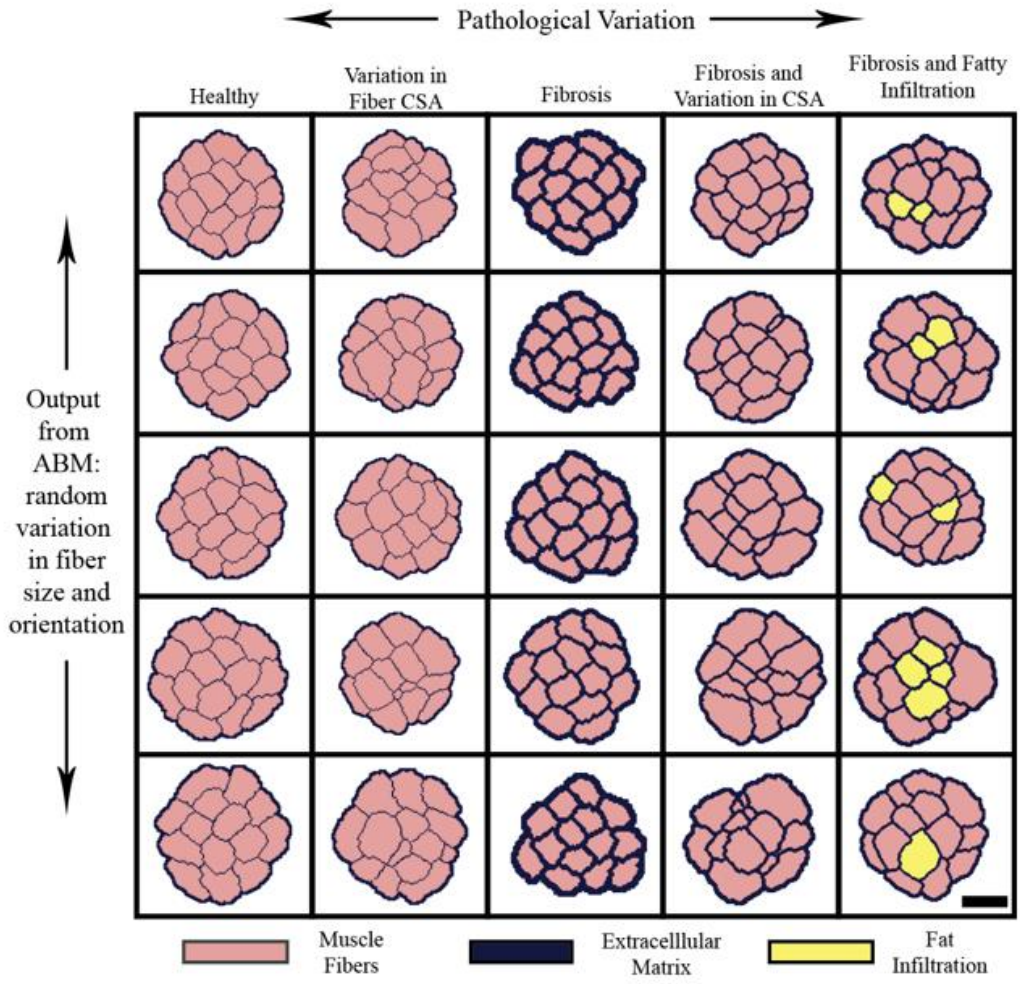

Figure 2.2. An agent-based model (ABM) is used to generate a variety of new fascicle cross-section geometries for different pathological variations commonly seen in musculoskeletal disease. The horizontal axis represents the different pathological conditions modeled, including: variation in fiber CSA, fibrosis and fatty infiltration. These symptoms are manifested as pseudohypertrophy in DMD patients where the total muscle volume increases due to increased fibrosis and fat infiltration. The vertical axis represents the variation in fascicle geometry created by the ABM's randomized generation of fascicle cross sections with differing fiber shapes and sizes. Scale bar, 100 mm.

2.3.2 Conversion from agent-based model to micromechanical model

We mapped the material elements from the agent-based model's discretized grid onto an initialized finite element mesh that represents the cross-section of a single muscle fascicle (Fig. 2.3). The mesh density was increased and a smoothing algorithm was applied to eliminate any ill-conditioned elements in narrow portions of the extracellular matrix. An initialized mesh, the size of the agent-based model grid, was created using TrueGrid (XYZ Scientific Applications). The hexahedral element mesh dimensions were: 390 x 390 elements in the cross-section plane and one element thick. Additional simulations were completed with a three-element-thick hexahedral mesh and the calculated shear modulus was within 0.5% of the one-element-thick mesh; therefore a one-element-thick mesh was utilized to decrease computational time.

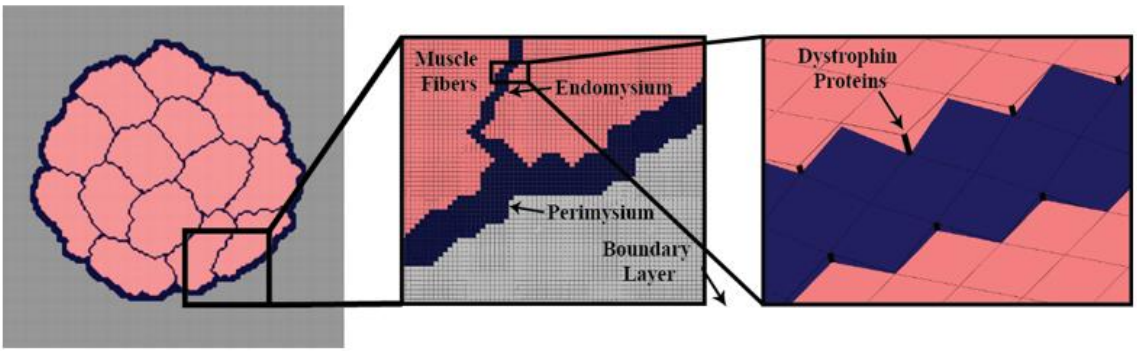

Figure 2.3. Components of the finite-element micromechanical model, including material types for ECM (endomysium and perimysium), muscle fibers, boundary layer and springs representing transmembrane proteins.

Since muscle fiber force is known to be transmitted laterally through shearing of the endomysium, we were interested in analyzing the muscle in shear (69, 141). We assigned the boundary conditions to prescribe simple shear deformation, representing the shear displacement of muscle fibers and fascicles relative to each other. The elements on one face were constrained in all directions and the opposite face was displaced in the -3 direction, creating a shear displacement in the 1-3 direction. All elements were constrained in the 1 and 2 directions.

2.3.3 Definition of constitutive model and material parameters

We used a transversely isotropic, nearly incompressible, hyperelastic constitutive model to represent the muscle fibers, extracellular matrix, and boundary layer. The deformation gradient (**F**) and right Cauchy-Green deformation tensor (**C**) are defined respectively as:

$$\boldsymbol{F} = \frac{\partial \boldsymbol{x}}{\partial \boldsymbol{X}} \text{ , and } \boldsymbol{C} = \boldsymbol{F}^T\boldsymbol{F} \tag{2.1}$$

Where **x** represents the deformed vector and **X** represents the reference vector. The stresses are derived from the strain energy density function (W), and the 2nd Piola-Kirchoff stress (**S**) is defined as:

$$\boldsymbol{S} = 2\,\frac{\partial W}{\partial \boldsymbol{C}} \tag{2.2}$$

This constitutive model uses an uncoupled form of the strain energy density function to enforce the incompressible behavior of the connective and muscle tissue. The strain energy density function separates the dilatational and deviatoric response of the muscle, resulting in the following strain energy density function (16):

$$W(\lambda, \psi, \beta, J) = W_\lambda(\lambda) + W_\psi(\psi) + W_\beta(\beta) + W_J(J) \tag{2.3}$$

where λ is the along-fiber stretch, ψ is along-fiber shear, β is cross-fiber shear, and J is the relative change in volume of the tissue. The fiber direction is defined along the axis of transverse isotropy. In this model it is assumed to run along the path of the muscle for both extracellular matrix and muscle fibers. Physically based strain invariants were utilized to relate material parameters to experimentally quantifiable measurements (32). $W_\lambda(\lambda)$ is a piece-wise function representing the

passive material properties of the tissue, dependent on the fiber length. W_ψ, W_β, W_J, were defined as follows:

$$W_\psi = G_\psi \psi^2,\ W_\beta = G_\beta \beta^2, W_J = \frac{K}{2} J^2 \tag{2.4}$$

where G_ψ is the along-fiber shear modulus, G_β is cross-fiber shear modulus, and $K$is the bulk modulus (16). Fat infiltration was modeled as a simple incompressible, hyperelastic, Neo-Hookean material with a single material parameter representing the Young's modulus of the material. Currently, there are no known measurements for the along-fiber shear modulus of muscle and extracellular matrix, G_ψ^{fiber}, G_ψ^{ECM}; however previous studies have shown that the ratio of $G_\psi^{fiber}/G_\psi^{ECM}$ is the critical factor in determining the contribution of structural variation on tissue-level properties (141). Furthermore, there remains a debate in the literature as to whether muscle fibers are more or less stiff than the ECM (69, 90, 124). Therefore, in order to explore the implications of these possible scenarios, G_ψ^{fiber} was held constant during simulations and G_ψ^{ECM} was adjusted to be both stiffer and more compliant in shear than the muscle fibers.

2.3.4 Definition of boundary material properties

Our method requires initialization of a finite element mesh so that only the material type for each element needs to be defined based on the output of the agent-based model. The boundary layer surrounding the muscle fascicle within the agent-based model grid allows for a unique opportunity to pre-allocate the mesh properties, boundary conditions, and applied displacements for the initialized finite element mesh (Fig. 2.4). In order to prevent the boundary layer from adversely affecting the model, its material properties were adjusted so that its behavior simulated the macroscopic shear properties of the muscle fascicle. Using rules of mixtures, the along-fiber shear properties of the boundary were defined as follows:

$$G_{\psi}^{boundary} = \frac{G_{\psi}^{fiber}(1 + V_{fiber}) + G_{\psi}^{ECM}(1 - V_{fiber})}{G_{\psi}^{fiber}(1 - V_{fiber}) + G_{\psi}^{ECM}(1 + V_{fiber})} G_{\psi}^{ECM} \quad (2.5)$$

where V_{fiber} is the volume fraction of fibers within the muscle fascicle. This created a homogenized, macroscopically representative material to which boundary conditions and displacements can be pre-imposed and used for all the unique fascicle geometries used in this study.

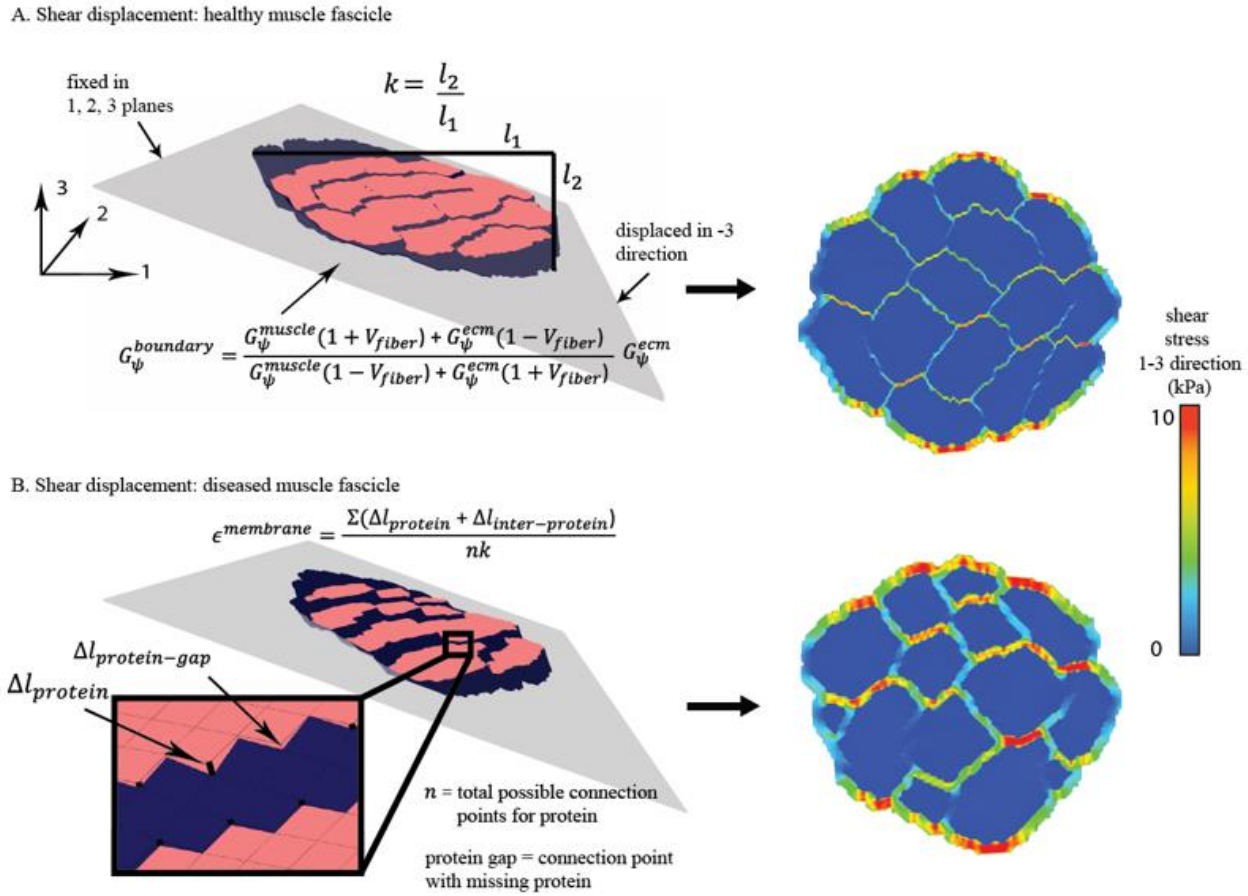

Figure 2.4. Finite-element model in shear for healthy (a) and diseased (b) muscle fascicles reveals variable shear stress profiles. The boundary layer properties were defined based on rules of mixtures to simulate macroscopic-fascicle properties. Fascicle displacement, k, was calculated as the fascicle displacement in the 3 direction (l2), divided by the width of the fascicle (l1). The displacement, k, and the shear stress in the 1–3 direction were used to calculate the fascicle shear modulus. Membrane strain is the average change in length between fiber and ECM nodes at both proteins and inter-protein regions, normalized by k.

2.3.5 Inclusion of transmembrane proteins

To analyze the effect of transmembrane proteins, such as dystrophin, we identified all nodes connecting the muscle fibers and ECM within the micromechanical model, added a node at that point, and then connected the two nodes with a spring. The transmembrane protein was modeled as nonlinear elastic spring (12, 52, 186). To represent a loss of proteins in the diseased state, a random number generator was used to randomly delete a specified quantity of the springs (ranging between 0% and 80%).

2.3.6 Determination of macroscopic along-fiber shear properties

Simulations were run using the nonlinear finite element solver, NIKE3D (126). The macroscopic along-fiber shear properties of the muscle fascicle were calculated based on the displacement and shear stress of the micromechanical model fascicle, excluding the boundary layer. The average shear stress (1-3 plane) in the fascicle was calculated using the post-processing software, Postview (94). The shear displacement of the fascicle, k, was also calculated in Postview, as the maximum 3-plane displacement across the fascicle, divided by the width of the fascicle at that point. The macroscopic along-fiber shear modulus was then calculated as follows:

$$G_{\psi}^{macro} = \frac{\sigma_{13}^{avg}}{2k} \tag{2.6}$$

2.3.7 Analyses

To initially validate the approach for defining geometries and boundary conditions, we performed simulations with a muscle to ECM shear modulus ratio ranging from 0.01 to 500 for a healthy muscle fascicle; the results replicated those found by Sharafi *et al.* (141). The micromechanical model was then used in a parameter analysis to test the individual effect of a number of variations in microstructures prevalent in musculoskeletal disease. We explored the

effects of volume fraction of fibers, density of transmembrane proteins, variance in fiber CSA, and volume fraction of fatty infiltration, all of which are structural variations that have been observed in DMD muscle. The agent-based model was used to generate new fascicle cross-sections for each simulation so that all analyses were completed with a unique geometry, accounting for typical variability seen in muscle fibers.

Because there is debate in the literature on whether muscle fibers are stiffer than the ECM or if the ECM is stiffer than muscle fibers, all parameter analyses were repeated at two ratios of $G_{\psi}^{fiber}/G_{\psi}^{ECM}$: one in which the muscle is 75 times stiffer than the ECM (141), and one in which the ECM is 25 times stiffer than the muscle (90). Total finite-element simulation time was eight minutes on 32-GB 8-processur IBM Linux workstation.

2.3.8 A case study investigating muscle disease

We performed a simulated case study of Duchenne muscular dystrophy in which the muscle fascicle was analyzed for healthy muscle and at three stages of disease. The early stage of the disease included only a loss of dystrophin proteins, the middle stage included loss of proteins, fibrosis, and increase in variance of fiber CSA, and the late stage included loss of proteins, increased fibrosis, fatty infiltration, and large variations in fiber CSA (68, 78). The macroscopic along-fiber shear moduli and ECM shear moduli were normalized by the muscle fiber modulus in order to simplify the presentation of the results. A second parameter, membrane strain, was used to analyze the potential for damage at the membrane. Membrane strain was calculated as the average change in length between fiber and ECM nodes at both proteins and inter-protein regions, normalized by the macro-scale shear displacement factor, k.

2.4 Results

2.4.1 Parameter Analysis

The effect of microstructural variations differs depending on whether the ECM is stiffer than the fibers or if the fibers are stiffer than the ECM. When the muscle fibers are stiffer than the ECM, increasing the volume fraction of fibers (Fig. 2.5A) and the density of trans-membrane proteins (Fig. 2.5B) both led to a significant increase in the macroscopic shear modulus of the fascicle. Incorporation of fatty infiltration decreased the shear stiffness of the muscle (Fig. 2.5C), while variability in the fiber CSA had no effect on stiffness (Fig. 2.5D). Conversely, when the ECM was stiffer than the muscle, only the volume fraction of fibers affected the tissue-level properties of the muscle, with an increasing volume fraction of fibers leading to a decrease in the macroscopic shear modulus (Fig. 2.5E). All other parameters had minimal effect on shear stiffness when the ECM was stiffer.

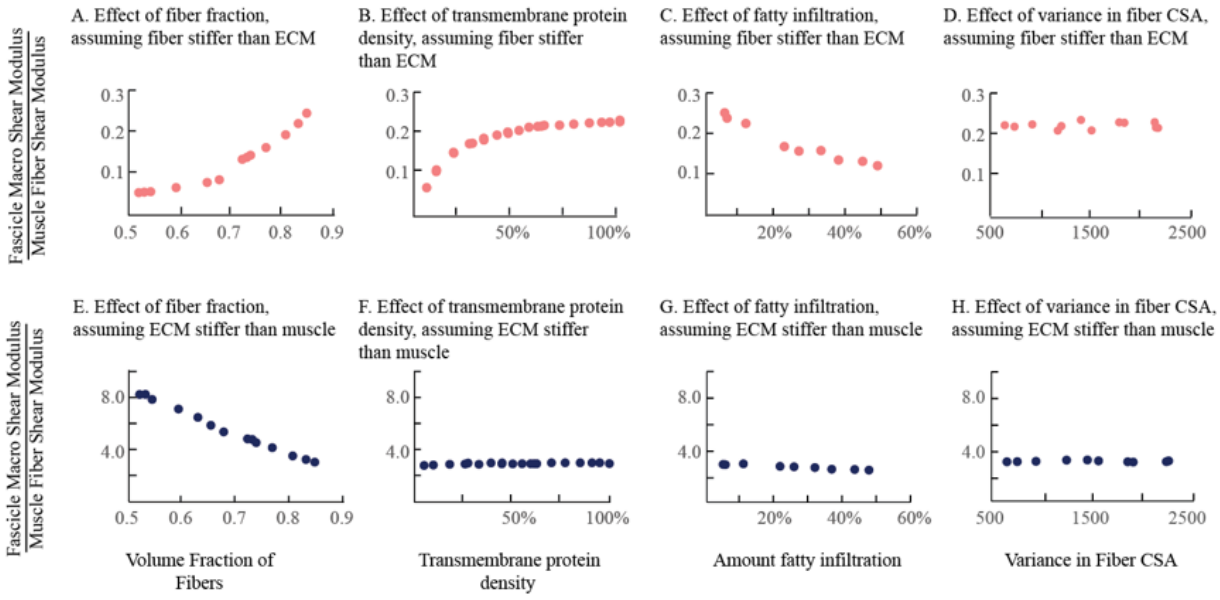

Figure 2.5. Macroscopic shear modulus is affected by stiffness of ECM, volume fraction of fibers, density of transmembrane proteins and amount of fatty infiltration. When the muscle fibers are stiffer than the ECM (a–d), both increasing the volume fraction of fibers (a) and increasing the density of transmembrane proteins (b) increase stiffness, while increasing fatty infiltration (c) decreases stiffness. When ECM is stiffer than muscle fibers (e–h), only the volume

fraction of fibers (e) has an effect, with an increase in volume fraction of fibers leading to a decrease in stiffness.

Regardless of the assumption of the relative stiffness of the fibers and the ECM, the density of transmembrane proteins had the most significant effect on membrane strain predictions, as compared to the other variations. However, in the case where the fiber was stiffer than the ECM, the protein density had a much more dramatic effect (Fig. 2.6B). These results highlight the fact that both protein density (which is decreased in DMD) and ECM properties both contribute to the damage susceptibly of muscle.

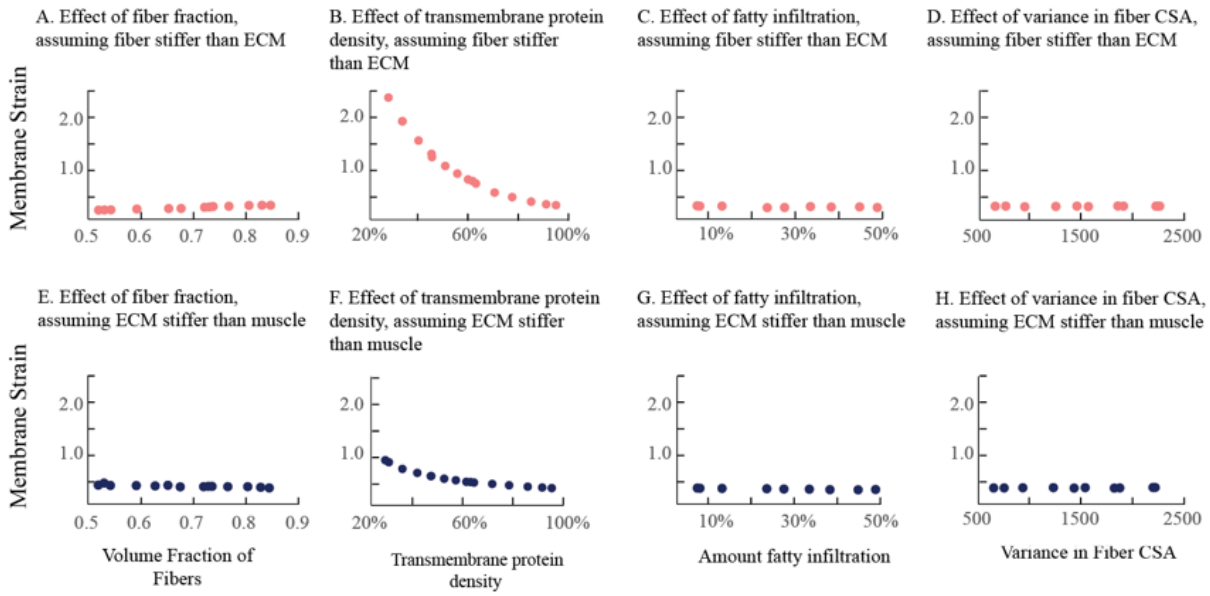

Figure 2.6. Membrane strain in the muscle fascicle is only affected by stiffness of ECM and density of transmembrane proteins. When the muscle is stiffer than the ECM (a–d), increasing the density of transmembrane proteins (b) decreases the strain on the membrane. When the ECM is stiffer than the muscles (e–h), increasing the density of transmembrane proteins (f) also decreases the strain on the membrane, but the effect is less significant.

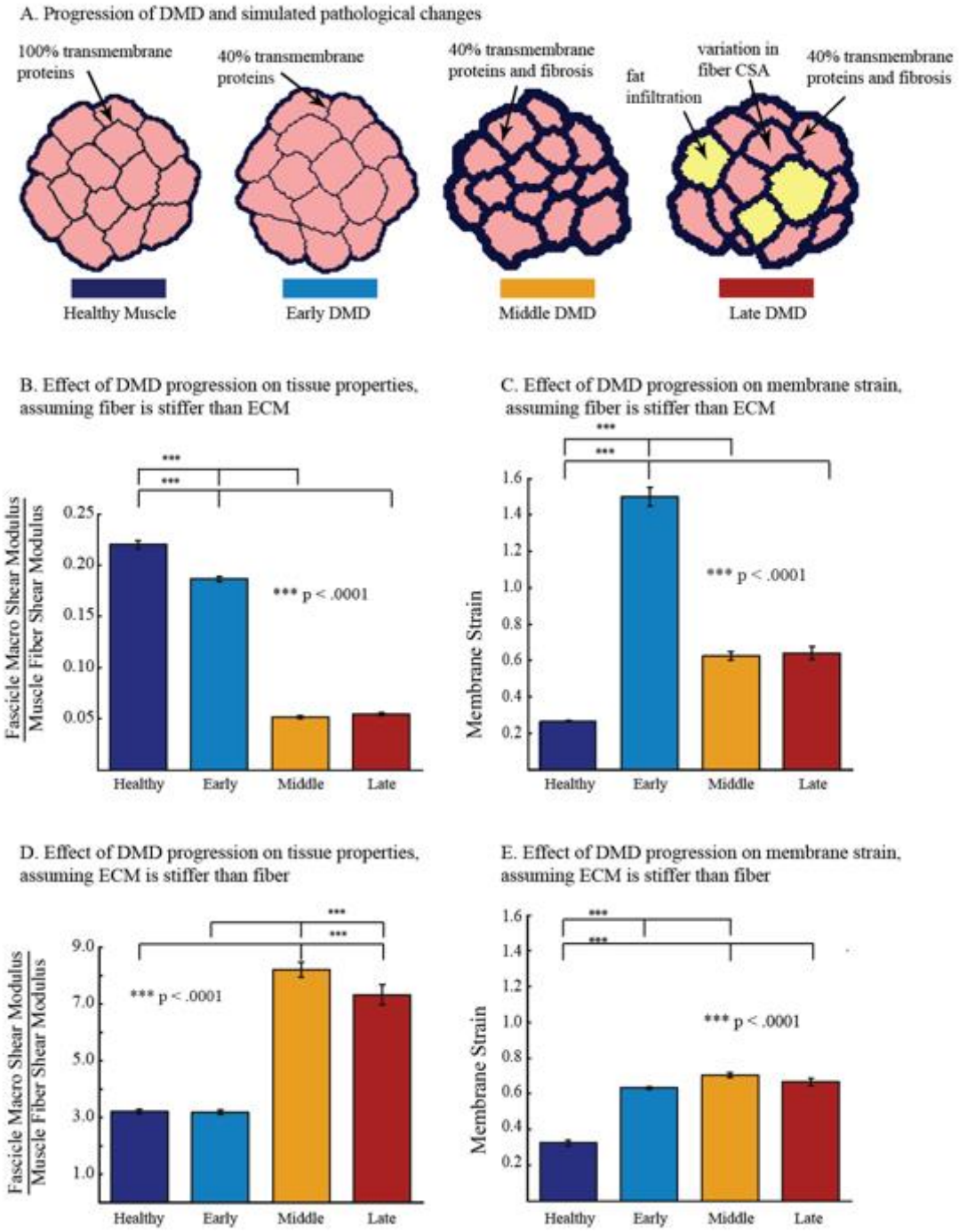

Figure 2.7. Fascicle geometries (a) for healthy, early, middle and late stage DMD muscle. Pseudohypertrophy of muscle is represented in the middle and late stages of DMD with fibrosis and fatty infiltration (a). When the muscle fiber is stiffer than the ECM (b,c), the macroscopic shear modulus decreases significantly during progression of disease (b) and the membrane strain increases significantly during the early stage, then decreases at the middle and late stages (c). When the ECM is stiffer than the fiber (d,e), the macroscopic shear modulus increases significantly in the middle stage and decreases slightly at the late stage (d), while the membrane strain increases less significantly throughout progression of the disease with a slight decrease at the late stage (e).

2.4.2 Case Study: Duchenne muscular dystrophy

The case study analysis demonstrated that pathological alterations associated with DMD progression influences both tissue properties and damage susceptibility, and the relative stiffness of the fiber and ECM dramatically influence the predicted results. In the case where the ECM remains more compliant than the fiber, tissue stiffness would decrease significantly over time (Fig. 2.7B). However, membrane strain initially increases (i.e., more damage susceptibility) but then decreases with fibrosis and fatty infiltration (Fig. 2.7C). When the ECM is stiffer than the fibers, the stiffness increases significantly in the middle and last stages (Fig. 2.7D) while the membrane strain increases less dramatically but remains elevated through the middle and late stages of disease progression (Fig. 2.7E).

2.5 Discussion

The goal of this work was to develop a computational framework to investigate how disease related changes in the muscle influence the tissue-level mechanical properties and susceptibly to membrane damage. By utilizing an agent-based model to generate geometries and mapping it to an initialized mesh, this novel modeling framework eliminates the cumbersome task of creating unique finite element meshes for each analysis, and allows for an unprecedented quantity of simulations to be run in a short amount of time. Additionally, the agent-based model generated new fascicle cross-section with varying muscle fiber shapes and sizes for each simulation, which incorporated architectural variability commonly seen *in-vivo*. This automation enabled us to explore a wide range of pathological variations commonly seen in muscle disease to first understand their influence independently, and to then analyze their compounding effects in a case study of Duchenne muscular dystrophy.

Analyzing the compounding effects of microstructural variations in the DMD case study revealed the importance of understanding fibrosis in DMD. The stiffness of the ECM relative to the fiber significantly affected the degree to which disease progression influenced the fascicle stiffness and membrane strain. Interestingly, other studies focusing on fibrosis in DMD have asserted that fibrosis not only exacerbates disease progression, but may also prevent the success of many targeted gene therapies (53, 109, 118). Further, the mechanical properties of fibrosis are likely altered throughout the course of disease, as its stiffness has been correlated with both amount of collagen and number of cross-links (65, 83, 113). Together, these results emphasize the complexity of fibrosis, and the need to better understand its development in DMD.

The model is also consistent with the theory that the transmembrane proteins protect the muscle cell from damage (17, 52, 153, 177) because deletion of membrane proteins resulted in increased strains in the membrane. However, the study further reveals that the function of the proteins is significantly affected by the nature of fibrosis. In the early stage DMD model, a 60% deletion of transmembrane proteins increased the membrane strain significantly (two-fold and five-fold) under both stiffness assumptions, with only a minimal effect on the stiffness of the muscle. This implies that even if there is not a measurable difference in stiffness at the beginning of the disease, which is supported in experimental studies (180), the protein-deficient muscle membrane may still be withstanding considerably elevated strains. The subsequent onset of fibrosis and fatty infiltration in the middle and late stages then either alleviates the membrane strain (muscle stiffer than ECM), or slightly increases it (ECM stiffer than muscle). This differential effect of fibrosis reveals a potential trade-off between functional preservation and protection of the membrane. When fibrosis decreases membrane strain the muscle stiffness also decreases, and when fibrosis increases membrane strain the muscle stiffness is increased. These insights further support the significance of understanding the nature of fibrosis.

Previous studies have predicted that damage to the muscle membrane is likely to be seen at the inter-protein regions where the dystrophin proteins are missing (17, 52, 177). We accounted for this effect in our predictions of membrane strain by determining the strain between the nodes across the entire border between muscle fibers and ECM, which included regions where dystrophin proteins existed as well as inter-protein gaps. Interestingly, when the muscle was stiffer than the ECM, there were higher strains at the inter-protein regions, than within the transmembrane proteins. When the ECM was stiffer than the fiber, the membrane strain was distributed more evenly between the protein and inter-protein regions.

Our predictions are consistent with recent studies which determined the influence of transmembrane protein density and stiffness on lateral force transmission (186). Supporting that study, we found that the stiffness of the protein had minimal effect on the fascicle shear modulus, while the density of proteins significantly affected the fascicle shear modulus. Interestingly, our analysis also revealed that, in the situation in which the ECM is stiffer than the fibers, the influence of protein density on tissue stiffness and membrane damage is diminished.

It is important to consider a number of limitations to the models presented here. First, the ECM was considered to be a continuous structure for both the endomysium and perimysium, and the same constitutive model was used for both components. However, it is known that these two layers have distinct structural compositions, and may have different material parameters (124, 125). Additionally, we did not account for the varying collagen directions seen in the ECM; though studies have postulated that the collagen direction in the endomysium does not have an effect on the shear properties (124). In our representation of fibrosis, we varied only the volume fraction of ECM while keeping the mechanical properties constant and homogenous across the sample. This simplification allowed us to focus on the effect of the volume fraction of ECM. However, this approach ignores the fact that the ECM stiffness is affected by additional factors, such as the amount of collagen within the ECM, the number of collagen cross-links, and the architectural

structure of the collagen (e.g. fiber orientation) (65, 83, 113). Indeed, increasing the volume fraction of ECM could be paired with changes in collagen content and architecture, which would also influence the tissue level properties and potential damage sensitivity of the membrane. Further, the mechanical properties of the transmembrane proteins were represented using a continuous nonlinear curve (186), although physiological models often represent it as a piece-wise function due to the unfolding of the protein (12, 52).

The analyses presented in this chapter focused on the behavior of muscle in simple shear. We focused on shearing of the fascicle because it is the dominant mode of lateral force transmission in muscle, and the behavior in shear cannot be simply intuited from the microstructure (as opposed to along-fiber tensile behavior). However, we acknowledge that simple shear does not fully represent physiologic loading patterns (69, 124, 142). In the future, coupling these models with macro-scale tissue level models (48) would enable us to study the behavior of the microstructures in the context of real physiological deformations. Additionally, we only effectively analyzed the passive mechanics of the muscle, whereas membrane damage primarily occurs during active lengthening contractions (29, 119). While the effects of activation on the shear properties of fibers are currently unknown, we would reason that muscle activation would further increase the stiffness of the muscle relative to the ECM. Therefore, we expect that the membrane damage profiles would be similar to the stiff fiber results in the DMD analysis (Fig 7C.) with potentially even greater membrane damage for a given level of shear deformation.

One of the critical challenges in creating multi-scale muscle models is the limited availability of experimental data for input parameters and validation of the model predictions. For this reason, the presented study focused on analyzing the effects of microstructural variations, given the uncertainty of specific parameters (such as the relative stiffness of the ECM and muscle fibers). We therefore utilized the presented analysis as a series of *in silico* experiments to explore the mechanics of DMD-associated modifications in microstructure, and to generate hypotheses that drive new experiments.

Future research to determine the shear properties of the ECM (and effect of pathological changes) would allow more focused analysis of disease progression. Additionally, correlations between the amount of collagen crosslinks and the stiffness of the muscle have revealed potential mechanisms through which disease may alter the mechanical properties of muscle, so it is critical to study how ECM properties differ in healthy and diseased populations. It is also important to understand the structural differences between the endomysium and perimysium within the ECM. Recent studies have developed novel methods for imaging the perimysium structure, and could be utilized to highlight these differences (55).

The modeling framework presented here can also be extended through a full coupling of the agent-based and micromechanical models to allow for the predictive analysis of DMD disease progression. Since the components of muscle are mechanosensitive, it would be informative to link the strain results of the micromechanical model with the agent-based model to predict the progression of DMD within a mechanical environment. Additionally, a fruitful area of future exploration would be to model the effects of pharmacological interventions on changes in DMD microstructure, such as the current standard-of-care, corticosteroids. Corticosteroids are known to reduce gene expression and inhibit myofibroblast activity, which potentially suppresses collagen production (78). Based on the findings in our DMD analysis, suppression of collagen production would have a differential effect on damage and function depending on the stiffness of the ECM. The integrated models would help reveal these mechanisms through which the corticosteroid's decreased collagen production prolongs ambulation; likewise they could be extended to predict other critical structure-function relationships of muscle.

Chapter 3

Agent-based model illustrates the role of the microenvironment in regeneration in healthy and *mdx* skeletal muscle

Acknowledgements: Kyle Martin, Shayn Peirce, Silvia Blemker

When my legs hurt, I say: “Shut up legs! Do what I tell you to do!” – Jens Voigt

"If you try to win, you might lose, but if you don't try to win, you lose for sure!" - Jens Voigt

3.1 Abstract:

Duchenne muscular dystrophy (DMD) is a progressive muscle wasting disease with no effective treatment. Multiple mechanisms are thought to contribute to muscle wasting, including increased susceptibility to contraction-induced damage, chronic inflammation, fibrosis, altered satellite stem cell (SSC) dynamics, and impaired regenerative capacity. The goals of this project were to: (i) develop an agent-based model of skeletal muscle that predicts the dynamic regenerative response of muscle cells, fibroblasts, SSCs, and inflammatory cells as a result of contraction-induced injury, (ii) calibrate and validate the model parameters based on comparison with published experimental measurements, and (iii) use the model to investigate how changing isolated and combined factors known to be associated with DMD (e.g. altered fibroblast or SSC behaviors) influence muscle regeneration. Our predictions revealed that the percent of injured muscle that recovered 28 days post injury was dependent on the peak SSC counts following injury. In simulations with near-full CSA recovery (healthy, 4 week *mdx*, 3 month *mdx*), the SSC counts correlated with the extent of initial injury; however, in simulations with impaired regeneration (9 month *mdx*), the peak SSC counts were suppressed relative to initial injury. The differences in SSC counts between these groups were emergent predictions dependent on altered microenvironment factors known to be associated with DMD. Multiple cell types influenced the peak number of SSCs, but no individual parameter predicted the differences in SSC counts. This finding suggests that interventions to target the microenvironment rather than SSCs directly, could be an effective method for improving regeneration in impaired muscle.

3.2 Introduction

Duchenne muscular dystrophy (DMD) is an X-linked recessive disorder caused by a mutation in the dystrophin gene, resulting in incomplete translation of the transmembrane

protein dystrophin (68, 79, 80). The lack of dystrophin makes the muscle more susceptible to contraction-induced damage and alters cell signaling processes, leading to a state of chronic inflammation (132, 153, 168). As the disease progresses, chronic damage and impaired regenerative capacity lead to muscle wasting as the contractile muscle tissue is replaced by fibrotic tissue and fatty infiltrate (75). Recent experiments have also shown that without dystrophin, SSCs undergo impaired asymmetric division resulting in either senescent cells or decreased differentiated myocytes (41). Despite extensive experimental research, there remains no cure for this disease. One of the reasons DMD is so challenging to treat is that all these mechanisms are hypothesized to contribute to the pathophysiology of the disease. Therefore, it is difficult to discern which cells and mechanisms would be the best targets for therapies.

Since impaired muscle regeneration is thought to drive disease progression in DMD, pre-clinical testing of potential treatments often utilizes a skeletal muscle injury and regeneration assay. Muscle regeneration, even in healthy muscle, is a complex, dynamic process involving numerous cell types, including SSCs, fibroblasts, and inflammatory cells. The inflammatory cell behaviors following injury have been well defined in the literature, and serve to breakdown debris and release growth factors that promote the downstream repair process (4, 25, 136, 166). A less well defined, but critical aspect of regeneration is the co-dependent interaction of SSCs and fibroblasts. Work by Murphy et al. has shown that both SSCs and fibroblasts are necessary for complete muscle regeneration (112). Fibroblasts and SSC counts peak approximately three to seven days post injury (72, 112). The SSCs divide to maintain the stem cell pool and differentiate into myocytes to repair the injured muscle (42, 84, 183).

Translating successful pre-clinical therapies in animal models, such as the *mdx* mouse, to humans is a critical barrier in developing effective therapies for DMD (61, 178). One challenge is the less severe phenotype in the *mdx* mouse compared to humans (111, 118).

Further, the temporal variations in disease phenotype as the *mdx* mouse ages, coupled with the multifaceted nature of DMD, make the results of experimental studies challenging to interpret. Therefore, we believe this is an opportunity to use computational models to aid experimental design and interpretation. We aim to develop a computational model to examine the interactions between these complex mechanisms of disease in a way that would be prohibitively difficult using experimental tools alone.

The extensive literature on muscle disease and regeneration provides a data-rich field to develop and test these computational models (9, 35, 115, 116, 118, 132, 167, 168, 176). A few recent computational models have made use of this wealth of information to examine specific aspects of disease in dystrophic muscle (34, 71, 169). We previously created micromechanical finite element models that examined the importance of the mechanical properties of the extracellular matrix (ECM) in determining the damage susceptibility of the muscle (170). Other studies used mathematical models to explore the extent to which the immune response in the *mdx* mouse contributes to the muscle degeneration and regeneration (34, 71). However, these previously published models were not developed to simulate the interactions between multiple mechanisms of disease in DMD. Therefore, we developed a new computational model to study the cellular pathophysiology contributing to muscle damage and regeneration in *mdx* mice. The specific goals of this work were to: (i) develop a computational model to predict mouse muscle regeneration following injury that focuses on the dynamics of SSCs and fibroblasts, (ii) tune the model such that it replicates key cell population dynamics from experimental studies in the literature, and (iii) use this model to analyze how known changes in the microenvironment contribute to impaired muscle regeneration in computational models of healthy and *mdx* mice.

3.3 Methods

3.3.1 Overview of approach to developing the ABM

There are extensive experimental studies that investigate the roles of individual factors, such as signaling molecules and cell types, on muscle regeneration following injury. The challenge of developing this model was to synthesize all these skeletal muscle regeneration studies to predict how muscle regeneration emerges from the behaviors and interactions of the various cell types in the muscle. To simulate these behaviors we utilized an agent-based model (ABM). ABMs simulate the actions of autonomous agents to analyze their effects on the system as a whole, providing an ideal platform for studying complex cellular dynamics (14, 59, 98, 134, 155, 158).

To develop our model of regeneration following contraction-induced injury, we used over 100 published experimental studies to define over 40 rules that govern the behaviors of muscle, SSC, fibroblast, and inflammatory cell agents. We determined that there were 13 model parameters that could not be determined from experimental data in the literature. To determine these parameters, we ran simulations and varied the unknown parameters within a physiologic range. The parameter values were determined based on the predictions that best replicated (i) cell counts and muscle fiber CSA for healthy muscle and (ii) the results of healthy muscle perturbation studies published in the literature. This process revealed that only a very specific combination of parameter values could provide predictions that met both criteria.

3.3.2 ABM Design

The ABM spatially represented a cross-section of a mouse lower limb muscle consisting of approximately 50 muscle fibers (Fig 3.1). We chose to model mouse muscle so that we could leverage the literature describing experimental studies performed in healthy and *mdx* mice. Our

ABM simulated the cellular behaviors governing muscle regeneration following an acute injury, as this is a common assay used to study regeneration experimentally. We defined an acute muscle injury as an injury induced by a single intervention (e.g. eccentric-contraction, freeze injury, cardiotoxin) that results in significant loss of strength that can recover within a time period of four-six weeks. We built the ABM in Repast, a java-based modeling platform (Argonne National Laboratory, Lemont, IL, USA). The spatial agents in the model included: muscle fibers, extracellular matrix (ECM), necrotic muscle tissue, fibroblasts, myofibroblasts, quiescent and activated SSCs, myoblasts, myocytes, and fused myotubes. The non-spatial agents included the following inflammatory cells: resident macrophages, neutrophils, three phenotypes of M1 macrophages, and M2 macrophages.

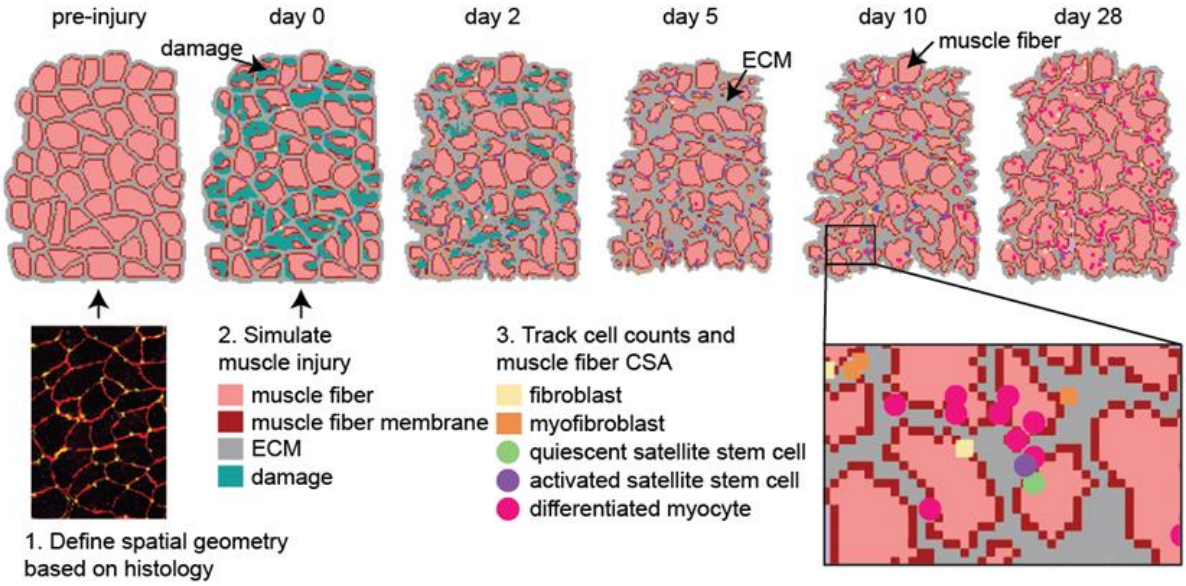

Figure 3.1. ABM simulates contraction-induced muscle damage and regeneration over 28 days. Histological images were imported into the ABM to define the spatial geometry. A contraction-induced muscle injury was simulated by replacing fiber elements with necrotic elements, and regeneration was tracked over time by measuring cell counts and fiber CSA.

The model represented 170,000 square microns with a 20-micron thickness cross-section of muscle using 13,000 grid elements. The muscle cross-section was generated by

importing muscle histology, masking the image (Mathworks, Natick, MA, USA) to differentiate the fibers and ECM, and mapping the masked image onto the ABM grid. Initial injury was simulated by stochastically replacing a percentage of the fiber elements with necrotic elements, according to the initial damage input parameter. For our healthy muscle simulations we varied the level of initial damage to determine its effect on muscle regeneration. In our *mdx* models we utilized data from the literature to define the extent of initial injury. While this approach simplified the mechanics of contraction-induced damage, it allowed us to focus on the cellular behaviors that lead to regeneration following the initial damage. Simulations were run with a 1-hour time step for a simulated 28 days following injury. All simulations were repeated 10 times to sample the stochastic nature of the model. The key model outputs included the cross-sectional area (CSA) of the muscle fibers and the time-varying counts for each cell type in the model. Muscle fiber CSA was determined by summing all of the healthy muscle fiber elements in the simulation. CSA recovery was defined as the current fiber CSA normalized to the original fiber CSA (pre-injury).

At each time step, literature-derived rules governed the behavior of the agents in the model. At model initialization, the ABM spatial representation and baseline cell (agents) numbers were defined. At subsequent time steps, each agent individually followed a probability-based decision tree to determine its action (Fig 3.2). For instance, based on the magnitude of the differentiation signal, SSC agents may differentiate into myoblasts or remain SSC agents. The collective actions of all of the autonomous agents (cells) lead to emergent, system-level behaviors (CSA changes, cell population dynamics) that were analyzed in the simulations.

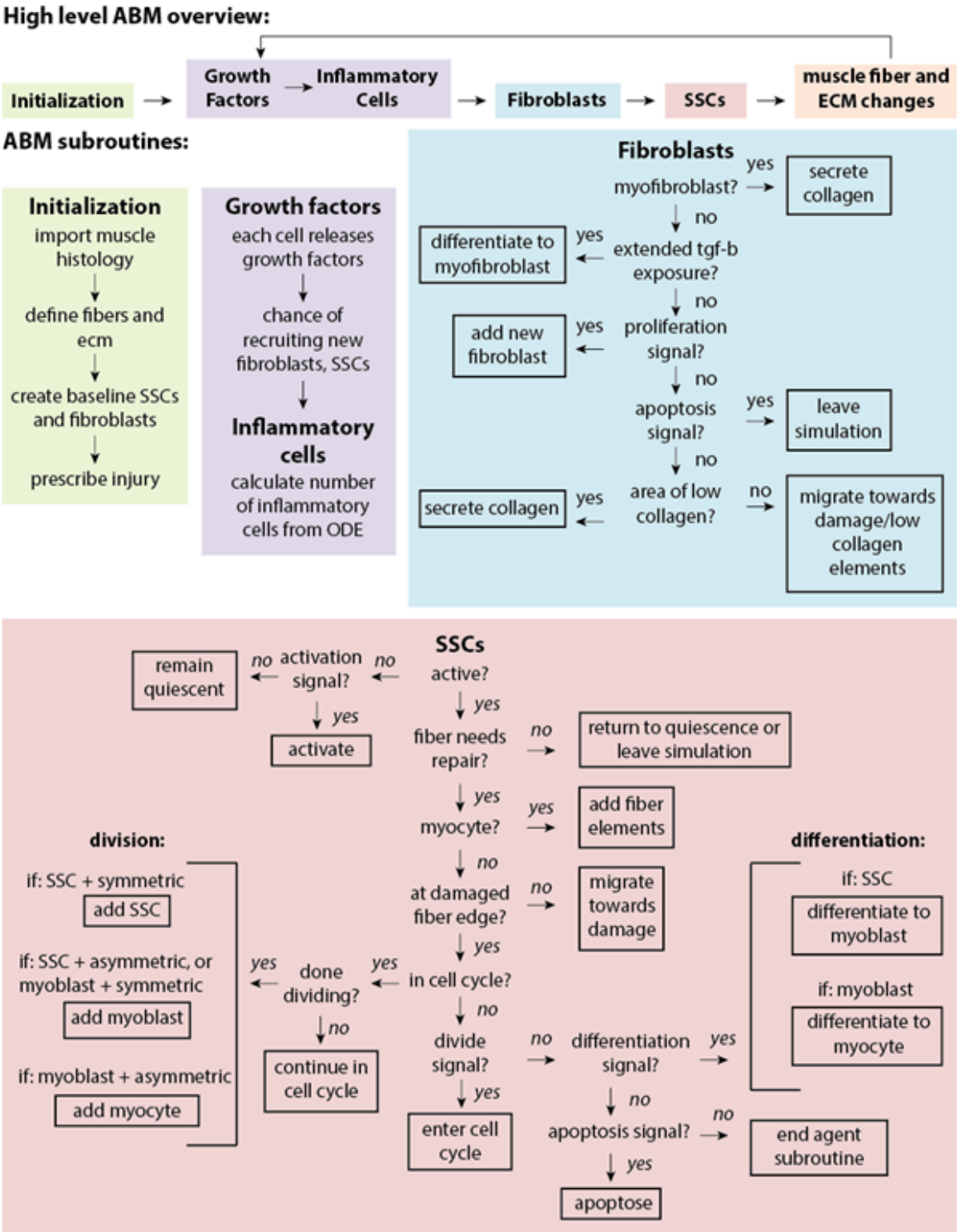

Figure 3.2. Flowchart of ABM rules. First the model is initialized, during each subsequent time step the inflammatory cells and growth factors are calculated. Then the spatial agents, fibroblasts, SSCs, fibers, and ECM follow a probability-based decision tree to guide their actions. In the flow chart, boxes represent a final action for the agent for the current time step.

3.3.3 Agent action overview

The simulated behaviors of the fibroblast and SSC agents included: secretion of growth factors, migration, quiescence, activation, recruitment, division, differentiation, and apoptosis. The 31 growth factors in the model represented the change in growth factors from homeostatic conditions (prior to injury) to levels following an eccentric contraction injury. At each time step, growth factors were added based on the defined secretions for each cell type. To migrate, the agents moved to a neighboring element within the model. Quiescent agents did not migrate or secrete growth factors until they were activated. If an agent was recruited, then a new agent was added to the simulation. An active agent could migrate, secrete growth factors, divide, differentiate, and apoptose. Agent division was represented by adding an additional agent to the simulation, and agent differentiation was represented by changing the agent type to the differentiated state. If an agent apoptosed, it was removed from the simulation.

3.3.4 Satellite stem cell (SSC) agents

(Table 3.1). At model initialization, the SSC agents were spatially located at the fiber edge in a quiescent state (130), with approximately 1 SSC agent per 4 fibers, for a 20 micron thickness cross-section. Following injury, SSC agents became activated by damage and the presence of HGF (3, 107, 156). Additionally, SSC agents were recruited to injured fibers based on a recruitment signal of growth factors (27, 57, 74, 144). SSC agents divided, both symmetrically (into two SSC agents) and asymmetrically (into one SSC agent, one committed myogenic progenitor agent), based on the microenvironmental cues and growth factors (outlined in Table 3.1). The probability that a SSC divided asymmetrically varied in the literature from 0.3 to 0.6, with the remaining divisions being symmetric (41, 85, 182). While the asymmetric cell division parameter is important to replicate experimental observations in the model, variation

within the range (0.3-0.6) did not greatly influence our model predictions. Therefore we selected a probability of 0.5 for both asymmetric and symmetric divisions. The SSC agents terminally differentiated (based on a differentiation signal) and fused with the injured fiber agents to repair the muscle (2, 4, 7). To simulate regeneration of the fiber, fused myocytes added muscle fiber elements to the periphery of the fiber. Approximately 10% of the SSC agents did not terminally differentiate and helped to restore the SSC agent pool until returning to quiescence (54, 85).

3.3.5 Fibroblast agents

(Table 3.2) At initialization, the fibroblast agents were distributed throughout the ECM (112). Following injury, additional fibroblast agents were recruited at a rate that was proportional to the amount of IL-4 secreted by eosinophil agents (66). Recent experiments have revealed that connective tissue fibroblasts in the muscle proliferate in the presence of SSCs; therefore, we incorporated a rule that caused fibroblast agents to proliferate in the presence of activated SSC agents (112). The likelihood of fibroblast agent apoptosis was elevated by the presence of TNF-α, while active TGF-β blocked the apoptosis (86). We modeled both inactive and active TGF-β as growth factors, and included a period of activation for TGF-β based on experimental data showing a 3-4 day delay between inactive TGF-β and active-TGF-β peaks (86). However, myofibroblast agents were able to immediately release activated TGF-β (39, 179). Fibroblast agents had an increasing likelihood of differentiating into myofibroblast agents when TGF-β was elevated for an extended period of time. We tuned the length of time at which high TGF-β exposure caused myofibroblast agent differentiation so that myofibroblast agent differentiation did not occur in the healthy muscle, consistent with published observations (30, 86). The fibroblast and myofibroblast agents (Table 3.2) secreted growth factors and collagen following injury (72, 98, 117, 120, 133, 146, 179, 185).

Table 3.1. Satellite stem cell (SSC) agent behaviors are defined based on literature-derived rules.

SSC Agent Behavior	Sources
SSC Activation	
Activation signal: Fiber damage; HGF	(3, 107, 156)
Recruitment signal: HGF + IGF + FGF + MMP – TGF-β	(2, 27, 74, 144, 172)
Migrate if MMP's break down dense ECM	(27, 172)
Migrate along fiber edge to damaged site	(57, 144)
SSC Division	
Enter cell cycle/divide: 3*IGF + 3*FGF + TNF-α + IFN + IL6 + VEGF + PDGF + GCSF – IL10 – TGF-β	(2, 4, 7, 51, 105, 136, 138, 152, 181);
50% cell divisions are symmetric, 50% asymmetric	(41, 85, 182)
10% of cells never express Myf5 and will not differentiate into myocytes	(54, 85)
Chance of division decreases with each cell division; 1st division 85%; 2nd 65%; 3rd 20%	(145)
After symmetric cell division, sister cells remain in contact for 3 hours	(144, 145)
After asymmetric cell division, sister cell remain in contact for 8 hours	(144, 145)
Time to initial division: 18-24 hours	(85, 131, 145)
Time to divide: 10 hours	(131, 145)
Decreased fibronectin = decreased chance of symmetric division	(11)
SSC Differentiation	
Exit cell cycle/terminally differentiate: 4*IL10 + IL4 - 2*FGF – 2*IGF – 2*HGF – IFN – TNF-α	(2, 4, 7, 107)
Activated SSCs differentiate into myoblasts; myoblasts differentiate into myocytes	(20, 173)
Differentiated myocytes fuse at damaged fiber edge	(20, 173, 183)
SSC Behaviors	
Initial count: 1 quiescent SSC per 4 fibers (assumes 20 micron thick slice)	(130)
Secretions: Fibronectin; MMPs; IL1; VEGF; CCL22	(11, 25, 88)
Inflammation dependent secretions: TNF-α; IL6; IL8; MCP	(25, 133)
Differentiated myoblasts fuse and repair muscle fiber	(91, 171)
If M1 macrophage count > SSC count, SSCs are protected from apoptosis	(25)

Table 3.2: Fibroblast agent behaviors are defined based on literature-derived rules.

Fibroblast Agent Behavior	Sources
Initial count: 1 per every 2 fibers (assumes 20 micron thick section)	(112)
Recruitment signal: eosinophil secreted IL-4	(66)
Proliferation signal: SSC proliferation	(86)
Extended TGF- β saturation causes fibroblast differentiation into myofibroblasts	(39, 179)
Secretions: TGF- β ; IGF1; PDGF; MMPs; IL6; FGF; Fibronectin	(72, 98, 117, 120, 146, 185)
Inflammation dependent secretions: IL1; IL8; MCP	(133)
Secrete collagen to rebuild ECM following injury	(137, 188)
Migrate towards damage/low collagen at 5-20 microns/hour	(40, 114)
Myofibroblast secretions: 2x Collagen; active-TGF-β	(120, 179, 185)
Apoptosis signal: TNF-α	(86)
TGF-β blocks TNF-α induced apoptosis	(86)

3.3.6 ECM and muscle fiber agents

The muscle fiber and ECM agents were comprised of multiple elements in the model. An average of 180 elements (2400 square microns) represented the area of a single muscle fiber. The ECM elements were prescribed a collagen density parameter based on literature measurements (118). To simulate injury, the initial damage parameter (input to the simulation) defined the percent of the healthy muscle fiber elements that were replaced by necrosis elements. The rate of necrosis element removal was dependent on the number of M1 macrophage agents. Elements corresponding to cleared necrosis converted to a low-density collagen element. Fibroblast agents secreted collagen in these locations to restore the stiffness of the damaged tissue (137, 188). Additionally, if areas of very low collagen remained, then two neighboring ECM elements with low collagen were merged into a single element (with the sum of both collagen density factors). This simulated behavior reduced the overall size of the muscle (muscle fibers and ECM) which is seen during muscle recovery (112). When myocyte agents

fused to the fiber edge, muscle fiber elements were added at the periphery of the fiber, increasing the muscle fiber size (20, 173, 183).

3.3.7 Inflammatory cell ODE

The inflammatory cell dynamics were defined based on previous work by Martin et al (100, 102). Our goal was to reduce the computational cost of the ABM, but still retain the dynamic behaviors of the inflammatory cells that were previously established. Therefore, we converted the rules for each of the inflammatory cells in the ABM described by Martin et al. into a system of seven coupled ordinary differential equations (ODEs). The seven ODEs represented the seven inflammatory cell phenotypes in Martin's model, including: resident macrophages (RM), neutrophils (N), apoptotic neutrophils (Na), M1 macrophages (M1), apoptotic neutrophil phagocytosing M1 macrophages (M1ae), debris phagocytosing M1 macrophages (M1de), and M2 macrophages (M2) (Equations 3.1-3.7). To test if our ODE was equivalent to the ABM by Martin et al., we ran simulations of the inflammatory cell dynamics following injury with both models and confirmed that the results of our ODE fell within the 95% confidence interval of the predictions from the Martin ABM.

The ODE was defined by 51 parameters that represented the recruiting and deterring interactions between the different cells types. The interactions were determined based on the growth factor secretions and the response to growth factors for each cell type. Within the ABM simulation framework, the inflammatory cell ODEs were solved non-spatially using the Euler method with a 1 hour time-step. To couple the inflammatory cell ODEs with the behaviors of the other spatial cell agents, we included the following rules for inflammatory cell agents, based on the cell counts at the beginning of each time step: (i) secretion of growth factors (ii) removal of necrosis elements and (iii) M1 macrophage-dependent protection of SSC apoptosis.

Additionally, the inflammatory cell ODEs are dependent on the spatial (fibroblast and SSC) agent counts at each time step. Detailed descriptions of the inflammatory cell ODEs are included in Appendix A.

3.3.8 Baseline model parameterization

To parameterize the baseline model, we ran simulations and iteratively adjusted the unknown model parameters (Table 3.3), such that the model predictions (95% confidence intervals) were consistent with published experimental data. The published experimental data included: (i) fibroblast and SSC counts (112), inflammatory cell counts (4) and CSA recovery measurements (123) for healthy muscle regeneration following injury, and (ii) results from healthy muscle regeneration perturbation studies. The perturbation studies included: (i) fibroblast depletion (112), (ii) SSC depletion (112), (iii) TNF-α blockade (86), and (iv) increased TGF-β (86).

When comparing the cell counts with published experiments, we focused on the critical window of 3-7 days post-injury, since this is when SSCs and fibroblasts peak in the literature. Cell counts were normalized such that the peak counts were similar for all the different cells in the model. The growth factor secretions from each cell were then scaled to be consistent with literature observations. In order to confirm the validity of this normalization scheme, we performed simulations with both normalized and un-normalized cell counts and found no differences in the simulations' predictions. The literature consistently uses percent of peak isometric torque as the biomarker of active muscle tissue regeneration; therefore, we tuned our unknown model parameters such that the fiber CSA predictions encompassed the peak torque measurements from the literature. Once the model parameters were tuned, we ran simulations to verify the models predictions. To verify the model predictions, we replicated experimental

perturbations in literature (Table 3.4) and compared our model predictions with the experimental results from the respective studies.

Table 3.3. Unknown model parameters were tuned to recapitulate published literature.

Parameter	Equation	Range Tested	Value
Normalization factor for fibroblast recruitment, x_1	Fibroblast recruitment probability = 1/(x_1-recruitment signal)	35-120	70
Maximum probability of fibroblast recruitment per hour, x_2	if fibroblast recruitment probability > x_2, recruitment probability = x_2	1/50 − 1/5	1/15
Normalization factor for fibroblast expansion, x_3	fibroblast expansion probability = 1/(x_3 – expansion signal)	50 − 140	90
Maximum probability of fibroblast expansion per hour, x_4	if fibroblast expansion probability > x_4, expansion probability = x_4	1/100 − 1/10	1/35
Minimum required time (hours) in high TGF- β environment for fibroblasts to differentiate into myofibroblasts, x_5	Minimum required time (hours) in high TGF-β environment for fibroblasts to differentiate into myofibroblasts = x_5	0 − 24	12
Normalization factor for SSC division, x_6	SSC division probability = 1/(x_6 – division signal)	150 − 300	220
Maximum probability of SSC division per hour, x_7	if SSC division probability > x_7, division probability = x_7	1/100 − 1/10	1/60
Normalization factor for SSC differentiation, x_8	SSC differentiation probability = 1/(x_8 – differentiation signal)	−30 − 40	0
Maximum probability of SSC differentiation per hour, x_9	if SSC differentiation probability > x_9, differentiation probability = x_9	1/50 − 1/2	1/5
Normalization factor for SSC migration, x_{10}	SSC migration probability = 1/(x_{10} – migration signal)	100 − 180	150
Maximum probability of SSC migration per hour, x_{11}	if SSC migration probability > x_{11}, migration probability = x_{11}	1/50 − 1/5	1/30
Probability of adding a fiber element, when SSC is fused with myofiber per hour, x_{12}	Probability of adding a fiber element, when SSC is fused with myofiber per hour = x_{12}	1/20 − 1	1/4
Maximum number of fiber elements added per SSC, x_{13}	Maximum number of fiber elements added per SSC = x_{13}	5 − 200	60

Table 3.4: Input parameters for model verification simulations.

Simulation	Revised model input	Source
Fibroblast depletion	Decreased baseline fibroblast counts by 60%, and fibroblast recruitment by 60%	(112)
Macrophage decrease	Decreased macrophage levels by 80%	(154)
SSC depletion	Set SSC counts to 0	(112)
No asymmetric division	Set the chance of asymmetric division to 0	(82)
Block TNF-α	Set TNF-α parameter to 0	(86)
Add TGF-β	Increased TGF-β 1.5x	(86)
Fibronectin knockdown	Set fibronectin parameter to 0	(11)
Block eosinophil secreted IL-4	Set eosinophil-secreted IL-4 parameter to 0	(66)

3.3.9 Analysis of individual mechanisms of disease

After developing the model to replicate various experimental observations of healthy muscle regeneration, we modified individual cellular behaviors to examine how each mechanism can contribute to the disease phenotype. To do this, we independently varied the number of fibroblast, SSC, and inflammatory cell agents, the ability to asymmetrically divide, and the extent of initial damage in a range from healthy to values relevant to dystrophic muscle. We then simulated a muscle injury and tracked the CSA recovery over time (fiber CSA relative to original CSA). We examined the simulation predictions in two ways. First, we quantified the time-varying muscle fiber CSA (relative to original size) for 10 repeated simulations of variations in each input parameter. Second, we compared muscle fiber CSA (relative to original size) at specific time points for all simulations within a physiologic range of the input parameters.

3.3.10 Analysis of *mdx* mouse models

We created variations of the ABM that represented *mdx* mice at three stages of disease (Table 3.5) by altering parameters consistent with observations of muscle pathophysiology at different ages of *mdx* mice. We selected three ages of *mdx* mice to differentiate between three

phenotypes of the disease that occur at different ages. The 4 week old *mdx* mouse has a significant inflammatory response and exhibits increased markers of degeneration. The 3 month old *mdx* mouse represents a more stable phenotype, in which the inflammatory cells, SSCs, and fibroblast are more similar to a healthy mouse with increased damage susceptibility. The 9 month old *mdx* mouse represents a more pro-fibrotic phenotype.

Table 3.5. Model input parameters were altered to develop models of *mdx* mice at three disease stages.

Parameter	**Healthy (3 month old)**	**4 week old *mdx***	**3 month old *mdx***	**9 month old *mdx***
Fibrosis (% ECM above healthy) (30, 118)	0%	0%	+ 5%	+ 10%
Relative initial fibroblast count (30)	1	1	1.5	2
Initial damage (35, 115)	10%	35%	26%	29%
Relative collagen density (63, 103, 118)	1	1	1.5	3
Relative initial SSC count (130, 139)	1	1	1	1
Relative telomere shortening (93, 135)	1	1	1	1
Probability symmetric division (41, 60, 85, 182)	0.5	0.5	0.5	0.5
Probability asymmetric division (41, 60, 85, 182)	0.5	0.1	0.1	0.1
Probability abnormal division (41, 60, 85, 182)	0.5	0.4	0.4	0.4
Relative resident macrophage count (166, 176)	1	2	1.3	1.8
Relative chance of secondary necrosis (166, 167)	1	2	1.5	1.5
Eosinophil scalar (23)	1	1.3	1	1
M1 macrophage scalar (166, 176)	1	1.25	1	1
M2 macrophage scalar (165, 166)	1	0.8	1.25	2.5
Relative initial active-TGF-B1 (97, 118)	1	1	1	1.3

The spatial representations were defined by importing histology from correspondingly aged *mdx* muscle. The histology defined the pathological variations in CSA, fibrosis, and collagen density (30, 118). To capture both the increased damage susceptibility in *mdx* mice, and a significant force-loss from injury, we used work by Dellorusso et al, that analyzed the injury from supra-physiologic strains in different ages of *mdx* mice (35). Our model representation of damage represents the factors that recover as a result of SSC behavior and

thus does not include factors that can recover without SSCs (e.g. excitation-contraction uncoupling). Therefore, we aimed to exclude the contribution of excitation-contraction coupling in our initial damage input parameter by excluding the percent of force-loss that recovers 15 minutes post injury, as this portion of the force deficit has been shown not to depend on SSC regeneration (35). We also reduced the level of initial damage, while maintaining the ratios of damage between the groups, based on the assumption that 50% of the torque-deficit can be recovered without SSCs (128). From these data, we calculated the ratio of damage between healthy, 3 month *mdx*, and 9 month *mdx* mice to be 10%:26%:29%. To predict the damage in the 4 week *mdx* mouse, we used a previously published finite-element model to simulate the contraction. The model predicted that the lack of dystrophin proteins (17, 52) and low-density collagen (prior to fibrosis) resulted in 35% damage. In these simulations, we have assumed that the mechanism of injury (damage to contractile muscle tissue) is the same between healthy and *mdx* mice.

Baseline cell counts for fibroblasts were altered according to experimental data (30). Baseline SSC counts were kept the same between healthy and *mdx* models because many studies have shown that *mdx* mice do not show direct changes in SSC counts or regeneration (measured by telomere shortening) in the lower limb for the age groups modeled (135, 139). However, asymmetric division of SSC agents were modified according to experimental observations (41). The inflammatory cell behaviors were altered to represent the significantly elevated pro-inflammatory environment in the 4 week *mdx* mouse model with increased cytotoxicity of macrophage agents (166, 167, 176). In the 3 month old *mdx* mouse model, the inflammatory response was elevated relative to the healthy values. In the 9 month old *mdx* mouse model, the inflammatory response was shifted to a highly anti-inflammatory phenotype (higher M2 macrophage agent counts relative to M1 agent counts) with a TGF- β enriched environment (added TGF-β) (97, 118, 166, 167).

3.4 Results

3.4.1 ABM simulated healthy muscle regeneration dynamics.

While tuning the unknown model parameters (Table 3.3), the simulations revealed emergent muscle regeneration behaviors that were consistent with key experimental studies in the field. For example, the fibroblast agents peaked between days 3 and 7 following injury (Fig 3.3A), with fibroblast agents remaining elevated throughout most of regeneration (10, 112). The SSC agents peaked between days 3 and 7, and the differentiating myocyte agents appeared in the simulated muscle by day 4, peaking in number by day 10 (10, 112). The inflammatory cell ODEs also recapitulated the timing of inflammatory cell peaks, including M1 macrophages at day 2-3, and M2 macrophages at day 4-5 (4, 25, 136, 166) (Fig 3.3B). The simulated muscle fiber CSA returned to 100% of its original fiber size by 14 days post injury (Fig 3.3C) (123).

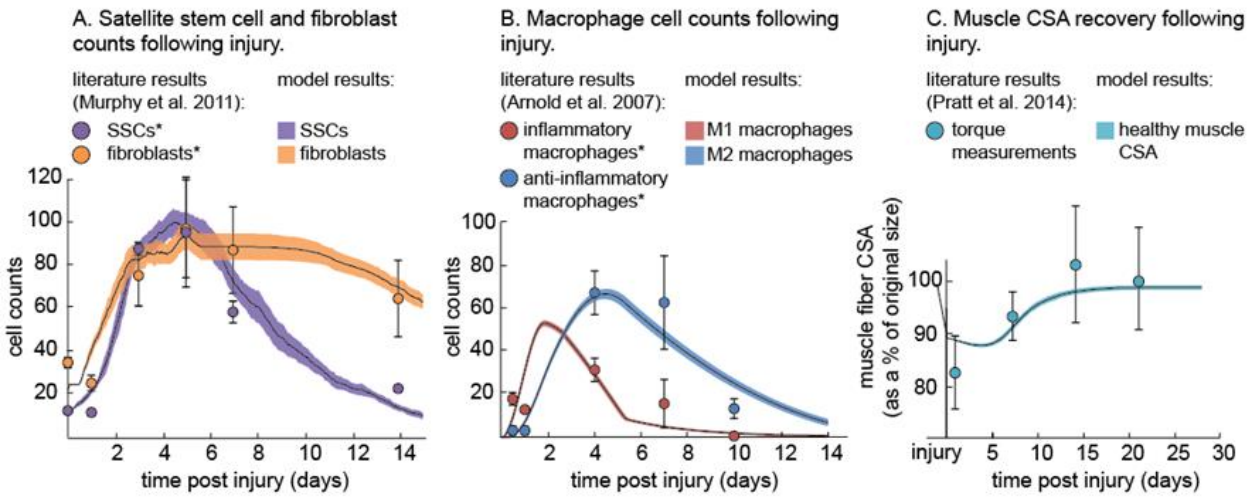

Figure 3.3. ABM of healthy muscle regeneration recapitulates peak cell populations and fiber CSA following injury. The model recapitulated experimental data for SSCs, fibroblasts, M1 macrophages and M2 macrophages following injury, within the models predicted 95% confidence interval for cell counts (4, 112) (A, B). Regeneration in the ABM is measured as a percent of the current fiber CSA relative to the original fiber CSA (pre-injury). The model recapitulated experimental regeneration data (peak isometric torque loss) for healthy muscle following injury (C). The day 0 time point has been excluded from this figure to reduce the contributions from neuromuscular failure (123). *Cell counts have been normalized for comparison to model results, as described in Methods section.

3.4.2 ABM simulations of initial damage perturbations.

We varied the amount of initial damage and tracked the CSA recovery (defined as the normalized CSA) over 28 days (Fig 3.4A). The ABM predicted that the time to recovery (time for the fiber CSA to return to 100%) is not linearly dependent on the extent of initial damage (Fig 3.4B). At early time points (day 7), the percent CSA recovery had a one-to-one relationship with the initial damage. However, at later time points (days 14 and 28), the CSA percent recovery was similar for the different damage levels. This implies that the magnitude of the regenerative response is positively correlated with the amount of muscle damage, and the timing of regeneration remains relatively constant across damage levels.

3.4.3 ABM simulations of fibroblast perturbations.

We simulated the effects of varying the number of fibroblast agents in the model across a physiologic range (0 to 2.5 fold change in the number of fibroblast agents, relative to healthy controls) (Fig 3.4D). With increased numbers of fibroblast agents in the muscle, we found no change in muscle regeneration (fiber CSA) compared to healthy muscle (Fig 3.4D). Simulations with a 0-0.5 fold change in fibroblast agents (relative to healthy controls) resulted in an 11% decrease in fiber CSA at the end of the 28 day simulation (Fig 3.4C).

3.4.4 ABM simulations of inflammation perturbations.

We varied the number of macrophages to investigate the effects of inflammation on muscle regeneration in our ABM (Fig 3.4E and 3.4F). Our model predicted that a 0-0.3 fold change in macrophage agents (relative to healthy controls) resulted in increased fiber CSA for the first 6 days following injury, but ultimately resulted in a 13% decrease in fiber CSA at the end

of the 28 day simulation. Additionally, we found that greatly increasing the number of macrophage agents (2.5-3 fold increase from healthy controls) resulted in a decreased fiber CSA at two time periods, days 0-5 and day 10-28, with a 7% decrease in fiber CSA at day 28.

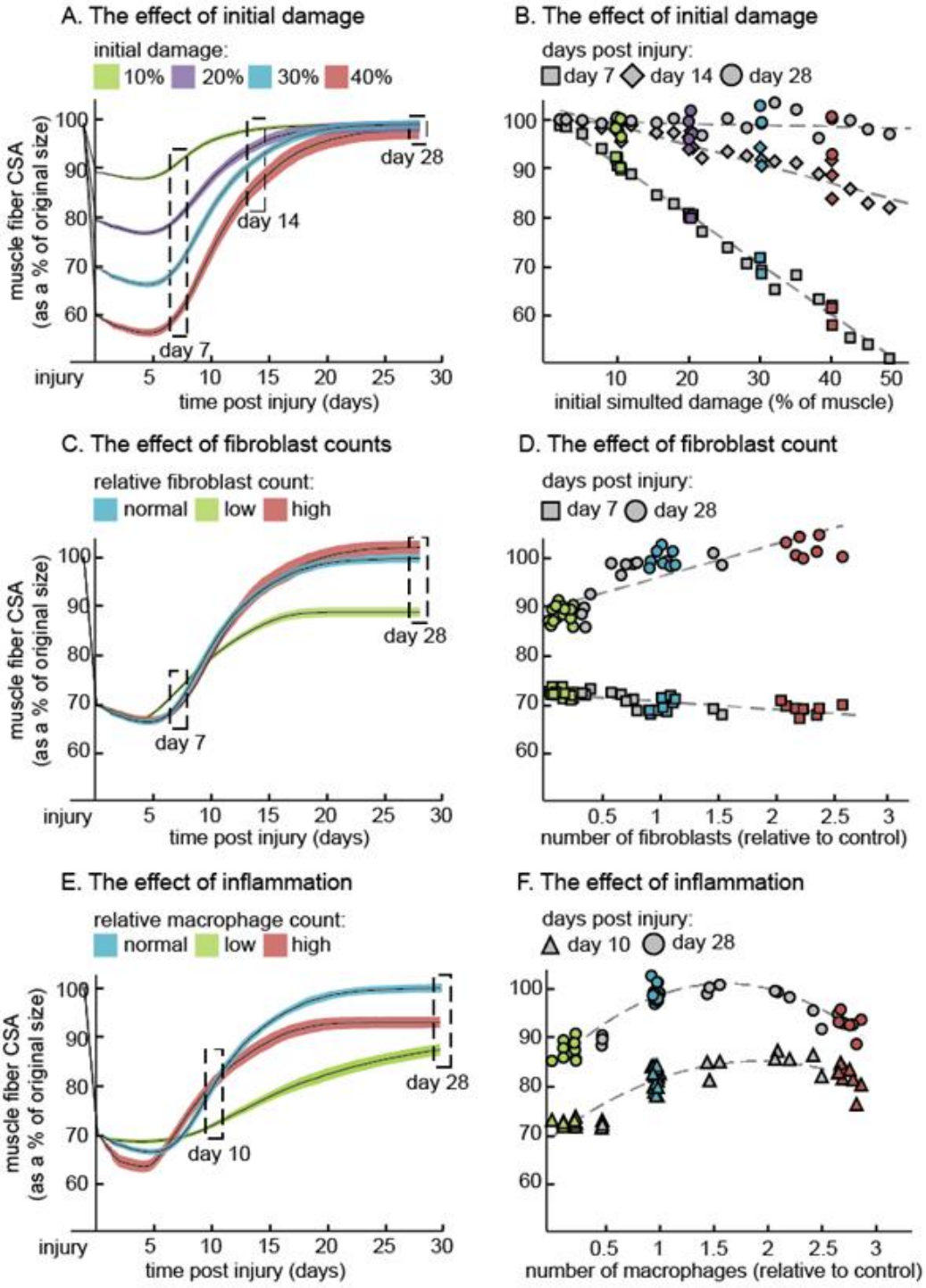

Figure 3.4. (From previous page). Altering initial damage, fibroblast agent counts, and macrophage agent counts revealed complex, temporal dynamics. We analyzed the effects of modifying initial damage (A, B), fibroblast agent counts (C, D), and macrophage agent counts (E, F) in our healthy muscle ABM. Parameters were varied in a range from healthy to expected values in dystrophic muscle. Output includes muscle regeneration curves for 10 repeated simulations with a single input parameter (A, C, E), and muscle fiber CSA (relative to original size) at specific time points for all simulations within a range of input parameters (B, D, F). Altering the initial damage revealed relatively consistent timing of recovery (A). Low fibroblast counts resulted in initial increased fiber CSA but ultimate impairment (C). Both high and low levels of macrophages were predicted to impair regeneration (E).

3.4.5 ABM simulations of SSC perturbations.

The simulations predicted that varying SSC agent counts by 0-1.5 fold (relative to healthy controls) affected muscle regeneration significantly (Fig 3.5A and 3.5B). Depletion of SSC agents (0 SSC agents) resulted in a 36% decrease (relative to healthy controls) in fiber CSA by day 28, while low SSC agent counts (0.1-0.4 fold change relative to healthy controls) resulted in a 22% decrease (relative to healthy controls) in fiber CSA by day 28. Increasing the SSC agent counts 1.5 fold only minimally enhanced the fiber CSA (3%) compared to the healthy controls. We simulated the effects of impaired SSC agent asymmetric division on the normalized fiber CSA. Allowing for 0% SSC agent asymmetric division (100% symmetric divisions) lead to impaired muscle regeneration at all time points after 7 days, with a 6% decrease in fiber CSA at day 28 (Fig 3.5C). 100% SSC agent asymmetric division resulted in no difference in fiber CSA at all time points.

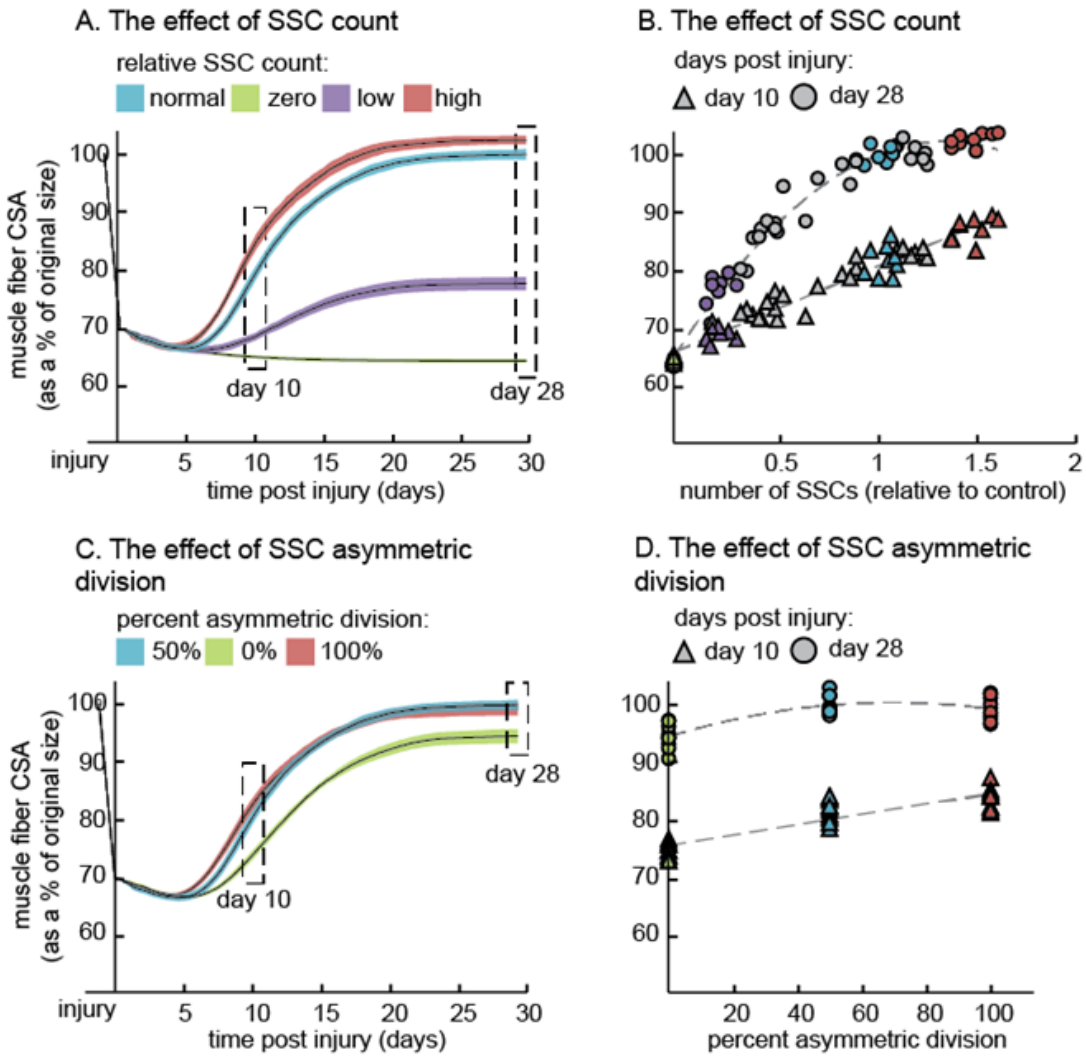

Figure 3.5. Altering SSC agent counts and impairing SSC agent asymmetric division revealed complex, temporal dynamics. We analyzed the effects of modifying SSC agent counts (A, B), and percent of SSC agent asymmetric divisions (C, D) in our healthy muscle ABM. Parameters were varied in a range from healthy to expected values in dystrophic muscle. Output includes muscle regeneration curves for 10 repeated simulations with a single input parameter (A, C), and muscle fiber CSA (relative to original size) at specific time points for all simulations within a range of input parameters (B, D). Depleted and low levels of SSC agents impaired regeneration, while high levels lead to a small but significant increase in fiber CSA (A). Zero SSC agent asymmetric divisions resulted in impaired regeneration for all time points (C).

3.4.6 Comparison of ABM perturbations with the published literature.

The results of fibroblast and inflammatory cell perturbation simulations were generally consistent with the available literature (Fig 3.6). For example, decreasing the number of fibroblast agents by 60% predicted decreased regeneration, and published experiments have shown that depletion of 60% of Tcf4+ fibroblasts resulted in premature differentiation of SSCs and impaired regeneration (47, 112). The model predicted that decreasing the number of macrophage agents impaired muscle regeneration, increased fibroblast agent counts, and had no effect on SSC agent counts. Comparable experimental studies similarly showed that decreased macrophage counts resulted in decreased regeneration at day 9 and 21 (4, 143, 154). Additionally, in mice with decreased monocytes (C-C chemokine receptor type 2 (Ccr2)-/- mouse strain), fibro/adipogenic progenitor cell (the main source of myofibroblasts in skeletal muscle (87, 162)) clearance is impaired, leading to increased fibro/adipogenic progentior cell counts (86). Experimentally, the effect of decreased macrophage counts on SSC counts is difficult to interpret in the literature, as some studies have shown no effect on SSCs (154, 175), while others have shown delayed proliferation and differentiation of SSCs (140).

The ABM predictions of *in silico* perturbations of SSC agents was also consistent with data in the literature. Our model predicted that decreasing the number of SSC agents resulted in decreased fibroblast agent counts and impaired regeneration. Similarly, experimental studies showed that depletion of Pax7+ SSCs resulted in decreased Tcf4+ fibroblast counts at day 5 and 28 (Tcf4+ cell density was increased following normalization to muscle area), and impaired regeneration (112). The model predicted impaired regeneration and decreased SSC agent counts following impaired SSC agent asymmetric division. A comparable experimental study similarly demonstrated that impaired SSC asymmetric division resulted in lower SSC counts and impaired regeneration (82)

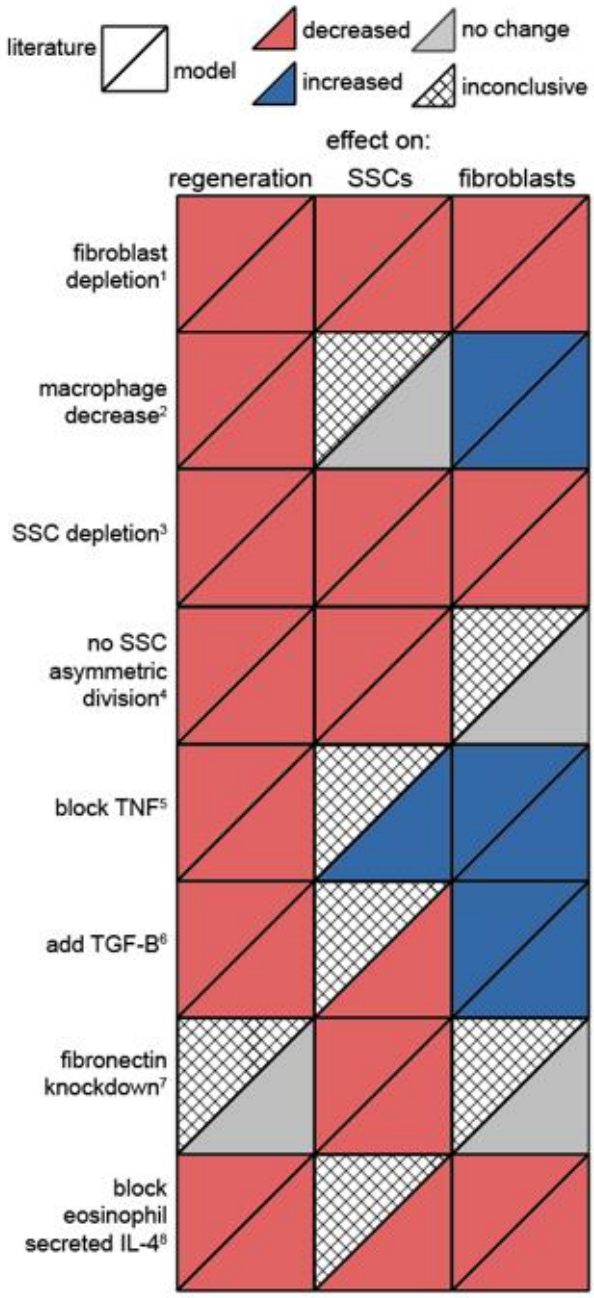

Figure 3.6. ABM predictions are verified through comparison with experimental results from published literature. Upper triangles represent a decrease (red), increase (blue), no change (gray), or inconclusive published data (checkered) for regeneration, SSC counts, or fibroblast counts. Lower triangles represent the model prediction. Inconclusive data is due to conflicting published data, or our inability to identify published experimental studies that recapitulated our ABM perturbations. Regeneration increases and decreases represent an increase or decrease in fiber CSA at the end of the 28 day simulation, respectively. To verify model predictions we simulated experiments in the literature and compared our model predictions to the experimental results. Experimental sources from the literature used for comparison: 1. (47, 112). 2. (4, 86, 143, 154). 3. (112). 4. (82). 5. (86, 174). 6. (86, 118) 7. (11, 92). 8. (66).

Finally, we evaluated the effects of varying four individual parameters that have been shown in the literature to be critical regulators of muscle regeneration: levels of TNF-α, TGFβ, fibronectin, and eosinophil-secreted IL-4. The model predicted that blocking TNF-α resulted in increased fibroblast agent counts and impaired regeneration at day 14. Similarly, experimental studies showed that blocking TNF-α resulted in increased fibroblasts at day 7 (86), and impaired regeneration at day 14 (174). Simulations with increased TGFβ expression predicted increased fibroblast agent counts and impaired regeneration. Comparable experimental studies showed increased fibroblasts at day 7 (86) and impaired regeneration, as measured by decreased force production one month following injury (118). The simulation of fibronectin knockdown predicted decreased SSC agent counts, in agreement with experimental studies (11, 92). Finally, simulations that blocked eosinophil-secreted IL-4 resulted in decreased regeneration and fibroblast agent counts. Similarly, experimental studies have shown that that blocking the IL-4 receptor resulted in decreased fibro/adipogenic progenitor cell numbers and impaired regeneration (66).

3.4.7 Simulated *mdx* mice displayed altered cell dynamics at all ages and impaired regeneration in 9 month old *mdx* mice.

Models of the 4 week old and 3 month old *mdx* mouse muscle recovered to within 96% of original fiber CSA (Fig 3.7A), while the model of the 9 month old *mdx* mouse recovered to 88% of its original size by day 28. Interestingly, although the predictions of fiber CSA regeneration appear similar for some of the *mdx* ages, the cellular dynamics driving the regeneration differ substantially for each *mdx* age. For example, following injury, the number of SSC agents was significantly increased (2.8x healthy controls) in the 4 week old *mdx* mice with a two-day delay in initial SSC agent differentiation (Fig 3.7B and 3.7C), while the 9 month old *mdx* mice had the highest levels of peak fibroblast agent counts (1.6x healthy controls) (Fig

3.7D). In the 4 week old *mdx* mice, the inflammatory response was dominated by pro-inflammatory macrophage agents (M1), and the activity of M2 macrophage agents was less substantial (Fig 3.7E and 3.7F). By contrast, both the young and 9 month old *mdx* mice were dominated by an anti-inflammatory phenotype with higher counts of M2 macrophage agents as compared to M1 macrophage agents. All the macrophage counts were elevated in the *mdx* mice relative to the healthy controls.

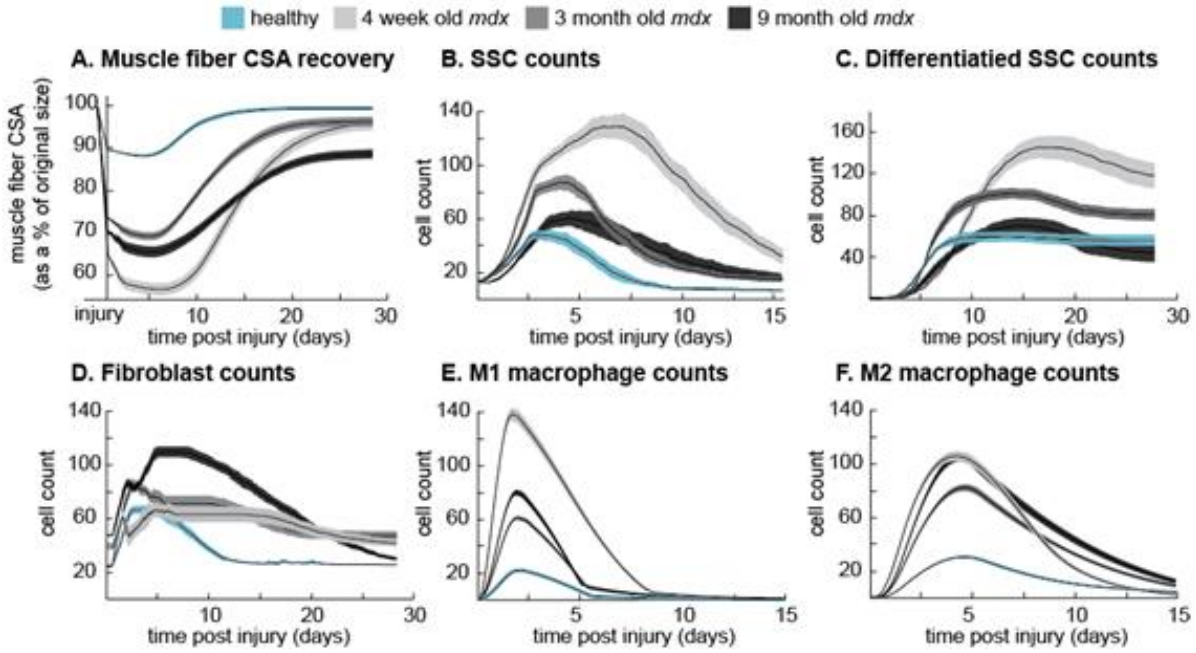

Figure 3.7. Three models of *mdx* mice simulate regeneration and cell counts following injury. Three models of *mdx* mice were developed for three stages of disease: 4 week old *mdx*, 3 month old *mdx*, and 9 month old *mdx*. Injury and regeneration were simulated and CSA and cell counts were tracked over time. The 4 week old and 3 month old *mdx* mouse recovered to 96% of the original fiber CSA 28 days post injury, while 9 month old *mdx* mice recovered to 88% of its original size (A). SSC agents were significantly increased in 4 week old *mdx* mice with delayed SSC agent differentiation (B, C). 9 month old *mdx* mice had high levels of fibroblast agents and low levels of SSC agents and differentiated SSC agents (B, C, D). The 4 week old *mdx* mouse was dominated by inflammatory (M1) macrophage agents, while the young and 9 month old *mdx* mice were dominated by anti-inflammatory (M2) macrophage agents.

We analyzed the relationship between the model cell counts and muscle CSA recovery in the healthy and *mdx* simulations. Peak SSC agent counts, normalized by the area of injury

(μm^2), correlated with the percent of the injured muscle that recovered 28 days post injury (Fig 3.8A). Since the initial SSC count parameter was not different in any of the *mdx* simulations, the predicted differences in peak SSC agent counts between the healthy and *mdx* mouse simulations were emergent model predictions that resulted from changes in the microenvironment. Therefore, we analyzed the relationship between SSC agent counts and other model predictions, to investigate how changes in individual factors associated with disease influence SSCs. Peak fibroblast agent and M2 macrophage agent counts, normalized by the area of injury, influenced the peak SSC agent counts, but no single model parameter was able to predict the differences in SSC counts (Fig 3.8B-D).

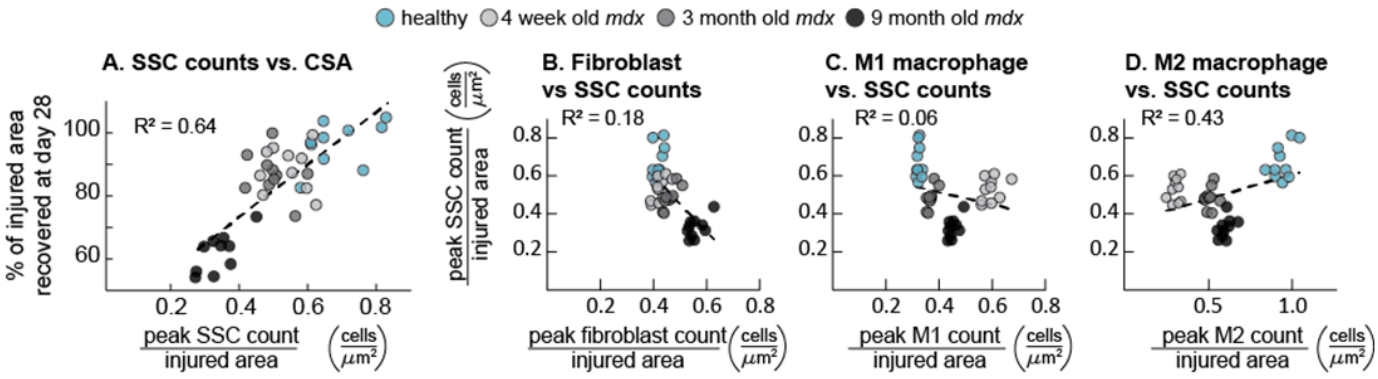

Figure 3.8. Peak SSC agent counts correlate with percent of injured muscle area recovered by day 28. Peak SSC agent counts from the healthy and *mdx* simulations, normalized by area of injury, correlate with the percent of injured muscle area recovered 28 days post injury (A). Percent of injured muscle area recovered is calculated as the (final fiber CSA – fiber CSA following injury)/area of the injury. Data points represent model results from individual simulations with n = 10 simulations per group (healthy, 4 week old *mdx*, 3 month old *mdx*, 9 month old *mdx*). Peak SSC agent counts are poorly correlated with fibroblast, M1 macrophage, and M2 macrophage agent counts (B, C, D).

3.5 Discussion

The goal of this study was to synthesize the available literature to develop a computational model that predicts muscle regeneration following injury based on the autonomous behaviors of skeletal muscle cells, fibroblasts, SSCs, and inflammatory cells. By

incorporating literature-derived rules from over 100 sources, we were able to capture behaviors from a wide breadth of experimental studies. We created a model that is sensitive to a broad range of parameters, yet able to simulate regeneration dynamics that are not explicitly defined in the model. We then used the model to probe disease mechanisms in insolation and within our models of the *mdx* mouse. The simulation results provided insight into the drivers of impaired regeneration in *mdx* muscle.

The simulations of healthy and *mdx* mice revealed that the percent of injured muscle recovered by day 28 is dependent on the peak number of SSC agents following injury (Fig 3.8A). In our healthy and *mdx* models with near full CSA recovery 28 days post injury, (healthy, 4 week *mdx*, and 3 month *mdx*), the peak number of SSC agents was directly correlated with the extent of initial damage, where higher levels of initial damage led to higher numbers of SSC agents (Fig 3.7B). Comparatively, in the 9 month *mdx* mouse with impaired regeneration, the peak SSC agent counts were suppressed relative to the initial damage. Since, in our model, SSCs are the primary cells responsible for repair and maintenance of skeletal muscle, it is not surprising that regeneration would correlate with SSC counts. However, it is important to note that we did not explicitly alter the SSC agent counts in our different models of *mdx* mice. Rather, the pathological differences in SSC agent counts during regeneration were an emergent model prediction driven by other microenvironmental factors. Our model analyses predicted that fibroblast and M2 macrophage agents influenced peak SSC counts, but no single model parameter was able to predict the differences in SSC populations that ultimately led to impaired regeneration. Since SSC counts have been implicated in DMD and used as therapeutic targets (135), our model suggests that it may be beneficial to target an upstream microenvironmental factor driving pathological differences in SSCs.

The model simulations also revealed that the cellular dynamics driving regeneration are time dependent, and that perturbing disease mechanisms often leads to temporally conflicting

regeneration results. For example, reducing the number of macrophage or fibroblast agents initially increased fiber CSA, but ultimately lead to impaired regeneration at the end of the 28 day simulation. Since these time-dependent cell types are often therapeutic targets, it is critical to understand the temporal variations that may occur following experimental perturbations. Current experimental techniques make continuous monitoring of the cellular and regenerative environment very difficult; therefore, computational modeling should be used to understand the temporal complexities and adequately define experimental time points to capture those dynamics.

The *mdx* simulation results compared favorably with the available published literature. Both our 3 month old *mdx* mouse simulation (Fig 3.7A) and comparable literature showed near-full CSA recovery by day 21 (123). The 4 week old *mdx* mouse simulation had 2.7 (Fig 3.7B) and 2.4 (Fig 3.7C) fold increases in SSC and differentiated SSC agents. Comparatively, a published experiment for the *mdx* diaphragm, a skeletal muscle that represents a more severe phenotype than the lower limb muscle in the model, showed similar increases in SSCs (116). The 4 week old *mdx* mouse simulation predicted a 4.8 fold increase in total macrophage agents, relative to healthy controls (Fig 3.7E and 3.7F), whereas an experimental study similarly showed a 4.5 fold increase in total macrophages between these groups (166). Additionally, the predictions from our healthy muscle model perturbations were similar to experimental results in the literature (Fig. 3.6). However, it is important to note that, while we aimed to include the most representative studies available in the literature, the perturbation analysis does not include the results of all studies.

It is important to consider the limitations of our model. In developing the healthy model, we focused on the complex dynamics of a subset of cells (particularly the SSCs and fibroblasts), rather than aiming to recapitulate all aspects of regeneration. As a result, some aspects of regeneration, such as additional cell types, excitation-contraction uncoupling, neuromuscular

junction changes, cytoskeletal disruption, myonuclei, and microvascular network, were not included. Therefore, we can only draw conclusions from perturbations of our modeled cell types. Further, we recapitulated the impaired regeneration in *mdx* mice by altering specific parameters in our healthy model. We modified parameters to represent the key differences between healthy and mdx cell behaviors, such as the increased cytotoxicity of macrophages, or increased fibroblast numbers. For the un-altered parameters, we assumed that the cell behaviors (Table 3.1 and 3.2), and the tuned model parameters (Table 3.3) remained constant. There were sufficient data to prescribe the altered input conditions; however, there was limited time-course data available to verify many of our *mdx* simulation predictions. This highlights the paucity of time course regeneration data in *mdx* mice, and future experiments could be used to verify the assumptions in our *mdx* model.

We originally tuned our models to Tcf4+ fibroblast and Pax7+ SSC counts. However, many rules were defined based on studies using different markers, potentially representing different cell phenotypes, such as fibro-adipogenic cells (FAPs) (72, 86). To address this, the agents in our model do not represent a marker for a specific cell type, such as Tcf4+ fibroblasts or Pax7+ SSCs. Rather, the agents represent a spectrum of phenotypes for the primary cell types. Based on agent parameters (e.g. cell cycle state, activation, or myogenic commitment), we can determine which population of agents in the model would be identified by experimental markers. We then use these agent populations to compare our model predictions to the respective published literature.

It is important to address the differences between muscle repair and regeneration, as well as the role of different injury mechanisms. We used published measurements of eccentric contractions to define our *mdx* model initial damage parameters to incorporate differences in damage susceptibility between *mdx* and healthy mice. However, experiments have shown that a significant portion of the force loss following eccentric contraction injuries can recover without

SSCs (128) (e.g. contributions from excitation-contraction uncoupling), and these contributions may be different between healthy and *mdx* mice. Our model does not include contributions from these factors, so we addressed this challenge into two ways. First, we used supra-physiologic strains from the literature to ensure there was sufficient damage to the contractile muscle tissue that required SSC regeneration. Lower strains would alter the injury mechanism to include a greater contribution from the factors that we have not included in our model. Second, we decreased the input damage parameter, while maintaining the ratio of damage between groups, since it has been shown that 50% of the force-deficit can be attributed to factors that do not require SSCs for regeneration (128). To address the uncertainty in this damage parameter we ran simulations at varying levels of initial damage (Fig 3.4A, 3.4B) and the model predicted that the magnitude of the regenerative response scaled with the input damage level. For instance, the peak SSCs counts increased with increasing levels of initial damage, but the time to recovery (in healthy muscle) was relatively conserved. This result supports our assumption that the most important aspect of the input damage parameter in our model was the ratio of damage between groups. Further, in our mdx simulation analyses we excluded the contribution of the initial damage parameter by normalizing the results (Fig 3.8) by the area of damage. From these results we drew our conclusions about the role of the SSCs.

Finally, to track recovery in our model, we used measurements of fiber CSA. However, experiments have shown that CSA does not perfectly predict muscle function, particularly between *mdx* and healthy mice where pseudohypertrophy contributes to increased muscle CSA, without subsequent increases in contractile fiber tissue (139). To address these factors, we measured CSA by summing the fiber elements and did not include ECM elements to reduce the contribution of pseudohypertrophic increases in CSA in the *mdx* models. Additionally, we excluded factors that contribute to force-deficits but do not require regeneration of muscle tissue to recover the force (e.g. excitation-contraction uncoupling and protein repair mechanisms as explained above). Therefore, the force deficits from eccentric contractions shown in the

literature are greater than the fiber CSA deficit that we have modeled, particularly in the first 24 hours following injury (e.g., Fig. 3.3) (123). Despite the fact that CSA does not perfectly predict muscle function, we believe our model is useful for comparing the effect of disease mechanisms on muscle regeneration between our simulation groups.

Future work aims to extend the model to represent more severe animal models and DMD patients, as well as incorporating chronic, long-term damage to the muscle. These models will be used for *in silico* testing to probe the effects of a wide range of potential therapies, such as therapies targeting upstream microenvironmental factors to alter SSC counts. The simulations will then be used to design insightful experiments to test those predictions. Ultimately, this new ABM recapitulated muscle regeneration following injury and suggested new hypotheses regarding the influence of the microenvironment on SSC behaviors and regeneration. The simulations revealed that regeneration is dependent on SSC counts, and that pathological differences in SSC counts may be driven by microenvironment factors. Broadly, this study also demonstrated the utility of computational models for providing insight into therapy development and experimental design for complex, multifaceted disease.

Chapter 4

In silico and *in vivo* experiments reveal that area fraction of collagen alone does not predict the regenerative capacity of *mdx* muscle

Acknowledgements: Brian Jones, Emily Miller, Elnaz Ghajar-Rahimi, Kyle Martin, Shayn Peirce, Silvia Blemker

"At some point, everything's going to go south on you... everything's going to go south and you're going to say, this is it. This is how I end. Now you can either accept that, or you can get to work. That's all it is. You just begin. You do the math. You solve one problem... and you solve the next one... and then the next. And if you solve enough problems, you get to come home"

– Mark Watney, The Martian

4.1 Abstract

Duchenne muscular dystrophy (DMD) is a fatal muscle wasting disease caused by the lack of the dystrophin protein. Fibrosis has been implicated in DMD, and strategies to reduce fibrosis are potential therapeutic targets. However, the mechanisms that cause fibrosis to impair regeneration in DMD are not fully understood. The goals of this study were to (1) test the hypothesis that fibrosis impairs regeneration, and (2) simulate the experiments *in silico* to test the model predictions and gain insight into the results. The study included WT, *mdx*, and *mdx*+TGFβ mice. TGFβ injections increased fibrosis in the *mdx* mouse, as measured by the increased area fraction of collagen. However, the injections decreased the passive stiffness of the TGFβ injected muscle, relative to the *mdx* muscle. During recovery from injury, there was no difference in fiber CSA (metric for muscle regeneration) between the three groups. This showed that increases in area fraction alone are not sufficient to impair regeneration. A computational model was used to simulate the experiments and the model similarly predicted no differences in regeneration between the groups. To investigate how differences in the fibrotic microenvironment would affect regeneration, the model parameters were altered to represent an increased ECM stiffness in the TGFβ mice. In contrast to the model predictions with a less stiff ECM network, these simulations predicted impaired regeneration and decreased peak SSC counts. The results of our experiment and computational analyses lead us to conclude that factors other than area fraction of collagen alone affect the passive properties and regenerative capacity of the muscle.

4.2 Introduction

Duchenne muscular dystrophy (DMD) is progressive muscle wasting disease affecting 1 in 3500 boys (26). It is caused by the lack of the dystrophin protein at the muscle fiber

membrane (68, 80, 108). Without dystrophin the muscle is more susceptible to contraction-induced damage, resulting in constant cycles of degeneration and regeneration (17, 52). This repetitive damage, coupled with altered cell signaling processes, leads to fibrosis and chronic inflammation (118, 132, 168). Despite extensive experimental research, there remains no cure for DMD. While therapies to replace the missing dystrophin protein are promising, there are many barriers to effective treatments (81, 104). Therefore, it is remains critical to develop effective therapies to treat symptoms of DMD.

Fibrosis, the excessive accumulation of collagen, impairs healthy muscle function in patients with DMD; therefore it is a promising potential target for therapies (187). In murine models, it has been shown that therapies that reduce fibrosis can dampen disease progression and increase the potential for therapeutics to effectively target the damaged muscle (1, 9, 109, 157). However, the mechanisms underlying the role of fibrosis in muscle regeneration and disease progression in DMD remain unclear, particularly because of the limited fibrosis in the most commonly used experimental model for DMD, the *mdx* mouse (118). The *mdx* mouse does not develop significant fibrosis in the lower limb muscles until much later in the disease.

To investigate how disease mechanisms, such as fibrosis, affect muscle regeneration, previous work in our lab has developed an agent-based model (ABM) of dystrophic muscle (Chapter 3). An ABM is a computational tool for modeling the actions of autonomous agents (cells), to analyze their effect on the system as a whole (muscle regeneration) (98, 99). The cells in the model include satellite stem cells (SSCs), fibroblasts, macrophages, and neutrophils. In model simulations of regeneration following injury in healthy and *mdx* mice at three ages (4 week old, 3 month old, and 9 month old +), the model predicted that regeneration (measured by fiber CSA) was only decreased in the 9 month+ *mdx* mouse. In this group, the peak number of SSCs were suppressed following injury, yet no individual factor in the model was able to predict the pathological decreases in SSCs that lead to impaired regeneration. One of the key

differences between the *mdx* models at the different ages was the increased fibrosis in the 9 month+ *mdx* mouse. From this, we predicted that the pro-fibrotic microenvironment at the later stages of disease impaired regeneration.

The goals of this study were to (1) experimentally test our hypothesis that fibrosis impairs regeneration in *mdx* mice, and (2) simulate the experiment *in silico* to test our models predictive capability and gain insight into our experimental results. We utilized a published experimental method for inducing fibrosis in *mdx* mice, injured the muscle, and measured muscle fiber CSA and cell counts during regeneration. Then we simulated the experiments *in silico* to compare our model predictions with the experimental results. Finally, the model was used to investigate how different fibrotic metrics would affect muscle regeneration.

4.3 Methods

4.3.1 Animals, TGFβ injections

All animal experiments were approved by the University of Virginia animal use and ethics committee. Three month old C57Bl/6J (referred to here as WT), and dystrophic C57Bl/10scsn-*mdx* male mice (Jackson Laboratories) were used in experiments. There were 4-5 animals per group per time point.

TGFβ mice were injected with 50 ng TGFβ (recombinant human TGFB1; R&D Systems, Minneapolis, MN, USA) in 50 µL PBS solution in the center of the muscle belly of the right TA (118). Sham injected mice were injected with 50 µL of PBS. 12 week old mice were injected two times (once per week), with the first injection 2 weeks prior to injury. Based on results from others that showed no effect of TGFβ in WT mice, WT-injected mice were not included in the study (118).

4.3.2 Injury method

To experimentally study regeneration we used a freeze injury method as described by others (154, 174). This is not a physiologic method representative of damage typically seen in dystrophic muscle, however it was utilized for a number of reasons. First, in order to study the effects on regeneration we had to induce a significant injury to the muscle. As described in previous chapters, an acute injury is a commonly utilized method for investigating the regenerative response in dystrophic muscle. Due to the extensive literature using this method, the ABM (Chapter 3) modeled an acute injury and the subsequent regeneration. A number of acute injury methods have been utilized in the literature, including cardiotoxins, freeze injuries, and eccentric contractions (64).

To test the regenerative response, we needed to induce a similar injury across all of the groups. Eccentric contractions, while physiologic, lead to differential levels of damage based on the disease state and the stiffness of the fibrosis (Chapter 2). Further, much of the force loss measured in eccentric contractions result from mechanisms such as excitation-contraction uncoupling that do not require regeneration to regain the force (123). Therefore a significant portion of the force-loss measured in eccentric contractions would not require SSCs for regeneration. Finally, the damage mechanisms are thought to be different between the different animal models, making it difficult to compare the resulting regenerative responses between the groups. Therefore, we chose to use a freeze injury method.

The freeze injury was completed as described by others (154, 174). Briefly, an incision was made through the skin over the TA muscle. A steel probe cooled with dry ice (for at least 30 minutes prior to injury) was held on the muscle belly of the TA muscle for 10 seconds. The incision was closed with silk suture. Mice were sacrificed at the defined time points by carbon

dioxide asphyxiation and muscles were immediately harvested, weighed, and snap frozen for immunohistochemistry and histological analysis.

4.3.2 Passive mechanical testing

For muscles undergoing passive mechanical testing, muscles were rapidly dissected and placed in 30mM 2,3-butanedione monoxime (BDM solution) to prevent cross bridge binding. The proximal attachment was kept intact and the muscle was secured with a pin through the tibia with a custom 3d printed attachment. The distal tendon was released and secured to a second custom 3d printed attachment. The muscles were placed in a bath in a biaxial testing apparatus (CellScale, Waterloo, Ontario), using only a single axis for mechanical testing. Muscles were subjected to 20 preconditioning cycles and three increasing ramp-holds of 4%, 6%, and 8% at 1%/second with 300 second hold periods.

4.3.3 Immunohistochemistry and histology

Cryosections (10 μm thick) of cross-sections of mouse muscle were stained with hematoxylin and eosin (H&E) staining and picrosirius red staining. Quantification of collagen content was completed by thresholding five 20x images and summing the number of red pixels. For immunohistochemistry, cryosections were fixed in 4% PFA, permeabilized with 0.3% triton as needed, blocked with 10% serum, and incubated with the following primary antibodies: PDGFR-α (1:200, R&D systems), CD68 (1:300, Invitrogen), CD206(1:300, ABCAM), Laminin-2-α (1:175, Sigma-Aldrich). The following secondary antibodies were incubated for 1 hour, followed by DAPI: Alexa fluor conjugated goat anti-rat 546, donkey anti-rabbit 647. CD68+/CD206- macrophages are indicative of pro-inflammatory macrophages, while CD206+ macrophages are indicative of anti-inflammatory macrophages (159). PDGFR-α+ cells are

representative of non-myogenic fibro-adipogenic progenitor cells (30, 162). Cells were counted manually in imageJ or through custom Matlab code to quantify the number of cells that were double positive for the respective marker and DAPI. Fiber CSA was calculated with custom Matlab code that quantified each fiber based on perimeters defined with Laminin-2-α antibody staining.

4.3.4 ABM *in silico* experiments

A previously developed computational model was used to simulate the experiment for the three study groups: WT (3 month old), *mdx* (3 month old), *mdx*+ TGFβ (3 month old). The model is described in detail previously (Chapter 3). Briefly, the ABM predicted muscle regeneration following injury from the autonomous actions of the different agents in the model. The ABM was built in Repast, a java-based modeling platform (Argonne National Laboratory, Lemont, IL, USA). The model spatially represented a cross-section of a mouse lower limb muscle, consisting of approximately 50 muscle fibers. Simulations represented an acute muscle injury followed by regeneration over 28 days with a 1 hour time step. The agents in the model included SSCs, fibroblasts, macrophages, neutrophils, muscle fibers, ECM, and necrotic elements. The key model outputs included the cross-sectional area (CSA) of the muscle fibers and time-varying counts for each cell type in the model. Muscle fiber CSA was determined in two ways. First, by summing all the healthy muscle fiber elements in the simulation, normalized by the number of healthy muscle fiber elements prior to injury. Second, by calculating the CSA of each individual fiber, normalized by the average fiber CSA across the simulation. This second metric provides insight into the range of damage and regeneration across individual fibers. At each time step, agents individually followed a probability-based decision tree to determine its action, based on literature defined-rules, (Chapter 3, Table 3.1 and Table 3.2).

The baseline experimental measurements and uninjured histology informed the baseline input parameters for the computational model, including the number of resident macrophages and fibroblasts. The histology was used to define the average fiber CSA, distribution of fiber sizes, and area fraction of collagen for the groups (*mdx*, *mdx*+TGFβ, WT). For the injury and regeneration simulations, an input damage parameter defined the percent of muscle fiber elements that were replaced with necrotic elements. Elements within each individual fiber were stochastically replaced with necrotic elements, such that the damage per fiber was between 0 and 100% for a given simulation. However, the total percent of necrotic elements in the muscle was equal to the input damage parameter. To represent the TGFβ injections, the baseline level of active TGFβ was increased 1.4 fold, based on literature that has shown increases in TGFβ in the TA muscle following two weeks of injections (118).

4.3.5 Statistics

Comparisons between groups were performed using one-way ANOVAs in Matlab (The Mathworks Inc., Natick MA). P-values = .01 unless otherwise noted in the figure. All model simulation were run 10 times to sample the stochastic nature of the model, and results are shown as 95% confidence intervals.

4.4 Results

4.4.1 Baseline experimental measurements following TGFβ injections

The percentage of Sirius red+ connective tissue was increased in TGFβ injected muscle compared with *mdx* muscle and WT controls prior to injury (Fig 4.1A). Mechanical testing

showed that the *mdx* muscles were stiffer than WT controls; however, TGFβ injections reduced the passive stiffness of the TA muscle, similar to WT controls (Fig 4.1B). TGFβ injections did not significantly alter baseline cell counts for PDGFRα+ fibroblasts, CD68+/CD206- macrophages, or CD206+ macrophages vs *mdx* mice (Fig 4.1 D, E). However, these baseline cell counts were increased in the TA of both *mdx* mice compared to WT controls.

4.4.2 WT and *mdx* mice exhibit a robust regenerative response following injury

Muscle fiber CSA was calculated in cross-sections of muscle prior to and following injury, this was used as a marker for muscle regeneration. Following injury, the muscle fiber CSA was reduced at day 5 relative to uninjured muscle at day 0 (Figure 4.2A). There was no significant difference at any of the time points between the three groups. By day 28, the muscle fiber CSA was not significantly different than the uninjured groups, signifying full regeneration. The area fraction of collagen, measured by the percentage of Sirius red+ pixels was significantly elevated in *mdx*+TGFβ baseline muscles; however, following injury there was no significant difference between the *mdx* and *mdx*+TGFβ groups (Figure 4.2B). During recovery, the area fraction of collagen was reduced in WT muscle, compared to *mdx*+TGFβ muscle, at day 2-14, but these groups were not different by day 28. The distribution of fiber sizes, in both uninjured groups and 28 days post injury are qualitatively skewed towards smaller fibers in *mdx* and *mdx*+TGFβ groups compared to WT controls with a more normal distribution (Fig 4.3).

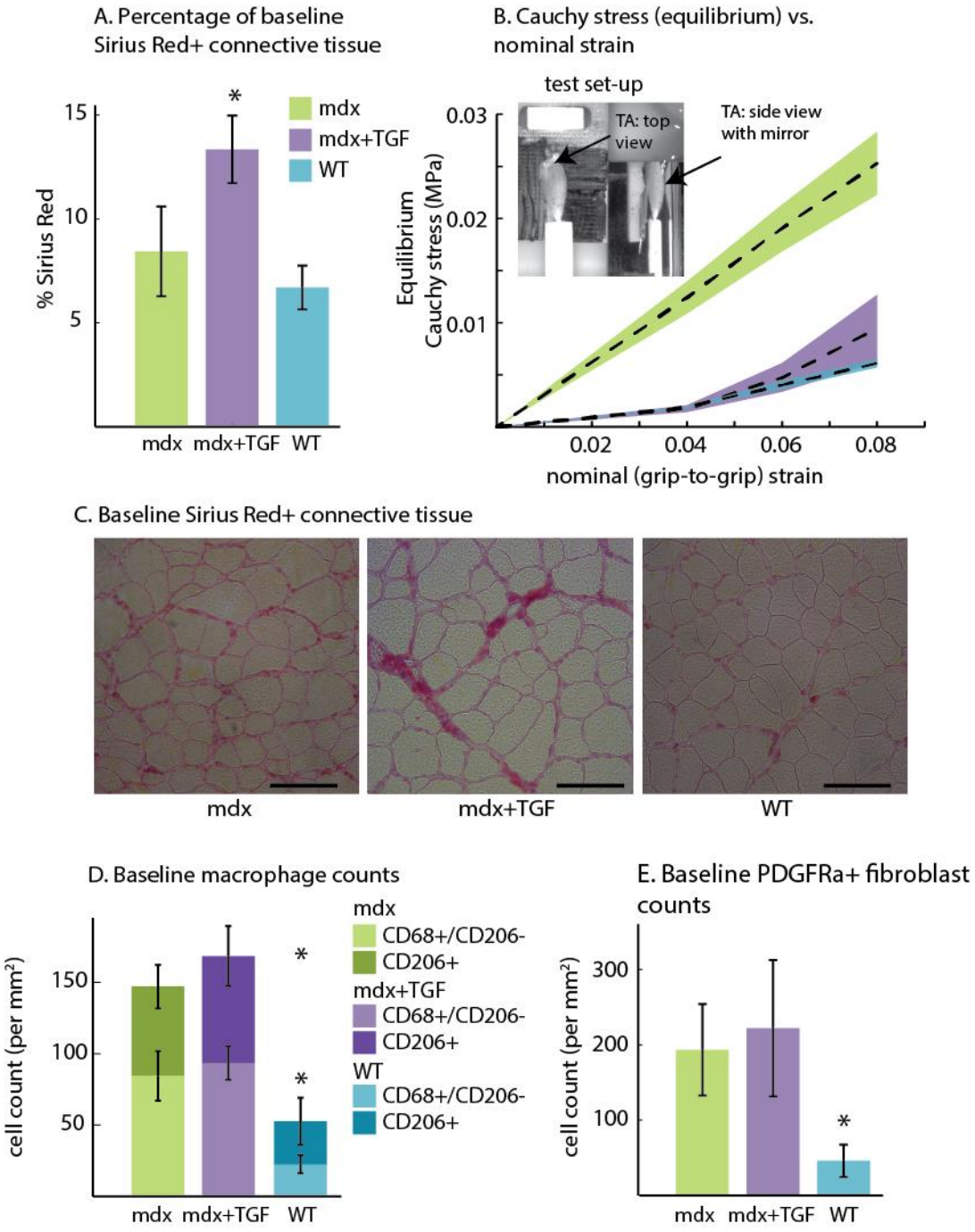

Figure 4.1: The percentage of red pixels with Sirius red+ connective tissue was increased in TGFβ injected mice compared to WT controls and *mdx* mice (A). The passive stiffness of the *mdx* muscle was decreased following TGFβ injections, similar to WT controls (B). Representative images of Sirius red staining in *mdx*, TGFβ -injected, and WT mice (C). Baseline CD206+ and CD68+/CD206- macrophages (D) and PDGFRa+ fibroblasts (E) were increased in *mdx* and TGFβ -injected *mdx* mice compared to WT controls. *p = .01 and n = 4-5 per group.

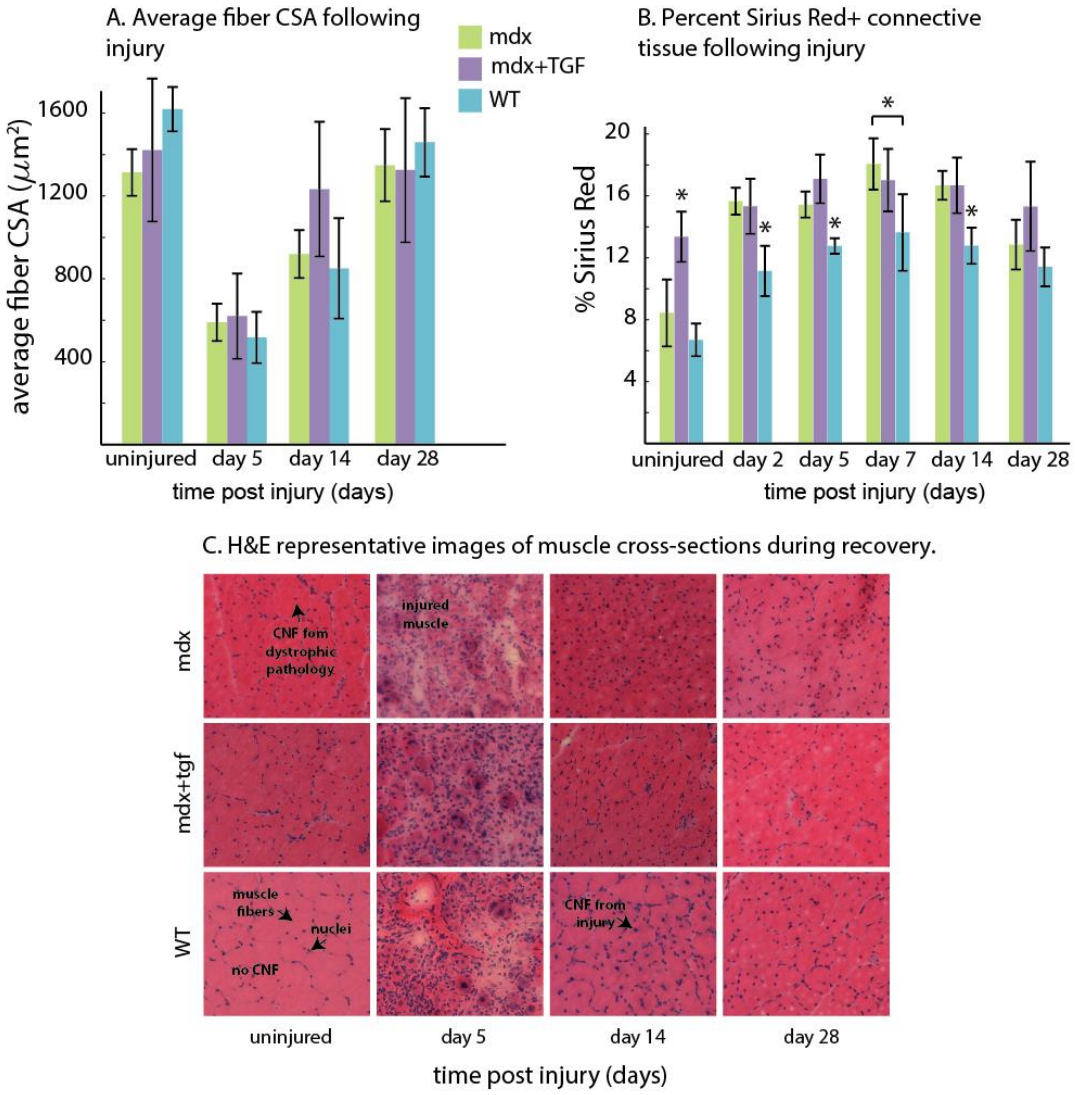

Figure 4.2: The muscle fiber CSA was decreased 5 days post injury, but there was no significant difference between the three groups at any of the time points (A). The percent of Sirius red+ connective tissue was elevated in *mdx*+TGFβ prior to injury (B). Following injury the WT red pixel percentage was decreased at day 2-14 compared to *mdx* mice. H&E staining shows the histological changes in muscle cross-sections prior to and during muscle recovery from injury (C). *p = .01 and n = 4-5 per group.

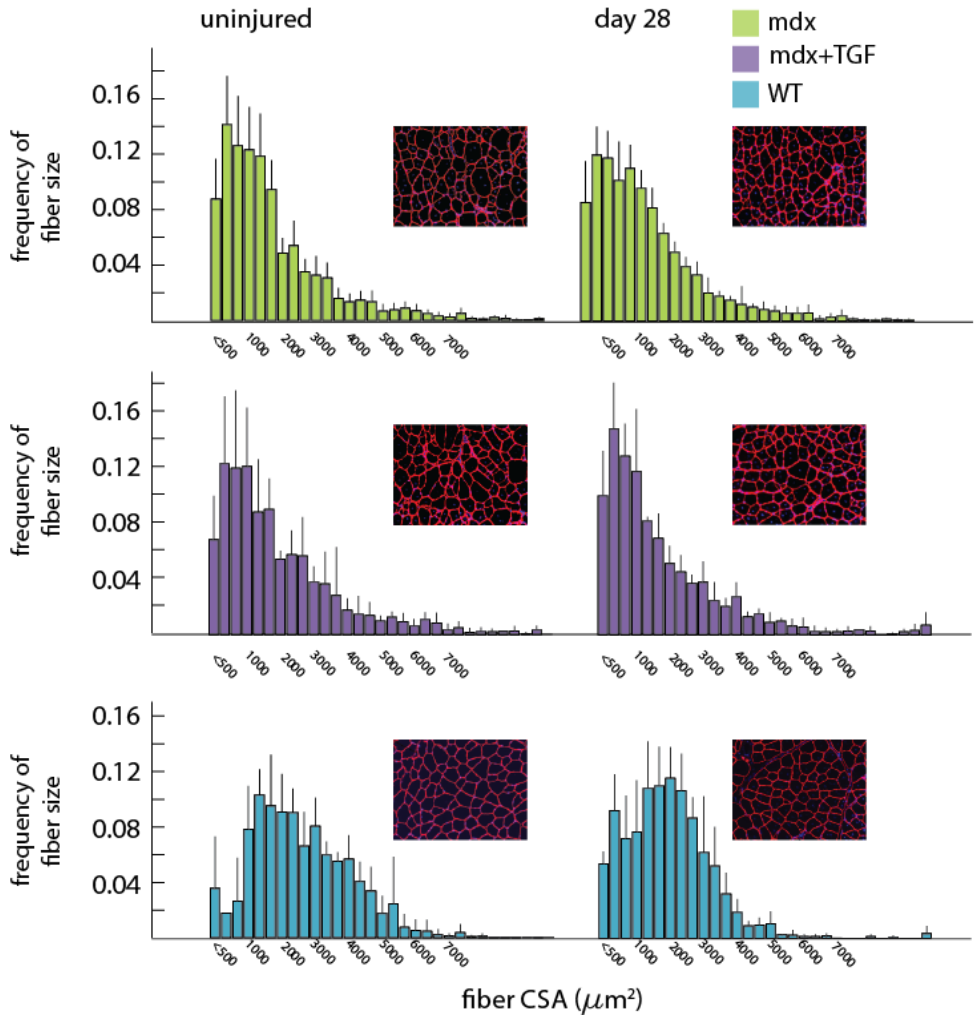

Figure 4.3. The distribution of fiber sizes prior to injury in uninjured mice and 28 days post injury qualitatively illustrates the skewed distribution of fiber sizes towards smaller fibers in *mdx* and *mdx*+TGFβ mice.

Prior to injury, the number of PDGFRα+ fibroblasts were significantly elevated in both *mdx* groups (Fig 4.4A). However, following injury the PDGFRα+ fibroblast counts were similar between groups until day 7 in which the counts in the WT mouse were decreased relative to *mdx*+TGFβ mice. Prior to injury, the CD68+/206- and CD206+ macrophages were increased in both *mdx* groups, compared to WT mice (Fig 4B,C). Following injury, there was no difference in cell counts until day 7 when the CD68+/206- cell counts were reduced in the WT mouse and CD206+ cell counts were increased in WT mice compared to *mdx*+TGFβ mice.

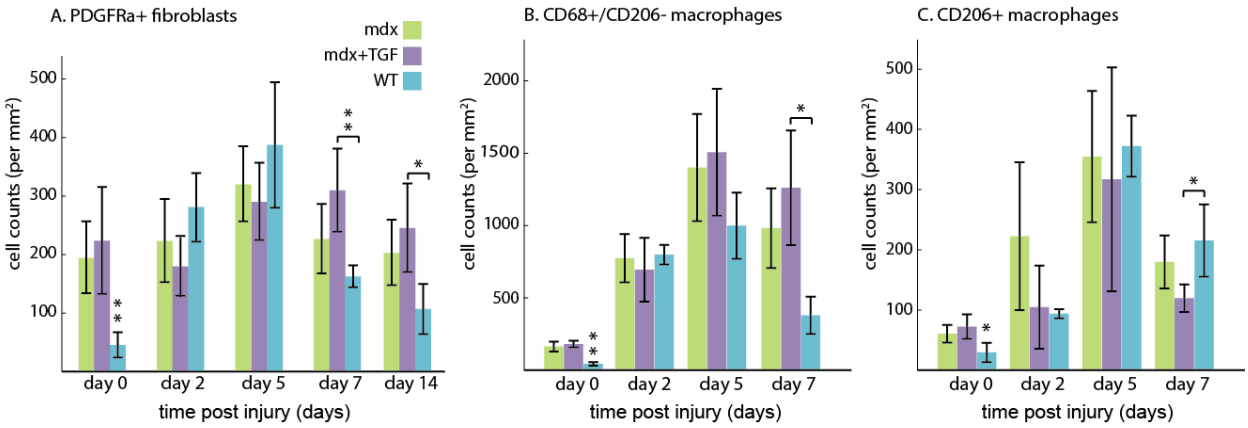

Figure 4.4: The number of PDGFRα+ fibroblasts were significantly reduced in WT uninjured mice (A). Following injury, the groups were not different until day 7 and 14, where counts in the WT mouse were decreased relative to *mdx*+TGFβ mice. CD68+/206- and CD206+ macrophages in uninjured WT mice were reduced compared to both *mdx* mice groups (B,C). Following injury, the groups were not different until day 7 when the CD68+/206- cell counts were reduced in the WT mouse and CD206+ cell counts were increased in WT mice compared to *mdx*+TGFβ mice.

4.4.2. *In silico* experiment predictions

The ABM of muscle injury and regeneration was used to simulate the experiments. Input parameters for the three groups were defined in the previous model (Chapter 3), or based on experimental measurements of uninjured muscles in this study (Fig 4.1). The input damage parameter was set to 55% based on the decreased fiber CSA measurements at day 5. The baseline number of resident macrophages and fibroblasts in both *mdx* groups were increased 2x and 3x from WT controls. Histology from the three groups was used to prescribe the initial fiber size, fiber size distribution, and area fraction of ECM. To account for complex differences in ECM structure, the ECM in the model is defined by both the area fraction of ECM elements, and a collagen density parameter for each ECM element. This collagen density parameter represents the total amount of collagen divided by the area fraction of ECM. We assume that the stiffness of the muscle positively correlates with the collagen density parameter, and that the collagen density parameter increases with DMD disease progression (5, 63, 103, 118). Based on these studies, the collagen density parameter was set at 1.0 for healthy WT mice, and 1.5 for

mdx mice. For the *mdx*+TGFβ muscles, the passive stiffness was decreased. We assumed that this decreased stiffness was a result of decreased stiffness of the ECM; therefore, we reduced the collagen density parameter in the model to 1.0 to match WT values. However, the area fraction of collagen remained elevated according to histology.

The average muscle fiber CSA, relative to the uninjured average fiber CSA, was used as the model metric for regeneration. In the simulations, the fiber CSA was reduced at day 5 and returned to the original size by day 28 (Fig 4.5A), with no significant differences between the groups at these times. The model fibroblast counts peaked and remained elevated from day 5-14 for the *mdx* and *mdx*+TGFβ simulation groups. In the WT simulation group, the model fibroblast counts peaked around day 5, and remained elevated until day 8 when they returned to basal levels. At day 14 the fibroblast counts were reduced in the WT model compared to *mdx* and *mdx*+TGFβ groups.

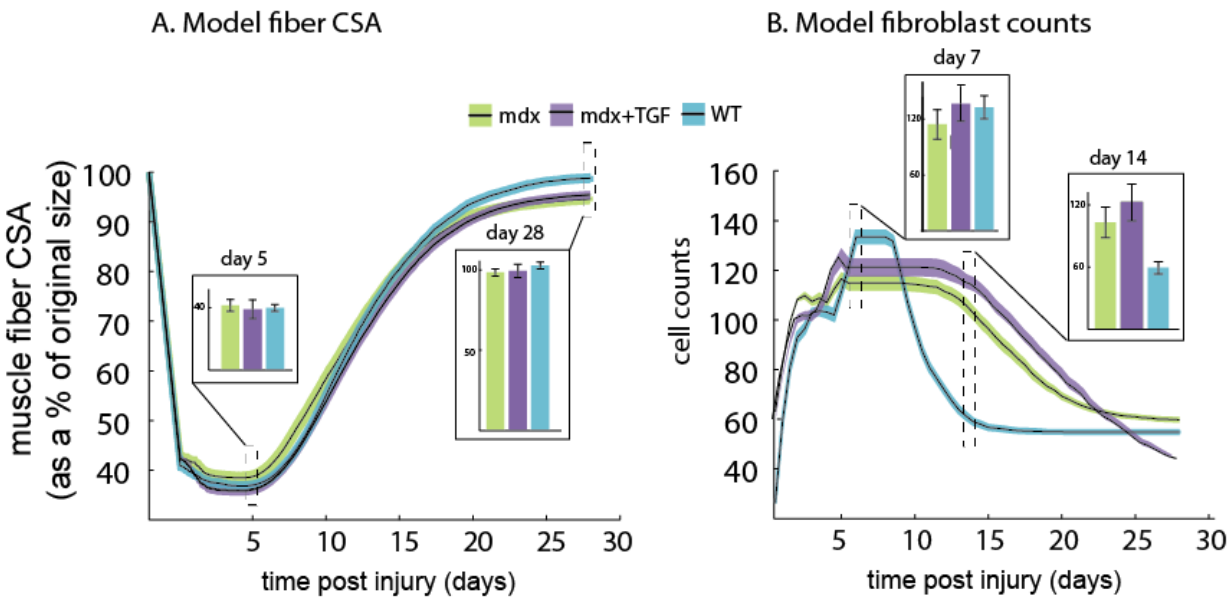

Figure 4.5. Simulation predictions for the *in silico* experiment with *mdx*, *mdx*+TGFβ, and WT mice. The model predicted that the fiber CSA would not be different for the three groups at all time points (A). The fibroblast counts peaked between day 5-10 in the *mdx* and *mdx*+TGFβ groups, but began to decrease at day 8 in the WT group (B).

The model predictions of fiber CSA were within one standard deviation of the experimental fiber CSA measurements for all groups and time points except the WT mouse at day 14 (Fig 4.6). The computational model also included a range of fiber CSAs based on representative histology from each group (Fig 4.6B). Qualitatively, the distributions were skewed towards smaller fibers in the *mdx* and *mdx*+TGFβ models, compared to the WT model both prior to injury and 28 days following injury. As explained in the methods section, the amount of damage is stochastically prescribed to each fiber, such that each fiber has a varying level of initial damage, but the total sum of the damage is equal to the input damage parameter. Due to this stochasticity, and the variability in fiber size (Fig 4.6B), there is a wide range of average fiber CSAs across the simulations. To represent this, Fig 4.6A includes the standard deviation from all the individual fibers (normalized by the average uninjured fiber CSA).

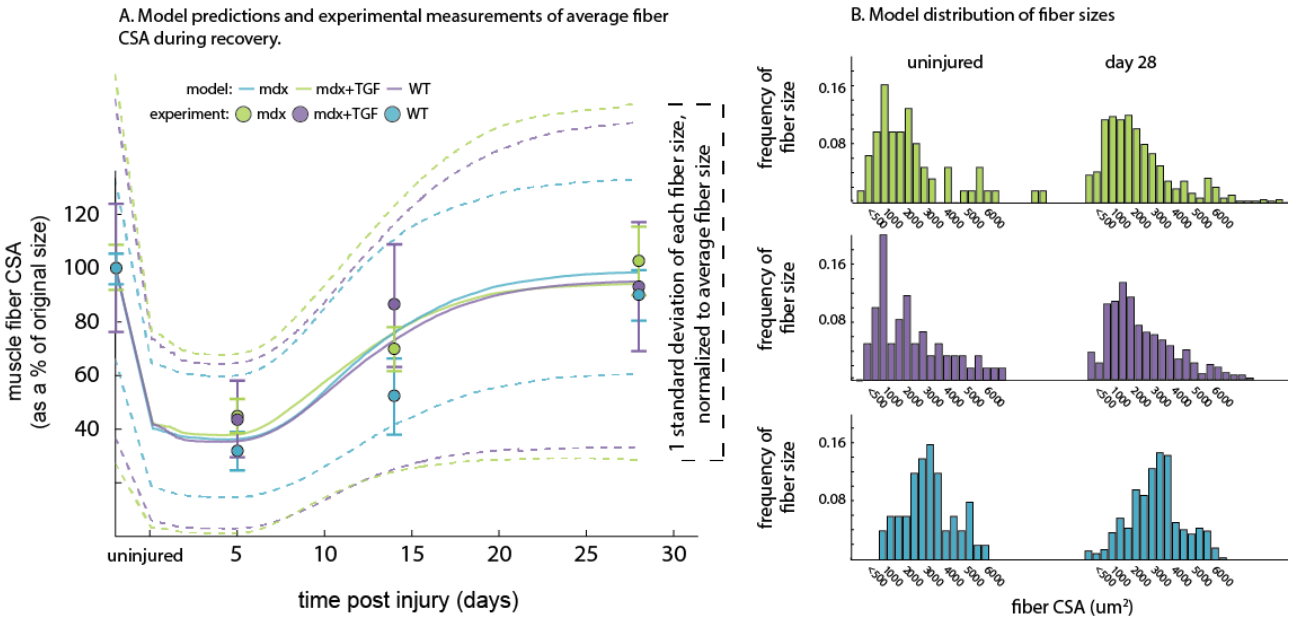

Figure 4.6. The average and standard deviation of each individual fiber CSA, normalized by the average uninjured fiber CSA, across all fibers in each group (n = 500-600 fibers/group) (A). Qualitatively, the distribution of fiber CSAs is skewed to the smaller fiber sizes in the *mdx* and *mdx*+TGFβ groups compared to WT controls.

Since the baseline experimental measurements of uninjured TAs showed that the stiffness of the TA in *mdx*+TGFβ muscle was decreased, the collagen density parameter was decreased in the simulation, as described above. However, in contrast to our results, it is expected that fibrosis which arises from aging in dystrophic muscle would increase the stiffness of the muscle (63). To probe how this difference would affect our predictions, we increased the collagen density parameter and ran the same set of simulations (Fig 4.7). The model predicted that with the increased collagen density parameter normalized fiber CSA would be reduced from 95% to 84%. Further, peak SSC counts would be decreased, but there would not be a significant decrease in the number of fibroblasts following injury.

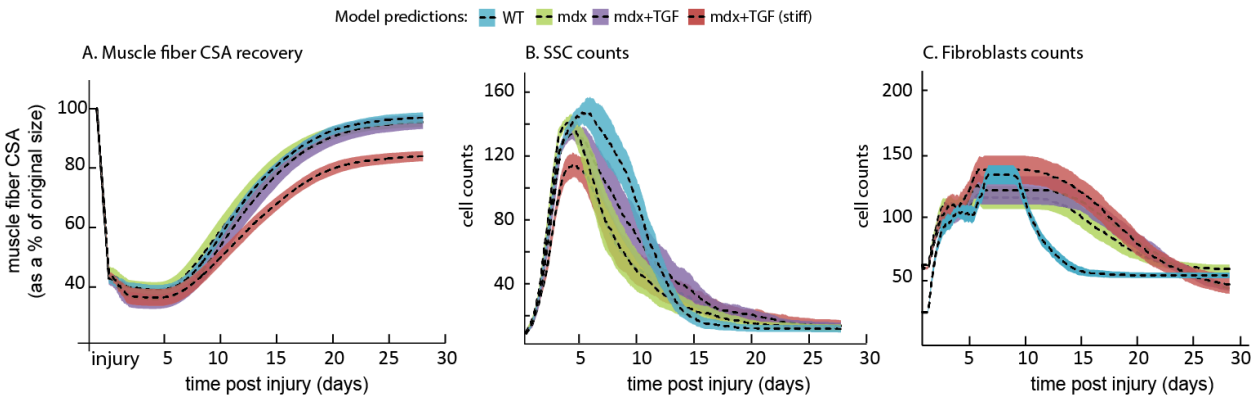

Figure 4.7. Model predicted that if the collagen density is increased in the *mdx*+TGFβ model (*mdx*+TGFβ-stiff), then fiber CSA would be decreased at day 28 (A), SSC counts would be decreased (B), but there would be no significant effect on fibroblast counts (C).

4.5 Discussion

The goal of this study was to test our hypothesis that increased fibrosis in the *mdx* mouse would impair regeneration. TGFβ injections were utilized to induce fibrosis in the muscle, which resulted in an increase in the area of collagen but a decrease in the stiffness of the muscle. While there were differences in macrophages and fibroblasts between our WT and *mdx*

muscles, our experimental measurements of fiber CSA showed no difference in regeneration in the three groups. To understand our experimental results, we simulated this experiment *in silico* with a previously published ABM of muscle injury and regeneration and similarly predicted no significant difference in regeneration. However, by altering input parameters to represent a stiff fibrotic microenvironment, our model predicted that peak SSC counts would be decreased and regeneration would be impaired.

We utilized a published experimental model for inducing fibrosis in skeletal muscle with TGFβ injections (22, 89, 118). TGFβ is potent stimulator of collagen production in fibroblasts, and intramuscular injections of TGFβ have been shown to increase signaling of fibrotic target genes such as CTGF and TIMP-1 (118, 137, 188). In agreement with these results, the TGFβ injections in this study, increased the area fraction of ECM. However, the passive stiffness of the muscle was reduced. In skeletal muscle, the passive stiffness is thought to be largely dependent on the ECM collagen (56, 106, 170), suggesting that the reduced stiffness following TGFβ injections was a consequence of the reduced stiffness of the ECM. Interestingly, across our three groups, the passive stiffness of the muscle was not correlated with the area fraction of collagen. Similarly, a study analyzing the passive properties of different *mdx* skeletal muscles found no correlation between the collagen area fraction (which was shown to strongly correlate with collagen content) and the passive stiffness of the muscle (148). From these results, we hypothesize that other factors in this study, such as collagen cross-linking, which is a post-translational modification to the collagen, or density of collagen, determines the passive stiffness of the ECM.

In our injury study, we aimed to analyze how the change in area fraction of collagen would affect regeneration, and found no difference between the *mdx*+TGFβ and *mdx* muscles. However, other studies in the literature have shown that reducing fibrosis improves muscle function (1, 161). This suggests that fibrosis affects regeneration, but that factors other than just

an increase in area fraction of collagen determine this effect. To investigate this we utilized an ABM of muscle injury and regeneration. Our ABM predictions of muscle fiber CSA following injury compared favorably to the experiments and similarly predicted no difference in fiber CSA across the three groups. The model also similarly predicted the timing of fibroblast peaks in the three groups, but it did not predict significant decreases in fibroblast counts until day 9, where they were significantly decreased at day 7 in the experiments. With confidence in the models predictive capability, we altered parameters associated with pathological changes in ECM properties to represent increased collagen density and re-simulated the same set of experiments with the altered input parameters. The model predicted decreased peak SSC counts and impaired regeneration following injury, predominantly due to impaired SSC migration to the site of damage. Similar to the conclusions from the passive mechanical testing, this suggests that the properties of the fibrosis, rather than just the area fraction of collagen, is a critical factor in determining its effect on muscle function and regeneration.

It is important to consider a number of limitations to the study. First, our study utilized TGFβ injection to induce fibrosis. While this lead to increased area fraction of collage, there was also reduced passive stiffness of the injected muscles. With our experimental measurements from this study, we were only able to determine the area fraction of collagen, and we found no correlation between the area fraction and the passive stiffness of the muscle. This is in agreement with results by Smith et al. that found no correlation between collagen content and stiffness. However, other groups have shown correlations between these two parameters (50, 63). We expect that this arises from differences in experimental design. In the work by Smith et al, the collagen content and passive properties were compared between different muscles, while the other studies analyzed progression of fibrotic muscle and scar tissue across time. In this study, collagen area was compared across two different animal models (*mdx* and WT controls). In addition, fibrosis was induced by cytokine injections which likely altered multiple factors

associated with the ECM. In a study describing this method there was a 40% increase in the collagen content, measured through biochemical quantification. However, if the area fraction of collagen increased similarly to our study (60%), then the collagen content per area would be decreased. Further, if the injections stimulated fibroblasts to secrete collagen, then this new ECM network may have both degraded and synthesized new collagen, without sufficient time to form cross-links and increase the collagen packing density. This means that our fibrosis induction method may not be akin to fibrosis seen in aged *mdx* mice or DMD patients. However, this provides a unique opportunity for probing the effect of a specific aspect of fibrosis (area fraction of collagen) on passive properties and muscle regeneration. Ultimately this lead us to conclude that area fraction alone is not a predictor of passive mechanical properties or muscle regeneration.

Another limitation is the use of fiber CSA as the metric for regeneration. Immediately following injury, fiber CSA does not scale well with muscle function (active force) due to neuromuscular changes (123); however for the time points analyzed in this study we believe that fiber CSA is a robust marker of regeneration. Since it is impossible to track muscle fiber CSA over time (all timepoints are terminal), fiber CSA introduces additional variability to the data. To illustrate this, the standard deviation in Figure 4.6A represents the variability in model fiber CSAs when normalized to average fiber CSA of an entire group. This normalization scheme is akin to normalizing average fiber CSA at each time point to the average fiber CSA of an uninjured group in an experiment.

Ultimately the study tested the hypothesis that fibrosis impairs regeneration in dystrophic muscle following injury. The experiments showed that increases in area fraction alone were not sufficient to impair regeneration. Interestingly, this increase in area fraction of collagen also resulted in decreased passive stiffness of the muscle, suggesting that the ECM stiffness was decreased. However, the area fraction of collagen across our three groups did not correlate with

muscle stiffness. We also utilized a computational model of the *mdx* mouse to simulate the experiments and similarly found no decrease in regeneration. Conversely, with an increased collagen density parameter, the model predicted decreased SSC counts and impaired regeneration. The results of our experiment and computational analyses lead us to conclude that factors other than area fraction of collagen affect the passive properties and regenerative capacity of the muscle.

Chapter 5

5.1 Overview

This dissertation was motivated by my desire to understand the role of different disease mechanisms on disease pathology in DMD. In this work, I posit that one of the reasons DMD is so challenging to treat is that DMD is a complex, multifaceted disease, in which multiple mechanisms contribute to the disease pathophysiology. I believe that computational models can help us unravel these complexities to answer a number of critical questions, such as: how does the nature of the fibrosis affect the damage susceptibility and function of the tissue, and how do changes in the microenvironment alter muscle regeneration? We believe the answers to these questions will help us answer our ultimate question: What are the best targets for therapies, and how can we design experiments to test their effectiveness?

From the motivation to develop my original micromechanical models to my final experiments, my dissertation work has had two key themes. The first theme, investigating how disease mechanisms contribute to disease pathology in DMD, was a primary goal defined within each aim. However, the second theme, the role of the ECM in function, damage susceptibility, and regeneration organically emerged at each stage of my research. Originally, I was fascinated by how the ECM, which only comprises 5-10% of the muscle volume fraction, can play such a significant role in force transmission. I was also intrigued by the ongoing debate in the literature about whether the ECM was stiffer or more compliant than the skeletal muscle fibers. I hypothesized that the ECM is more compliant than the fiber in healthy muscle, particularly in shear displacements, and stiffer than the fiber in fibrotic disease. The role of the ECM was paramount in the micromechanical finite element models developed in Chapter 2. We developed models of cross-sections of muscle fascicles to investigate how changes in the

microstructure during DMD affect function and damage susceptibility. The models predicted a trade-off between function and damage susceptibility that was dependent on the relative stiffness of the ECM.

During my literature review to build and validate our micromechanical models, it became readily apparent that I would be remiss to not investigate how pathological changes in cell physiology affect disease progression in DMD. Therefore, in Chapter 3, I developed an ABM of the key cells involved in muscle regeneration following injury. Ultimately, this avenue of research seeks to understand how chronic, low level damage, from activities such as walking and breathing, leads to muscle degeneration in DMD. However, the limited experimental data from chronic damage made it prohibitively difficult to initially develop chronic computational models. Therefore, the first step for this long-term project was to develop an ABM that incorporated the cell types implicated in DMD and also replicated an experimental assay with sufficient literature. Regeneration from injury is impaired in DMD, and is affected by all the disease mechanisms that we were interested in studying –increased susceptibility to damage, chronic inflammation, fibrosis, and altered SSC dynamics. Additionally, there is extensive data in the literature for acute muscle injuries and regeneration in healthy and dystrophic muscle. Therefore, we developed an ABM of muscle injury and regeneration in healthy and *mdx* mice, the most commonly utilized animal model of DMD.

Developing an ABM that predicts muscle regeneration from the autonomous actions of agents in our model (neutrophils, macrophages, SSCs, fibroblasts, muscle cells, ECM, necrotic elements) is not a trivial process. To build the ABM, I iteratively incorporated rules, ran repeated simulations to sample the stochastic results, and then compared the results to the literature. If the simulation results did not match the literature, I incorporated additional literature-based rules until our model was able to replicate results from both healthy muscle regeneration and perturbation studies.

We used the model to understand how isolated mechanisms of disease altered healthy muscle regeneration. While experimental studies aim to test isolated disease mechanisms, it is very difficult to control and analyze all variables in an experiment. However, our ABM is a powerful tool for isolating the effect of single disease mechanisms to determine how they affect regeneration in healthy and dystrophic muscle. The simulations revealed that the cellular dynamics driving regeneration are time dependent, and that perturbing disease mechanisms often leads to temporally conflicting results. For example, reducing the number of macrophage or fibroblast agents initially increased fiber CSA, but ultimately lead to impaired regeneration at the end of the 28 day simulation. Since these time-dependent cell types are often therapeutic targets, it is critical to understand the temporal variations that may occur following experimental perturbations. Computational models can be used to understand these temporal complexities and adequately define experimental time points to capture the dynamics.

After analyzing the effect of isolated disease mechanisms, we extended the models by altering parameters to replicate three different ages of *mdx* mice. Our ABM predicted that in the late stages of disease, there were pathological decreases in the number of SSCs following injury which ultimately lead to impaired regeneration. Even with the same number of baseline SSCs prior to injury, our model predicted varied peak SSCs counts for the different ages of *mdx* mice. No individual model factor was able to predict these differences in SSC counts. Rather, a combination of factors at the late stages of disease lead to a pro-fibrotic microenvironment that resulted in suppressed SSC counts and impaired regeneration. This emergent model result once again aligns with the second theme of this dissertation – the critical role of the ECM.

As a final component of this dissertation work, we used the ABM to design an experiment to test the effect of fibrosis on muscle regeneration in *mdx* mice. We used a known experimental intervention (TGFβ) to induce fibrosis in the tibialis anterior muscle of the *mdx* mouse and then measured the effect two weeks later. Similar to the literature, the muscle had

increased area fraction of collagen; however passive testing showed that the stiffness of the muscle was significantly decreased compared to *mdx* mice. This suggested that the ECM stiffness was decreased in our *mdx*+TGFβ mouse. We induced an injury in the muscle and measured regeneration with muscle fiber CSA measurements. The experiment showed no significant difference between our three groups (WT, *mdx*, and *mdx*+TGFβ) at all time points measured. Then we simulated these experiments in our ABM of muscle regeneration and similarly found no difference in regeneration between the three groups in the model. Although there were differences in cell counts between the *mdx* and WT muscles. Since we assumed that the stiffness of the ECM was decreased following TGFβ injections, we altered a model parameter that represented collagen density (assumed to correlate with stiffness), to be similar to healthy values, in our original simulations. To investigate the effect of this parameter, we increased the collagen density parameter in the model to be more similar to values expected in aged *mdx* muscle and DMD patients. These simulations predicted that the stiff fibrotic microenvironment would impair regeneration. Together, our experimental and computational analyses predicted that the area fraction of collagen alone was not able to predict the passive properties and regenerative capacity of dystrophic muscle.

Ultimately, I developed two computational models to study how mechanics and physiology affect disease pathology in DMD. The models highlighted how the complex dystrophic microenvironment alters muscle function, damage susceptibility, and regeneration from injury. Throughout this dissertation our models elucidated the complex role of the ECM, and how different pathological factors associated with the ECM alter its effects. The models were then used to design an experiment to test our model predictions and inform our model hypotheses. Given the opportunity to revisit this work, we would have included an aged, fibrotic *mdx* mouse to test our hypothesis that the fibrotic microenvironment at the late stages of disease results in increased muscle stiffness and impaired regeneration. Moving forward, this modeling framework provides the groundwork to develop long-term, chronic DMD models to

predict muscle degeneration and *in silico* therapeutic testing to discern the best targets for therapies.

5.2 Contributions

Micromechanical models of dystrophic skeletal muscle

I have developed the first micromechanical models of skeletal muscle to understand how disease adaptations affect tissue level function and fiber level damage. Previous models had been developed to derive tissue level constitutive properties from the muscle microstructure, but these models did not probe the effect of disease. Our model simulations revealed that the volume fraction and stiffness of the fibrosis significantly altered function and damage susceptibility. From the model results, we predicted that the fibrosis protected the muscle from contraction induced damage but impaired function by increasing the stiffness of the muscle. This prediction aligns with observations in the literature where at the early stages of disease the measurements of damage are significantly elevated, prior to the onset of fibrosis. Then at the later stages of disease, there is decreased function but the measurements of acute damage are suppressed. These models additionally highlighted the importance of understanding the material properties of the ECM and the muscle fibers.

Another key contribution was our novel method for generating these micromechanical models. In order to study the effect of microstructural changes, we needed to generate a significant number of fascicle cross-sections to build our models. Therefore, we used an ABM to generate new, stochastic fascicle cross-sections, and mapped them onto a discretized FE mesh. By using an ABM to generate the muscle cross-sections, we were able to rapidly generate FE meshes of muscle fibers, ECM, and dystrophin proteins, which incorporated both variability commonly seen *in vivo* and microstructural disease modifications.

SSC and fibroblast focused ABM of muscle regeneration

I have developed the first cell physiology based model of muscle regeneration to study disease mechanisms in DMD. While previous models in the lab focused on inflammatory cells during healthy muscle regeneration, this model probed the complex relationships of SSCs and fibroblasts, and then adapted the model to study disease. I have extended the field by developing a model that is able to analyze the effect of altering isolated, pathological changes associated with DMD, a task that is prohibitively difficult with experimental tools alone. I then used the model to reveal how the microenvironment alters SSC dynamics during regeneration. The model predicted that the pro-fibrotic environment at the late stages of disease in the *mdx* mouse resulted in suppressed SSC counts and impaired regeneration. This model has developed the framework for modeling more severe phenotypes in DMD patients, and *in silico* therapeutic testing.

Another key contribution of this model is its utility for simulating experiments to test model predictions and gain insight into experimental results. Based on the ABM predictions, we designed an experiment to test the role of fibrosis on muscle regeneration and then used the model for *in silico* simulation of these experiments. Our experiments showed no significant difference in regeneration between our two *mdx* groups. However, we were able to use the model to predict that the decreased stiffness of the muscle with our fibrosis intervention enabled full regeneration of the muscle; while a simulated stiff fibrotic ECM network did not fully repair. Without our model, it would have been difficult to interpret the results of these experiments, and we may not have gained insight following our extensive experimental study.

Converting previous ABM to a system of ODEs

One of the most useful contributions of this body of work is the method of simplifying a previous ABM into a system of ODEs. A significant challenge of developing a complex model is being able to extend it to study new behaviors or incorporate additional complexity. This is

particularly true for ABMs, where it is extremely challenging to replicate system-level, emergent behaviors from the stochastic actions of autonomous agents. Therefore, it is often prohibitively difficult and computationally expensive to incorporate additional rules into an ABM to study a new phenomenon. When I was building off work from a previous model by Kyle Martin, I addressed this challenge by developing a method for converting the former ABM into a system of seven coupled ODEs. I determined the cumulative effect of one cell on another cell by calculating the growth factor secretions from each cell type and the effect of the growth factors on each cell type. This calculation defined the 51 model parameters for the system of ODEs that were solved non-spatially in the background of the ABM. This method allowed me to develop an entirely new ABM of muscle regeneration based on the behaviors of fibroblasts and SSCs, but still determine the cell counts and growth factors from the inflammatory cells at each time step. I believe this method could be utilized to simplify the ABM presented in this work, so that it can be extended to predict long-term chronic changes in the muscle.

5.3 Current and future applications

5.3.1 Future modeling work to study DMD

The long term goal of the modeling framework developed in this dissertation is to predict degeneration from chronic, repetitive damage in DMD patients. With these models we aim to predict selective degeneration across muscles to discern the primary mechanisms contributing to disease progression. Then the models can be used for *in silico* therapeutic testing, and to design experiments to test these potential therapies. The work presented in this dissertation has developed the foundation for this avenue of research. The next steps include (1) modeling more severe disease phenotype in DMD patients, (2) developing a coupled FE-ABM framework for predicting chronic damage, and (3) *in silico* therapeutic testing. Details for how to address these future directions are included herein.

Model more severe phenotypes in DMD patients

The ABM (Chapter 3) developed in this work was developed from available data in the literature; therefore, we used the most common experimental model of DMD, the *mdx* mouse. However, the disease pathology in the *mdx* mouse is significantly less severe than human patients. We believe this contributes to the failure to translate successful therapies in the mouse to DMD patients. Computational models can help bridge this gap by incorporating these differences in order to elucidate which treatments have the greatest translational potential. The work in this dissertation developed the *mdx* models through a combination of literature-derived and experimentally-tested data. To build models of the more severe DMD phenotype, key parameters can be altered to represent the differences between the *mdx* mouse and humans. Examples of known differences include (1) impaired regenerative potential of SSCs in DMD patients, (2) increased fibrosis in DMD patients, and (3) increased *in vivo* strains in DMD patients. To capture these differences, rules or input parameters would be altered. For instance, the rules for SSC division in DMD patients could be altered to represent the decreased regenerative potential of SSCs following repetitive divisions. Second, patient (rather than mouse) histology could be used to define the baseline spatial geometry that defines the amount of fibrosis in the muscle cross-section. Further, the *in vivo* loads from DMD patients could be used to prescribe the input strain for predicting damage with a coupled FE-ABM model.

Develop coupled FE-ABM framework for chronic damage

After developing the model of DMD patients, a logical next step is to use a coupled FE-ABM framework to predict the effect of chronic, repetitive damage in dystrophic muscle (modeling framework outlined in Figure 5.1). The work in this thesis coupled the FE and ABM models in Repast; however, only a single acute injury at different stages of disease was used to predict the input level of damage. For the chronic model, repetitive activities such as walking or breathing would be used as the input deformations to the FE model. FE meshes would be

generated of the ABM cross-sections with fibers, ECM, and dystrophin proteins (Chapter 2). To account for changes in the muscle microstructure over time, new FE models would be built from the updated muscle cross-sections every 7-30 days, based on a sensitivity analysis to determine how frequently the FE model should be updated. Each time the FE model is updated, the eccentric contraction simulations would be repeated and the calculated membrane strains would be spatially mapped to the ABM.

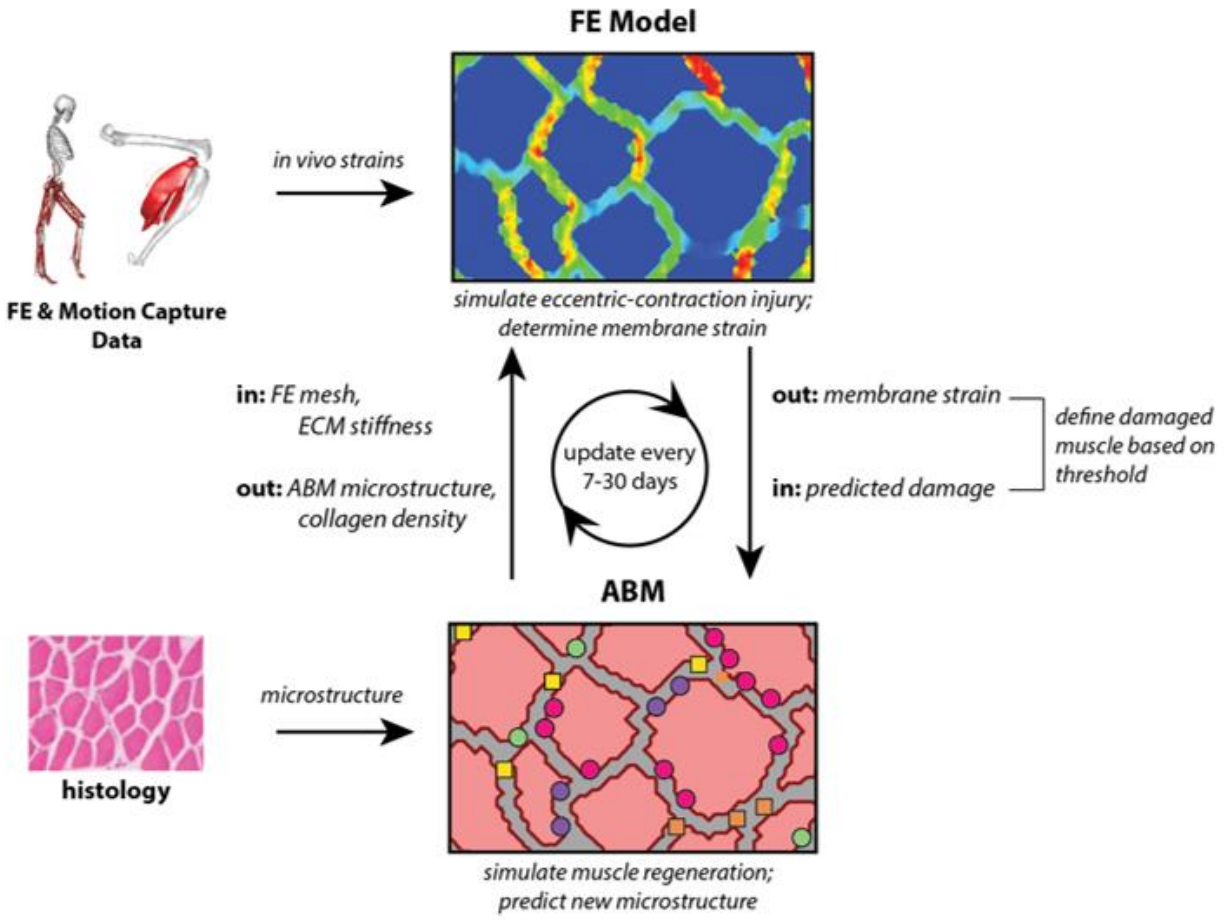

Figure 5.1. FE-ABM framework for predicting long-term chronic damage in dystrophic muscle.

In order to finalize the coupled modeling framework two key modeling parameters must be determined, (1) the relationship between the membrane strain and the amount of muscle damage, and (2) the passive material properties of the ECM and muscle fibers. The quantity of muscle damage that results from different strain levels is currently unknown in the field. Ongoing

work with Kate Bukovec and Robert Grange at Virginia Tech is exploring this relationship by inducing eccentric contractions at different strain levels and then submerging the muscle in procion orange dye. Muscle cross-sections are imaged and the area of procion orange dye is quantified as a metric of damage to the fiber. These experiments can be used to define the model parameter that prescribes the quantity of muscle damage based on the amount of membrane strain. To determine this parameter (or equation), eccentric contractions would be simulated in the model at the same length changes as the experiment, and the associated membrane strain would be calculated. Then an equation or parameter would be tuned that relates the membrane strain with the predicted amount of damage (corresponding with the amount of procion orange dye uptake).

The second unknown for the coupled models is how the collagen density parameter in the ABM relates to the ECM stiffness in the FE model. In this work, we assumed that the along fiber shear stiffness of the ECM linearly increases with the collagen density model parameter (in the fibrotic, dystrophic muscle). Since the micromechanical models apply an along-fiber shear displacement, it is important to determine the stiffness of the ECM in shear, and how this parameter depends on the collagen density. Biaxial mechanical testing experiments to determine the shear passive properties of the tissue are outlined in section 5.3.3. By using the protocol outlined in that section, and altering the collagen density (by aging mice or digesting collagen), the relationship between the collagen density and stiffness of the tissue can be determined.

Use coupled modeling framework to predict selective degeneration

Once this coupled modeling framework is finalized, an ideal avenue for testing and tuning the chronic model simulations is to predict selective degeneration in dystrophic muscle. In DMD, all muscles are missing the dystrophin protein, yet some muscles degenerate faster than others. To investigate this, literature and experimental data could be used to define the

altered factors in the ABM and FE models to represent specific muscles. In the ABM, differences in fiber type distribution and the number of SSCs would alter the baseline model parameters. In the FE model, the prescribed boundary conditions for the eccentric contraction simulations would be adjusted based on the magnitude and frequency of the repetitive damage for that specific muscle. For instance, the diaphragm muscle would have lower strains but increased frequency of repetitive damage, while a lower limb muscle would have a lower frequency of use but higher magnitude of strain. Simulations for specific muscles could be run for 90-120 days in *mdx* mice, and 6 months-3 years in DMD patients to predict the selective degeneration across muscles. Initial simulations of repetitive injuries are shown in Figure 5.2, where the model predicts that the fibrosis and fiber CSA are sensitive to the level and frequency of damage. We believe that if we can develop a modeling framework to predict why some muscles degenerate faster than others, we can gain critical insight into the mechanisms driving disease progression.

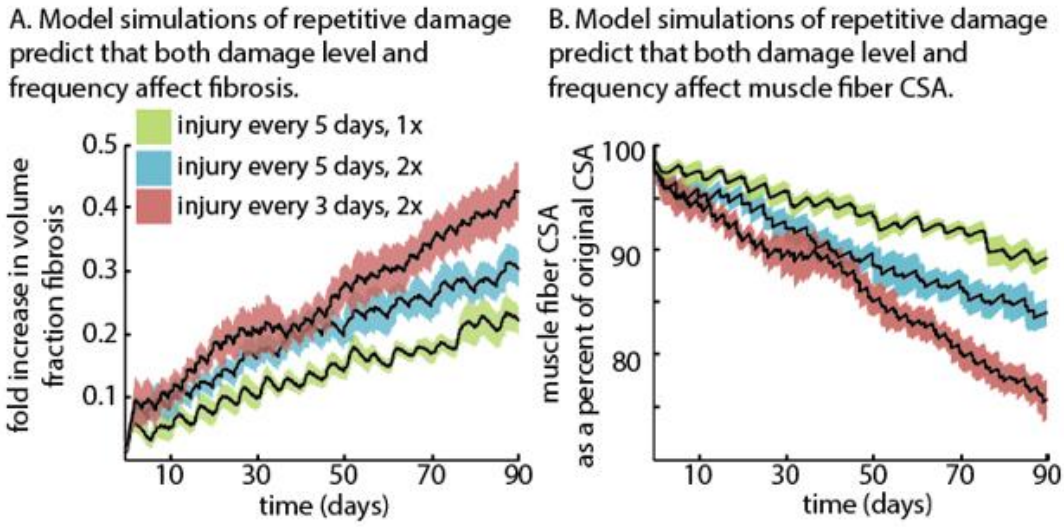

Figure 5.2. Simulations of repetitive acute-injuries predict that the fibrosis (A) and fiber CSA (B) are sensitive to level and frequency of damage.

In silico therapeutic testing

This coupled FE-ABM framework is a powerful tool for *in silico* therapeutic testing. Computational models allow us to simulate an extensive number of therapies and combinations of therapies that would be impossible with experiments alone. Therapeutics would be modeled by altering baseline parameters and specific rules to match the effects of the drugs. Then either an acute or chronic injury model could be used to test the therapy's effectiveness for improving regeneration or preventing degeneration. For instance, in Figure 5.3, we have simulated the effect of membrane protection, anti-inflammatory, and anti-fibrotic therapies in the *mdx* mouse. Future work would simulate these therapies in more severe phenotypes or DMD muscle models. By using computational models of DMD muscle, we can understand why a therapy may appear effective in the mouse but not the human. Simulations in the *mdx* and DMD models would enable researchers to design in vivo experiments that best test therapeutics in the *mdx* mouse that would successfully translate to DMD patients.

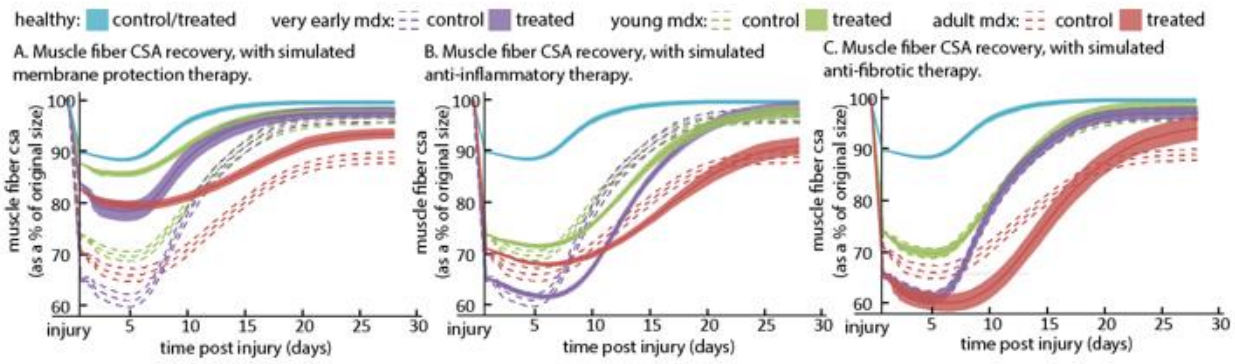

Figure 5.3. Simulations of potential therapies for membrane protection (A), anti-inflammatory (B), and anti-fibrotic (C) treatments at three ages of disease in the *mdx* mouse.

5.3.2 Modeling extensions for other applications

Use ABM to test therapies for volumetric muscle loss recovery and cerebral palsy

Both the ABM (Chapter 3) and FE micromechanical models (Chapter 2) were developed to represent muscle injury and regeneration in healthy muscle. Therefore, the models are not specific to DMD, and could be extended to study other skeletal muscle diseases or injuries. For instance, one application is to simulate recovery from volumetric muscle loss (VML). Volumetric muscle loss is defined as the "traumatic or surgical loss of skeletal muscle with resultant functional impairment" (31). Current work at UVA aims to improve recovery from these extensive injuries, and we believe that computational models can be used to investigate what factors would aid in the recovery process. The ABM could be used to simulate the border between the healthy and injured tissue. For the injured tissue, both the fibers and ECM structure would be eliminated or disrupted, and the resident cells would be seeded. While many of the rules would be altered to replicate the lack of functional recovery and chronic inflammation in VML, many of the cellular behaviors for inflammatory cells, SSCs, or fibroblasts would be similar. The model could be used to investigate what factors would best improve the recovery in this region.

Figure 5.4. Representative images of simulations of volumetric muscle loss at the border between healthy and damaged muscle.

This modeling framework could also be used to model diseases in which healthy muscle function is impaired, such as cerebral palsy (CP). In CP, it has been shown that the number of SSCs in muscles of children with contractures is significantly decreased. Current work with

Geoff Handsfield and Stephanie Khuu is using the ABM in this dissertation as the foundation for modeling contracture in CP patients. By altering the microenvironment (e.g. decreasing the number of SSCs), the ABM could be used to predict how these factors could lead to impaired muscle function.

Predict how accumulated microtears can lead to acute muscle injury

The micromechanical models developed in Chapter 2 could also be used to investigate new hypotheses for muscle injury in healthy muscle. In a previous application of this model, we proposed a new mechanism in which transmembrane proteins, such as dystrophin, are damaged during high-strain eccentric contractions. The protein damage creates a cascade effect of accumulated damage and ultimately results in an acute muscle injury. To analyze this hypothesis we first determined the along-fiber shear strain from tissue level simulations of sprinting (48). Then the tissue level output was used to apply boundary conditions to the micromechanical FE model (Chapter 2). We ran micro-level eccentric contraction simulations and calculated the membrane strain for each protein. Any proteins strained above the prescribed threshold had a probability of breaking. If the proteins broke, they were deleted from the micro-model and simulations were re-run. This process was repeated for a number of simulated contractions. Our initial analysis revealed that this mechanism stochastically predicted large membrane damage for both different fascicle geometries and within the same fascicle geometries.

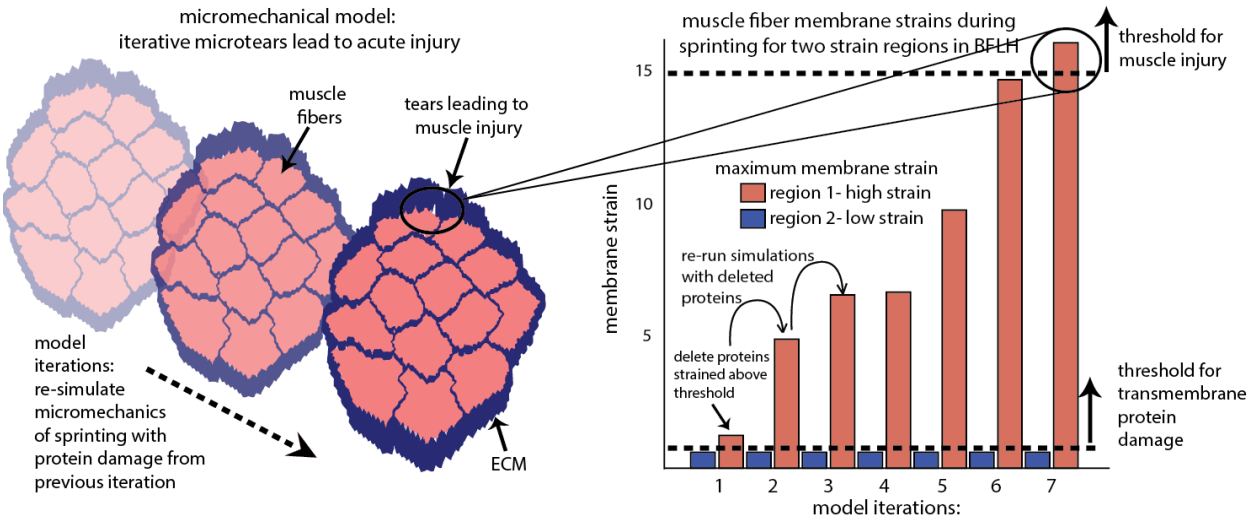

Figure 5.5. Iterations of the model analyses illustrate how small losses in membrane proteins could instantaneously lead to an acute muscle injury during eccentric contraction. After each simulation, proteins above the threshold for protein damage were deleted and a simulation with the remaining proteins was re-run. Model iterations represent the progressive increase in maximum membrane strain as proteins are deleted.

5.3.3 Experimental testing of the role of fibrosis

In Chapter 4, we aimed to test the role of fibrosis on muscle regeneration from injury through injections of TGFβ in 3 month *mdx* mice. These injections have been shown to increase both the mass and area fraction of collagen in the literature. While our injections increased the area fraction of collagen, the stiffness of the muscle was decreased, suggesting that the increased ECM was more compliant than the ECM in the *mdx* muscle. Both the experimental results, and the model predictions based on the baseline parameters showed no effect on regeneration between these two groups. We then used the model to predict that if the fibrosis leads to a stiffer ECM network, which we hypothesize occurs at the late stages of disease, then regeneration is impaired. Therefore, the next step experimentally is to test this prediction in a dystrophic muscle with a stiff fibrotic microenvironment, such as the 12 month *mdx* mouse. By using an older *mdx* mouse an intervention can be used to reduce fibrosis, rather than induce

fibrosis. Then regeneration from injury can be compared between the two groups to test our hypothesis of the role of the ECM on muscle regeneration in dystrophic muscle.

Passive testing of skeletal muscle to determine along-fiber and cross-fiber shear and properties of muscle

A key conclusion from our micromechanical models is that the muscle function and damage susceptibility is dependent on the tissue microenvironment, particularly the relative stiffness between the muscle fibers and the ECM. In our *mdx* mouse experiments (Chapter 4) we developed a system for testing the passive properties of whole muscles. However, due to the complex architecture of the TA muscle, we were unable to experimentally determine the specific contributions from along-fiber stretch, along-fiber shear, and cross-fiber shear properties. Therefore, an extension of this work would be to use biaxial mechanical testing to determine the material properties of the muscle.

The mouse diaphragm is an ideal muscle for biaxial testing since the muscle tissue is thin and there is a known fiber direction (Figure 5.6). Assuming that the two halves of the diaphragm are symmetrical in microstructure, one side can be used for mechanical testing and one for histological analysis. The half used for mechanical testing can be divided into four samples. The samples would be cut such that the fibers are 1) aligned with the edge 2) at a 22 degree angle or 3) at a 45 degree angle. The samples would be marked for speckle tracking and placed in a muscle bath.

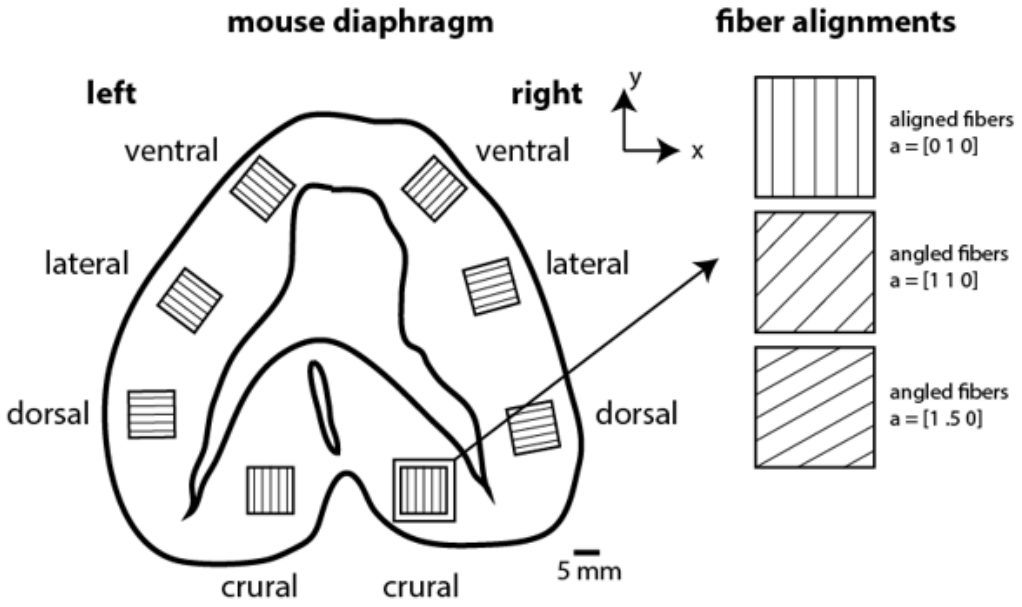

Figure 5.6. Schematic for how to use the mouse diaphragm to determine the passive mechanical properties of the muscle.

The skeletal muscle constitutive model used in this work is based on physically based strain invariants. Therefore, the sample protocol outlined in Figure 5.7 could be used to isolate the along-fiber stretch and cross-fiber shear strain invariants. The sample data would be averaged to fit parameters to the stress-deformation data. Additional test protocols could be used to validate the parameter fits. With this set up, the along-fiber shear strain parameter cannot be isolated. However, if the fiber direction is rotated, it will induce shear in the sample. In these protocols, there is a linear relationship between the along-fiber shear modulus and the stress in x and y direction (Figure 5.7). Therefore, the along-fiber shear modulus can be determined by fitting the along-fiber shear strain and test axis stress data.

A. Biaxial testing to protocol

Protocol function:	Fiber direction	Y stretch	X stretch
Preconditioning	All samples	1:1.1	1:1.1
Isolate along-fiber stretch	Aligned [0 1 0]	1:1.4	free edge
Isolate cross-fiber shear		constant at 1	1:1.4
Model validation		1:1.3	1:1.15
		1:1.15	1:1.3
Indirectly calculate along-fiber shear	Angled [1 1 0]	1:1.4	constant at 1
		constant at 1	1:1.4
	Angled [1 .5 0]	1:1.3	1:1.15
		1:1.15	1:1.3

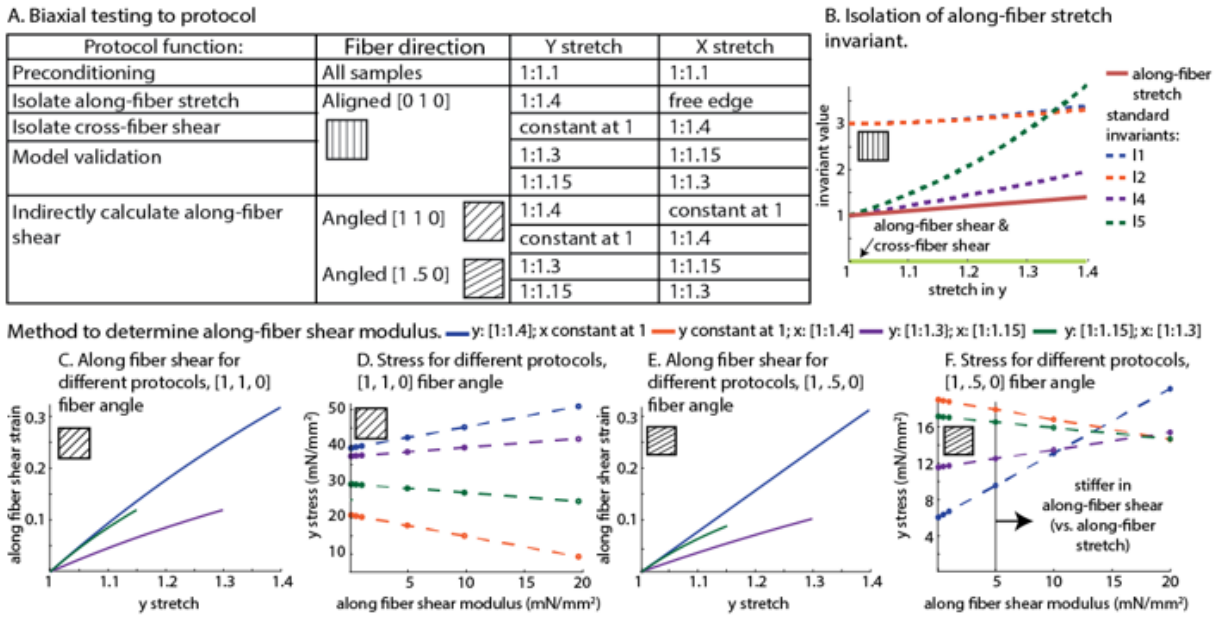

Figure 5.7: Biaxial testing protocol to isolate three physically-based strain invariants (A), such as the along-fiber stretch (B). An indirect method utilizing the relationship between along-fiber shear modulus and test axis stress will be used to determine the along-fiber shear modulus (C-E).

This protocol can be used to determine the four unknown parameters for our skeletal muscle constitutive model. Further, through testing of the diaphragm at different stages of disease or with altered fibrotic levels, we can infer the individual parameters for the muscle fibers and the ECM. This analysis assumes that the changes in the mechanical properties with disease result from changes to the ECM. By comparing the relative stiffness and volume fraction of fibrosis (as measured by picrosirius red staining) of different tissues, we can determine if the ECM is stiffer or more compliant than the muscle in all modes of deformation.

5.4 Final Remarks

In the past three decades since the cause of DMD was discovered, the rapidly advancing experimental tools have provided extensive experimental data and insight into this complex, multifaceted disease. However, there remains no effective treatment for DMD. I

believe that computational models can be a powerful tool for synthesizing the extensive experimental results to elucidate how the multiple disease mechanisms – damage susceptibility, fibrosis, chronic inflammation, impaired regeneration, and altered SSC dynamics – contribute to the progression of DMD. In this dissertation, I have developed mechanics and physiology-based computational models to probe the effect of these disease mechanisms on function, susceptibility to damage, and regeneration. The models revealed new hypotheses about the role of the fibrotic microenvironment, and provided insight into our experimental results. These models can serve as the foundation for future work to predict degeneration from chronic, repetitive injuries and for *in silico* therapeutic testing in DMD muscle. I believe that computational models can help us unravel the complexity of DMD to provide insight into the best therapies to treat boys living with DMD today.

Appendix: Converting the inflammatory cell ABM into a system of ODEs

One of the significant contributions of this body of work was the method of simplifying a complex ABM (99, 102) into a system of ODEs in order to focus on different cell types and applications. The complex rule sets and stochasticity of an ABM often makes it prohibitively difficult to incorporate new agents and rule sets. Additionally, new applications often require the use of different spatial or temporal constraints. However, as we continue to develop and extend our models, it is important to retain the insight and information from former models. Therefore, a method to simplify the predictions and relationships determined in an ABM is a critical step in the advancement of new models. To address this for our research aims, we developed a method to simplify a former ABM into a system of ODEs that incorporated the physiologic relationships between the different cell types.

We determined that the growth factors in the ABM by Martin et al. best characterized the relationships between the different cell types; therefore, we used these growth factors to calculate the relationships between the cells. First, we determined the amount of growth factors secreted from each cell type in the model (at each 1 hour time step) as shown in Figure A.1. Then we determined the effect each of those growth factors had on the different cell types. We did this for the 32 growth factors and 9 agents in the model: neutrophils (N), apoptotic neutrophils (Na), resident macrophages (RM), M1 inflammatory macrophages (M1), M1 inflammatory debris-phagocytosing macrophages (M1de), M1 inflammatory apoptotic-neutrophil phagocytosing macrophages (M1ae), M2 anti-inflammatory macrophages (M2), fibroblasts (F), and SSCs. Then we calculated the product of the growth factors to define parameters that represented the effect of each cell type on the other cell types in the model. The data is represented as a heat map in Figure A.2. The red, negative values represent a cell that induces an inhibitory response on a specific cell type through their growth factor secretions (e.g. M2 macrophages secrete growth factors that cause M1 macrophages to apoptose). The blue,

positive values represent a cell that induces a proliferative response on a specific cell type (e.g. neutrophil secretions lead to M1 macrophage proliferation).

	Secretion										Cell response								
	RM	N	Na	M1	M1ae	M1de	M2	F	SSC		RM	N	Na	M1	M1ae	M1de	M2	F	SSC
tgf	0	0	0	0	1	0	2	1	0		0	0	0	-2	0	0	-1	1	0
tnf	1	1	0	2	2	2	0	0	0.2		0	0	0	0.5	0	0	0	-1	0
igf1	0	0	0	1	1	1	1	2	0		0	0	0	0	0	0	0	0	1
pdgf	0	0	0	0	0	0	0	1	0		0	0	0	0	0	0	0	0	0
mmp12	0	0	0	0	0	0	0	1	1		0	0	0	0	0	0	0	0	0
collagen4	0	0	0	0	0	0	0	1	0		0	0	0	0	0	0	0	0	0
ecmprot	0	0	0	0	0	0	0	2	1		0	0	0	0	0	0	0	0	0
il1	2	1	0	1	1	1	0	0.2	1		0	1	0	0	0	0	0	0	0
il8	1	1	0	1	0	2	0	0.2	0.2		0	1	0	0	0	0	0	0	0
cxcl2	1	0	0	0	0	0	0	0	0		0	1	0	0	0	0	0	0	0
cxcl1	1	0	0	0	0	0	0	0	0		0	1	0	0	0	0	0	0	0
ccl3	1	1	-1	0	0	0	0	0	0		0	0	0	1	0	0	1	0	0
ccl4	1	1	0	0	0	0	0	0	0		0	1	0	1	0	0	1	0	0
il6	0	1	0	3	0	3	0	1	1		0	-0.5	0	1	0	0	1	0	0
mcp	0	1.7	0	0	0	0	0	0.2	1		0	1	0	1	0	0	1	0	0
ifn	0	5	0	0	0	1	0	0	0		0	0	0	1	0	0	-1	0	0
lactoferins	0	0	5	0	0	0	0	0	0		0	-1	0	0	0	0	0	0	0
hgf	0	0	1	0	0	0	0	0	0		0	0	0	0	0	0	0	0	1
vegf	0	0	1	1	1	1	0	0	1		0	0	0	0	0	0	0	0	0
mmp12	0	0	0	2	2	2	0	0	1		0	-1	0	0	0	0	0	0	0
gcsf	0	0	0	1	1	1	0	0	0		0	1	0	0	0	0	0	0	0
il10	0	0	0	1	0.1	0.5	1	0	0		0	-1	0	-1	0	0	2	0	0
lipoxins	0	0	0	0	1	1	0	0	0		0	-1	0	-1	0	0	-1	0	0
resolvins	0	0	0	0	3	2	0	0	0		0	-1	0	0	0	0	0	0	0
ccl17	0	0	0	0	1	0	2.8	0	0		0	0	0	1	0	0	1	0	0
ccl22	0	0	0	0	1	0	1	0	1		0	0	0	0	0	0	0	0	0
collagen4	0	0	0	0	0	0	1	0	0		0	0	0	0	0	0	0	0	0
pge2	0	0	0	0	0	0	3	0	0		0	-1	0	-1	0	0	-1	0	0
fgf	0	0	0	0	0	0	0	1	0		0	0	0	0	0	0	0	0	1

Figure A.1. Growth factor secretions from the different cell types in the ABM by Martin et al, and the effect of the growth factors on the different cell types in the model. A positive cell response represents a growth factor that causes the cell to proliferate, while a negative value represents a growth factor that leads to cell death, or differentiation to a new phenotype.

The calculated values (Fig A.2) were used as the initial predictions for the ODE model parameters for the 9 cell types in the model. To incorporate behaviors that were not captured directly by the growth factors, we incorporated additional parameters to represent cell death and phenotypic transition to different cell types. For instance, based on the microenvironment, neutrophils could transition to apoptotic neutrophils or M1 macrophages could transition to M2 anti-inflammatory macrophages. Many of the cell counts that initiated the inflammatory and regenerative response were also dependent on the amount of damage in the muscle. The initial set of ODEs was defined by 51 different modeling parameters. Once this initial set of ODEs was defined, we ran simulations (in Matlab with the Euler method) to predict the number of cells and

the timing of the cell peaks. We then incorporated and tuned a scaling factor until the ODE model predictions replicated the ABM model predictions. ODEs are shown in equation A.1-A.7 and Figure A.3, where $\%_{necrotic}$ is the current percent of the muscle that is necrotic, and RM_0 is the starting number of resident macrophages.

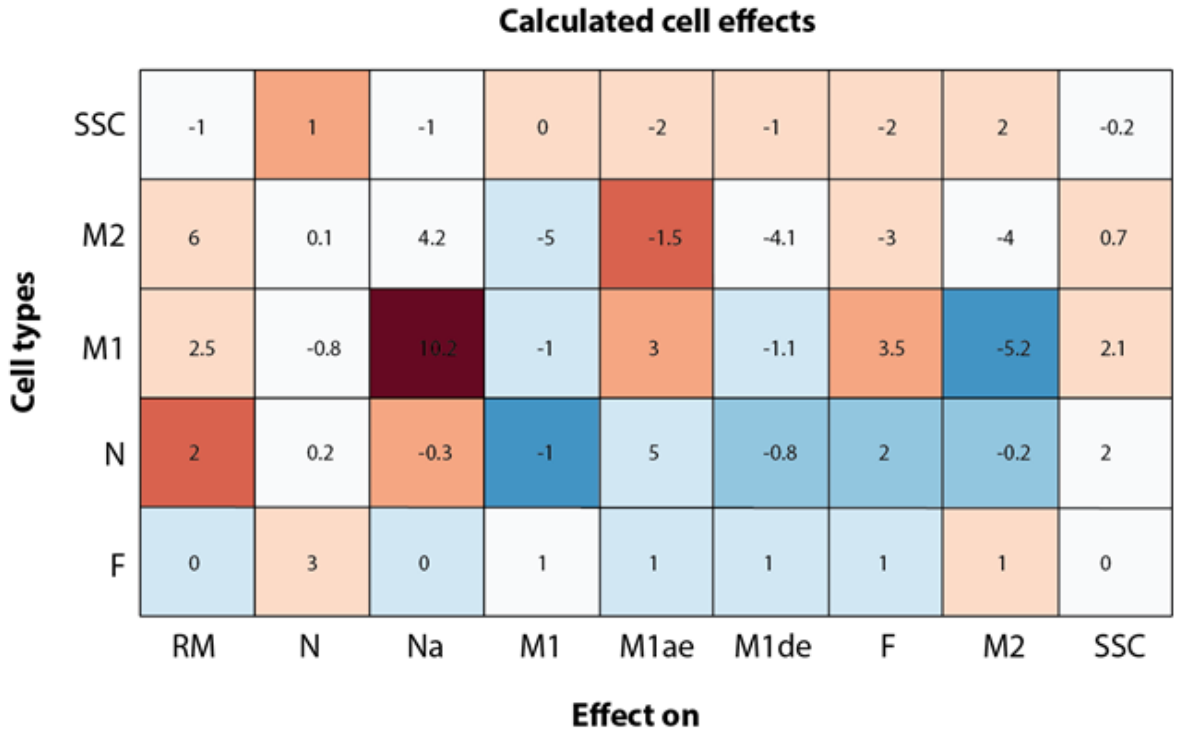

Figure A.2. Heat map represents the effect a cell type (rows) has on the other cell types (columns).

$$\frac{dRM}{dt} = 1.054RM_0 - 0.18RM \tag{A.1}$$

$$\frac{dN}{dt} = 2.40RM * \%_{necrotic} + 0.00033Fb + .016N - .024N_a - 0.082M1 - 0.020M1_{ae} - 0.0019M1_{de} - 0.045M2 + 0.0023SSC - 0.13N * \%_{necrotic} \tag{A.2}$$

$$\frac{dN_a}{dt} = 0.13N * \%_{necrotic} - 0.0058M1 * N_a - 0.0058N_a \tag{A.3}$$

$$\frac{dM1}{dt} = 0.0046RM * \%_{necrotic} - 0.0018Fb + 0.033N - 0.0018N_a + 0.0058M1 \quad \text{(A.4)}$$

$$- 0.0054M1_{ae} + 0.0096M1_{de} - 0.0092M2 + 0.0017SSC - 0.0011M1 * N_a$$

$$- 0.0046M1 * \%_{necrotic}$$

$$\frac{dM1_{ae}}{dt} = 0.003M1 * N - 0.018M1_{ae} \quad \text{(A.5)}$$

$$\frac{dM1_{de}}{dt} = 0.012M1 * \%_{necrotic} - 0.012M1_{de} \quad \text{(A.6)}$$

$$\frac{dM2}{dt} = 0.0054RM * \%_{necrotic} - 0.0026Fb - 0.019N - 0.00079N_a + 0.043M1 \quad \text{(A.7)}$$

$$+ 0.0053M1_{ae} + 0.015M1_{de} - 0.0096M2 + 0.0026SSC$$

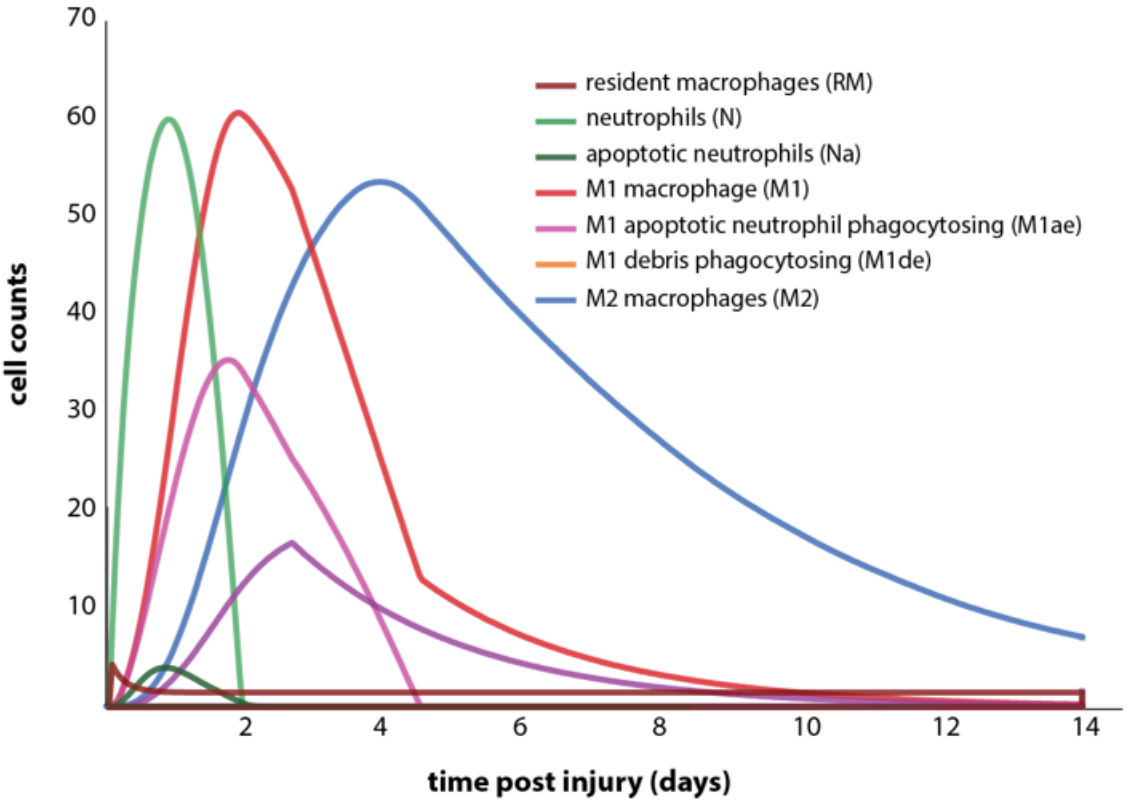

Figure A.3 Inflammatory cell counts predicted from ODEs

We incorporated the system of ODEs for the inflammatory cells (not including the fibroblasts and SSCs) non-spatially in the ABM. At each time step, the ABM used the Euler method to calculate the number of inflammatory cells in the model. Based on the number of cells, growth factors were secreted (non-spatially) at each time step, and a second set of ODEs defined the amount of growth factors in the model at each time step. The behaviors of the sptail agents (fibers, ECM, fibroblasts, and SSCs) were dependent on these growth factor secretions, as well as the number of inflammatory cells in the model.

References:

1. **Acuña MJ**, **Pessina P**, **Olguin H**, **Cabrera D**, **Vio CP**, **Bader M**, **Muñoz-canoves P**, **Santos R a.**, **Cabello-verrugio C**, **Brandan E**. Restoration of muscle strength in dystrophic muscle by angiotensin-1-7 through inhibition of TGF-β signalling. *Hum Mol Genet* 23: 1237–1249, 2014.

2. **Allen RE**, **Boxhorn LK**. Regulation of skeletal muscle satellite cell proliferation and differentiation by transforming growth factor-beta, insulin-like growth factor I, and fibroblast growth factor. *J Cell Physiol* 138: 311–315, 1989.

3. **Allen RE**, **Sheehan SM**, **Taylor RG**, **Kendall TL**, **Rice GM**. Hepatocyte growth factor activates quiescent skeletal muscle satellite cells in vitro. *J Cell Physiol* 165: 307–312, 1995.

4. **Arnold L**, **Henry A**, **Poron F**, **Baba-Amer Y**, **van Rooijen N**, **Plonquet A**, **Gherardi RK**, **Chazaud B**. Inflammatory monocytes recruited after skeletal muscle injury switch into antiinflammatory macrophages to support myogenesis. *J Exp Med* 204: 1057–1069, 2007.

5. **Avery NC**, **Bailey AJ**. Enzymic and non-enzymic cross-linking mechanisms in relation to turnover of collagen: Relevance to aging and exercise. *Scand J Med Sci Sport* 15: 231–240, 2005.

6. **Bailey AM**, **Thorne BC**, **Peirce SM**. Multi-cell agent-based simulation of the microvasculature to study the dynamics of circulating inflammatory cell trafficking. *Ann Biomed Eng* 35: 916–936, 2007.

7. **Bakkar N**, **Wang J**, **Ladner KJ**, **Wang H**, **Dahlman JM**, **Carathers M**, **Acharyya S**, **Rudnicki MA**, **Hollenbach AD**, **Guttridge DC**. IKK/NF-κB regulates skeletal myogenesis

via a signaling switch to inhibit differentiation and promote mitochondrial biogenesis. *J Cell Biol* 180: 787–802, 2008.

8. **Bassett DI**, **Bryson-Richardson RJ**, **Daggett DF**, **Gautier P**, **Keenan DG**, **Currie PD**. Dystrophin is required for the formation of stable muscle attachments in the zebrafish embryo. *Dev Dis* 130: 5851–60, 2003.

9. **Benedetti S**, **Hoshiya H**, **Tedesco FS**. Repair or replace? Exploiting novel gene and cell therapy strategies for muscular dystrophies. *FEBS J* 280: 4263–80, 2013.

10. **Bentzinger CF**, **Wang YX**, **Dumont NA**, **Rudnicki MA**. Cellular dynamics in the muscle satellite cell niche. *EMBO Rep* 14: 1062–1072, 2013.

11. **Bentzinger CF**, **Wang YX**, **Von Maltzahn J**, **Soleimani VD**, **Yin H**, **Rudnicki MA**. Fibronectin regulates Wnt7a signaling and satellite cell expansion. *Cell Stem Cell* 12: 75–87, 2013.

12. **Bhasin N**, **Law R**, **Liao G**, **Safer D**, **Ellmer J**, **Discher BM**, **Sweeney HL**, **Discher DE**. Molecular extensibility of mini-dystrophins and a dystrophin rod construct. *J Mol Biol* 352: 795–806, 2005.

13. **Bhui R**, **Hayenga HN**. An agent-based model of leukocyte transendothelial migration during atherogenesis. *PLoS Comput. Biol.* (2017). doi: 10.1371/journal.pcbi.1005523.

14. **Bhui R**, **Hayenga HN**. An agent-based model of leukocyte transendothelial migration during atherogenesis. *PLoS Comput Biol* 13: 1–23, 2017.

15. **Blemker SS**, **Delp SL**. Three-dimensional representation of complex muscle architectures and geometries. *Ann Biomed Eng* 33: 661–673, 2005.

16. **Blemker SS**, **Pinsky PM**, **Delp SL**. A 3D model of muscle reveals the causes of nonuniform strains in the biceps brachii. *J Biomech* 38: 657–65, 2005.

17. **Bloch RJ**, **Gonzalez-Serratos H**. Lateral Force Transmission Across Costameres in Skeletal Muscle. *Exerc Sport Sci Rev* 31: 73–78, 2003.

18. **Bonabeau E**. Agent-based modeling: methods and techniques for simulating human systems. *Proc Natl Acad Sci* 99: 7280–7287, 2002.

19. **Brinkmeyer-Langford C**, **Kornegay JN**. Comparative Genomics of X-linked Muscular Dystrophies: The Golden Retriever Model. *Curr Genomics* 14: 330–42, 2013.

20. **Ten Broek RW**, **Grefte S**, **Von Den Hoff JW**. Regulatory factors and cell populations involved in skeletal muscle regeneration. *J Cell Physiol* 224: 7–16, 2010.

21. **Brown DG**, **Robinson DT**. Effects of heterogeneity in residential preferences on an agent-based model of urban sprawl. *Ecol Soc* 11, 2006.

22. **Cabello-Verrugio C**, **Santander C**, **Cofré C**, **Acuña MJ**, **Melo F**, **Brandan E**. The internal region leucine-rich repeat 6 of decorin interacts with low density lipoprotein receptor-related protein-1, modulates Transforming Growth Factor (TGF)-β-dependent signaling, and inhibits TGF-β-dependent fibrotic response in skeletal muscles. *J Biol Chem* 287: 6773–6787, 2012.

23. **Cai B**, **Spencer MJ**, **Nakamura G**, **Tseng-Ong L**, **Tidball JG**. Eosinophilia of dystrophin-deficient muscle is promoted by perforin-mediated cytotoxicity by T cell effectors. *Am J Pathol* 156: 1789–1796, 2000.

24. **Cantini M**, **Giurisato E**, **Radu C**, **Tiozzo S**, **Pampinella F**, **Senigaglia D**, **Zaniolo G**, **Mazzoleni F**, **Vitiello L**. Macrophage-secreted myogenic factors: A promising tool for greatly enhancing the proliferative capacity of myoblasts in vitro and in vivo. *Neurol Sci* 23: 189–194, 2002.

25. **Chazaud B**, **Sonnet C**, **Lafuste P**, **Bassez G**, **Rimaniol a. C**, **Poron F**, **Authier FJ**,

Dreyfus P a., **Gherardi RK**. Satellite cells attract monocytes and use macrophages as a support to escape apoptosis and enhance muscle growth. *J Cell Biol* 163: 1133–1143, 2003.

26. **Chelly J**, **Desguerre I**. Progressive muscular dystrophies. *Handb Clin Neurol* 113: 1343–66, 2013.

27. **Chen X**, **Li Y**. Role of matrix metalloproteinases in skeletal muscle: migration, differentiation, regeneration and fibrosis. *Cell Adh Migr* 3: 337–341, 2009.

28. **Chen Y-W**, **Nagaraju K**, **Bakay M**, **McIntyre O**, **Rawat R**, **Shi R**, **Hoffman EP**. Early onset of inflammation and later involvement of TGFbeta in Duchenne muscular dystrophy. *Neurology* 65: 826–34, 2005.

29. **Claflin DR**, **Brooks S V**. Direct observation of failing fibers in muscles of dystrophic mice provides mechanistic insight into muscular dystrophy. *Am J Physiol Cell Physiol* 294: C651–C658, 2008.

30. **Contreras O**, **Rebolledo DL**, **Oyarzún JE**, **Olguín HC**, **Brandan E**. Connective tissue cells expressing fibro/adipogenic progenitor markers increase under chronic damage: relevance in fibroblast-myofibroblast differentiation and skeletal muscle fibrosis. *Cell Tissue Res.* (2016). doi: 10.1007/s00441-015-2343-0.

31. **Corona BT**, **Ward CL**, **Baker HB**, **Walters TJ**, **Christ GJ**. Implantation of In Vitro Tissue Engineered Muscle Repair Constructs and Bladder Acellular Matrices Partially Restore In Vivo Skeletal Muscle Function in a Rat Model of Volumetric Muscle Loss Injury. *Tissue Eng Part A* 20: 131219054609007, 2013.

32. **Criscione JC**, **Douglas AS**, **Hunter WC**. Physically based strain invariant set for materials exhibiting transversely isotropic behavior. *J Mech Phys Solids* 49: 871–897,

2001.

33. **Deconinck A**, **Rafael J**, **Skinner J**, **Brown S**, **Potter A**, **Metzinger L**, **Watt D**, **Dickson J**, **Tinsley J**, **Davies K**. Utrophin-dystrophin-deficient mice as a model for Duchenne muscular dystrophy. *Cell* 90: 717–727, 1997.

34. **Dell'Acqua G**, **Castiglione F**. Stability and phase transitions in a mathematical model of Duchenne muscular dystrophy. *J Theor Biol* 260: 283–289, 2009.

35. **Dellorusso C**, **Crawford RW**, **Chamberlain JS**, **Brooks S V.** Tibialis anterior muscles in mdx mice are highly susceptible to contraction-induced injury. *J Muscle Res Cell Motil* 22: 467–475, 2001.

36. **Delp SL**, **Anderson FC**, **Arnold AS**, **Loan P**, **Habib A**, **John CT**, **Guendelman E**, **Thelen DG**. OpenSim: Open-source software to create and analyze dynamic simulations of movement. *IEEE Trans Biomed Eng* 54: 1940–1950, 2007.

37. **Deng B**, **Wehling-Henricks M**, **Villalta SA**, **Wang Y**, **Tidball JG**. Interleukin-10 triggers changes in macrophage phenotype that promote muscle growth and regeneration. *J Immunol* 187: 5419–5428, 2012.

38. **Desguerre I**, **Arnold L**, **Vignaud A**, **Cuvellier S**, **Yacoub-Youssef H**, **Gherardi RK**, **Chelly J**, **Chretien F**, **Mounier R**, **Ferry A**, **Chazaud B**. A new model of experimental fibrosis in hindlimb skeletal muscle of adult mdx mouse mimicking muscular dystrophy. *Muscle Nerve* 45: 803–14, 2012.

39. **Desmoulière a**, **Geinoz A**, **Gabbiani F**, **Gabbiani G**. Transforming growth factor-B1 induces alpha-smooth muscle actin expression in granulation tissue myofibroblasts and in quiescent and growing cultured fibroblasts. *J Cell Biol* 122: 103–111, 1993.

40. **Dickinson RB**, **Guido S**, **Tranquillo RT**. Biased cell migration of fibroblasts exhibiting

contact guidance in oriented collagen gels. *Ann Biomed Eng* 22: 342–356, 1994.

41. **Dumont NA**, **Wang YX**, **von Maltzahn J**, **Pasut A**, **Bentzinger CF**, **Brun CE**, **Rudnicki MA**. Dystrophin expression in muscle stem cells regulates their polarity and asymmetric division. *Nat Med* 21: 1455–1463, 2015.

42. **Dumont NA**, **Wang YX**, **Rudnicki MA**. Intrinsic and extrinsic mechanisms regulating satellite cell function. *Development* 142: 1572–1581, 2015.

43. **Dumont N**, **Bouchard P**, **Frenette J**. Neutrophil-induced skeletal muscle damage: a calculated and controlled response following hindlimb unloading and reloading. *Am J Physiol Regul Integr Comp Physiol* 295: R1831–R1838, 2008.

44. **Dumont N**, **Frenette J**. Macrophages Protect against Muscle Atrophy and Promote Muscle Recovery in Vivo and in Vitro. *Am J Pathol* 176: 2228–2235, 2010.

45. **Emery AEH**. The muscular dystrophies. *Lancet* 359: 687–95, 2002.

46. **Evans NP**, **Misyak SA**, **Robertson JL**, **Bassaganya-Riera J**, **Grange RW**. Immune-Mediated Mechanisms Potentially Regulate the Disease Time-Course of Duchenne Muscular Dystrophy and Provide Targets for Therapeutic Intervention. *PM R* 1: 755–768, 2009.

47. **Fiore D**, **Judson RN**, **Low M**, **Lee S**, **Zhang E**, **Hopkins C**, **Xu P**, **Lenzi A**, **Rossi FM V**, **Lemos DR**. Pharmacological blockage of fibro/adipogenic progenitor expansion and suppression of regenerative fibrogenesis is associated with impaired skeletal muscle regeneration. *Stem Cell Res* 17: 161–169, 2016.

48. **Fiorentino NM**, **Blemker SS**. Musculotendon variability influences tissue strains experienced by the biceps femoris long head muscle during high-speed running. *J Biomech* 47: 3325–33, 2014.

49. **Fiorentino NM**, **Rehorn MR**, **Chumanov ES**, **Thelen DG**, **Blemker SS**. Computational models predict larger muscle tissue strains at faster sprinting speeds. *Med Sci Sports Exerc* 46: 776–786, 2014.

50. **Fomovsky GM**, **Holmes JW**. Evolution of scar structure, mechanics, and ventricular function after myocardial infarction in the rat. *Am J Physiol Heart Circ Physiol* 298: H221–H228, 2010.

51. **Fu X**, **Xiao J**, **Wei Y**, **Li S**, **Liu Y**, **Yin J**, **Sun K**, **Sun H**, **Wang H**, **Zhang Z**, **Zhang B-T**, **Sheng C**, **Wang H**, **Hu P**. Combination of inflammation-related cytokines promotes long-term muscle stem cell expansion. *Cell Res* 25: 655–73, 2015.

52. **García-Pelagio K**, **Bloch R**, **Ortega A**, **González-Serratos H**. Biomechanics of the sarcolemma and costameres in single skeletal muscle fibers from normal and dystrophin-null mice. *J Muscle Res Cell Motil* 31: 323–36, 2011.

53. **Gargioli C**, **Coletta M**, **De Grandis F**, **Cannata SM**, **Cossu G**. PlGF-MMP-9-expressing cells restore microcirculation and efficacy of cell therapy in aged dystrophic muscle. *Nat Med* 14: 973–8, 2008.

54. **Gayraud-Morel B**, **Chrétien F**, **Jory A**, **Sambasivan R**, **Negroni E**, **Flamant P**, **Soubigou G**, **Coppée J-Y**, **Di Santo J**, **Cumano A**, **Mouly V**, **Tajbakhsh S**. Myf5 haploinsufficiency reveals distinct cell fate potentials for adult skeletal muscle stem cells. *J Cell Sci* 125: 1738–49, 2012.

55. **Gillies AR**, **Bushong EA**, **Deerinck TJ**, **Ellisman MH**, **Lieber RL**. Three-Dimensional Reconstruction of Skeletal Muscle Extracellular Matrix Ultrastructure. *Microsc Microanal* 20: 1835–40, 2014.

56. **Gillies AR**, **Lieber RL**. Structure and function of the skeletal muscle extracellular matrix.

Muscle Nerve 44: 318–31, 2011.

57. **Goetsch KP**, **Myburgh KH**, **Niesler CU**. In vitro myoblast motility models: Investigating migration dynamics for the study of skeletal muscle repair. *J Muscle Res Cell Motil* 34: 333–347, 2013.

58. **Gopalakrishnan V**, **Kim M**, **An G**. Using an Agent-Based Model to Examine the Role of Dynamic Bacterial Virulence Potential in the Pathogenesis of Surgical Site Infection. *Adv Wound Care* 2: 510–526, 2013.

59. **Gopalakrishnan V**, **Kim M**, **An G**. Using an Agent-Based Model to Examine the Role of Dynamic Bacterial Virulence Potential in the Pathogenesis of Surgical Site Infection. *Adv Wound Care* 2: 510–526, 2013.

60. **Le Grand F**, **Jones AE**, **Seale V**, **Scime A**, **Rudnicki MA**. Wnt7a Activates the Planar Cell Polarity Pathway to Drive the Symmetric Expansion of Satellite Stem Cells. *Cell Stem Cell* 4: 535–547, 2009.

61. **Grounds MD**, **Radley HG**, **Lynch GS**, **Nagaraju K**, **De Luca A**. Towards developing standard operating procedures for pre-clinical testing in the mdx mouse model of Duchenne muscular dystrophy. *Neurobiol Dis* 31: 1–19, 2008.

62. **Guyon JR**, **Goswami J**, **Jun SJ**, **Thorne M**, **Howell M**, **Pusack T**, **Kawahara G**, **Steffen LS**, **Galdzicki M**, **Kunkel LM**. Genetic isolation and characterization of a splicing mutant of zebrafish dystrophin. *Hum Mol Genet* 18: 202–11, 2009.

63. **Hakim CH**, **Grange RW**, **Duan D**. The passive mechanical properties of the extensor digitorum longus muscle are compromised in 2- to 20-mo-old mdx mice. *J Appl Physiol* 110: 1656–1663, 2011.

64. **Hardy D**, **Besnard A**, **Latil M**, **Jouvion G**, **Briand D**, **Thépenier C**, **Pascal Q**, **Guguin**

A, **Gayraud-Morel B**, **Cavaillon J-M**, **Tajbakhsh S**, **Rocheteau P**, **Chrétien F**. Comparative Study of Injury Models for Studying Muscle Regeneration in Mice. *PLoS One* 11: e0147198, 2016.

65. **Haus JM**, **Carrithers JA**, **Trappe SW**, **Trappe TA**. Collagen, cross-linking, and advanced glycation end products in aging human skeletal muscle. *J Appl Physiol* 103: 2068–76, 2007.

66. **Heredia JE**, **Mukundan L**, **Chen FM**, **Mueller AA**, **Deo RC**, **Locksley RM**, **Rando TA**, **Chawla A**. Type 2 innate signals stimulate fibro/adipogenic progenitors to facilitate muscle regeneration. *Cell* 153: 376–388, 2013.

67. **Hill AV**. The Heat of Shortening and the Dynamic Constants of Muscle.pdf. *Proc R Soc London Ser B, Biol Sci* 126: 136–195, 1938.

68. **Hoffman EP**, **Brown RH**, **Kunkel LM**. Dystrophin : The Protein Product of the Duchenne Muscular Dystrophy Locus. *Cell* 51: 919–928, 1987.

69. **Huijing PA**. Muscle as a collagen fiber reinforced composite: A review of force transmission in muscle and whole limb. *J Biomech* 32: 329–345, 1999.

70. **Huxley AF**. Muscle structure and theories of contraction. *Prog Biophys Biophys Chem* 7: 255–318., 1957.

71. **Jarrah AS**, **Castiglione F**, **Evans NP**, **Grange RW**, **Laubenbacher R**. A mathematical model of skeletal muscle disease and immune response in the mdx mouse. *Biomed Res Int* 2014: 871810, 2014.

72. **Joe AW**, **Yi L**, **Natarajan A**, **Le Grand F**, **So L**, **Wang J**, **Rudnicki MA**, **Rossi FM**. Muscle injury activates resident fibro/adipogenic progenitors that facilitate myogenesis. *Nat Cell Biol* 12: 153–163, 2010.

73. **Johansson T**, **Meier P**, **Blickhan R**. A finite-element model for the mechanical analysis of skeletal muscles. *J Theor Biol* 206: 131–49, 2000.

74. **Kawamura K**, **Takano K**, **Suetsugu S**, **Kurisu S**, **Yamazaki D**, **Miki H**, **Takenawa T**, **Endo T**. N-WASP and WAVE2 acting downstream of phosphatidylinositol 3-kinase are required for myogenic cell migration induced by hepatocyte growth factor. *J Biol Chem* 279: 54862–54871, 2004.

75. **Kharraz Y**, **Guerra J**, **Pessina P**, **Serrano AL**, **Muñoz-Cánoves P**. Understanding the process of fibrosis in Duchenne muscular dystrophy. *Biomed Res Int* 2014: 965631, 2014.

76. **Kim S**, **Campbell KA**, **Fox DJ**, **Matthews DJ**, **Valdez R**. Corticosteroid Treatments in Males With Duchenne Muscular Dystrophy: Treatment Duration and Time to Loss of Ambulation. *J. Child Neurol.* (November 20, 2014). doi: 10.1177/0883073814558120.

77. **Kjær M**. Role of Extracellular Matrix in Adaptation of Tendon and Skeletal Muscle to Mechanical Loading. *Physiol Rev* 84: 649–698, 2004.

78. **Klingler W**, **Jurkat-Rott K**, **Lehmann-horn F**, **Schleip R**. The role of fibrosis in Duchenne muscular dystrophy. *Acta Myol* 31: 184–195, 2012.

79. **Koenig M**, **Hoffman EP**, **Bertelson CJ**, **Monaco AP**, **Feener C**, **Kunkel LM**. Complete Cloning of the Duchenne Muscular Dystrophy (DMD) cDNA and Preliminary Genomic Organization of the DMD Gene in Normal and Affected Individuals. *Cell* 50: 509–517, 1987.

80. **Koenig M**, **Monaco AP**, **Kunkel LM**. The Complete Sequence of Dystrophin Predicts a Rod-Shaped Cytoskeletal Protein. *Cell* 53: 219–228, 1988.

81. **Kole R**, **Krieg AM**. Exon skipping therapy for Duchenne muscular dystrophy. *Adv Drug*

Deliv Rev 87: 104–107, 2015.

82. **Kollu S**, **Abou-Khalil R**, **Shen C**, **Brack AS**. The Spindle Assembly Checkpoint Safeguards Genomic Integrity of Skeletal Muscle Satellite Cells. *Stem cell reports* 4: 1061–1074, 2015.

83. **Kragstrup TWW**, **Kjaer M**, **Mackey ALL**. Structural, biochemical, cellular, and functional changes in skeletal muscle extracellular matrix with aging. *Scand J Med Sci Sports* 21: 749–57, 2011.

84. **Kuang S**, **Gillespie MA**, **Rudnicki MA**. Niche Regulation of Muscle Satellite Cell Self-Renewal and Differentiation. *Cell Stem Cell* 2: 22–31, 2008.

85. **Kuang S**, **Kuroda K**, **Le Grand F**, **Rudnicki MA**. Asymmetric Self-Renewal and Commitment of Satellite Stem Cells in Muscle. *Cell* 129: 999–1010, 2007.

86. **Lemos DR**, **Babaeijandaghi F**, **Low M**, **Chang C-K**, **Lee ST**, **Fiore D**, **Zhang R-H**, **Natarajan A**, **Nedospasov S a**, **Rossi FM V**. Nilotinib reduces muscle fibrosis in chronic muscle injury by promoting TNF-mediated apoptosis of fibro/adipogenic progenitors. *Nat Med* 21: 786–794, 2015.

87. **Lemos DR**, **Paylor B**, **Chang C**, **Sampaio A**, **Underhill TM**, **Rossi FM V**. Functionally convergent white adipogenic progenitors of different lineages participate in a diffused system supporting tissue regeneration. *Stem Cells* 30: 1152–1162, 2012.

88. **Lewis MP**, **Tippett HL**, **Sinanan ACM**, **Morgan MJ**, **Hunt NP**. Gelatinase-B (matrix metalloproteinase-9; MMP-9) secretion is involved in the migratory phase of human and murine muscle cell cultures. *J Muscle Res Cell Motil* 21: 223–233, 2000.

89. **Li Y**, **Foster W**, **Deasy BM**, **Chan Y**, **Prisk V**, **Tang Y**, **Cummins J**, **Huard J**. Transforming Growth Factor-β1 Induces the Differentiation of Myogenic Cells into Fibrotic

Cells in Injured Skeletal Muscle. *Am J Pathol* 164: 1007–1019, 2004.

90. **Lieber RL**, **Ward SR**. Cellular mechanisms of tissue fibrosis. 4. Structural and functional consequences of skeletal muscle fibrosis. *Am J Physiol Cell Physiol* 305: C241-52, 2013.

91. **Lipton BH**, **Konigsberg IR**. A fine-structural analysis of the fusion of myogenic cells. *J Cell Biol* 53: 348–364, 1972.

92. **Lukjanenko L**, **Jung MJ**, **Hegde N**, **Perruisseau-Carrier C**, **Migliavacca E**, **Rozo M**, **Karaz S**, **Jacot G**, **Schmidt M**, **Li L**, **Metairon S**, **Raymond F**, **Lee U**, **Sizzano F**, **Wilson DH**, **Dumont NA**, **Palini A**, **Fässler R**, **Steiner P**, **Descombes P**, **Rudnicki MA**, **Fan C-M**, **von Maltzahn J**, **Feige JN**, **Bentzinger CF**. Loss of fibronectin from the aged stem cell niche affects the regenerative capacity of skeletal muscle in mice. *Nat Med* 22: 897–905, 2016.

93. **Lund TC**, **Grange RW**, **Lowe DA**. Telomere shortening in diaphragm and tibialis anterior muscles of aged mdx mice. *Muscle and Nerve* 36: 387–390, 2007.

94. **Maas S a**, **Ellis BJ**, **Ateshian GA**, **Weiss JA**. FEBio: finite elements for biomechanics. *J Biomech Eng* 134, 2012.

95. **Mann CJ**, **Perdiguero E**, **Kharraz Y**, **Aguilar S**, **Pessina P**, **Serrano AL**, **Muñoz-Cánoves P**. Aberrant repair and fibrosis development in skeletal muscle. *Skelet Muscle* 1: 21, 2011.

96. **Manzur A**, **Kuntzer T**, **Pike M**, **Swan A**. Glucocorticoid corticosteroids for Duchenne muscular dystrophy. *Cochrane Database Syst Rev* , 2008.

97. **Maranhão JB**, **Moreira D de O**, **Mauricío AF**, **de Carvalho SC**, **Ferretti R**, **Pereira JA**, **Santo Neto H**, **Marques MJ**. Changes in calsequestrin, TNF-α, TGF-β and MyoD levels during the progression of skeletal muscle dystrophy in mdx mice: A comparative analysis

of the quadriceps, diaphragm and intrinsic laryngeal muscles. *Int J Exp Pathol* 96: 285–293, 2015.

98. **Martin KS**, **Blemker SS**, **Peirce SM**. Agent-based computational model investigates muscle-specific responses to disuse-induced atrophy. *J Appl Physiol* 118: 1299–309, 2015.

99. **Martin KS**, **Kegelman CD**, **Virgilio KM**, **Passipieri JA**, **Christ GJ**, **Blemker SS**, **Peirce SM**. In Silico and In Vivo Experiments Reveal M-CSF Injections Accelerate Regeneration Following Muscle Laceration. *Ann Biomed Eng* 45, 2017.

100. **Martin KS**, **Kegelman CD**, **Virgilio KM**, **Passipieri JA**, **Christ GJ**, **Blemker SS**, **Peirce SM**. In Silico and In Vivo Experiments Reveal M-CSF Injections Accelerate Regeneration Following Muscle Laceration. *Ann Biomed Eng* 45: 747–760, 2017.

101. **Martin KS**, **Virgilio KM**, **Peirce SM**, **Blemker SS**. Computational modeling of muscle regeneration and adaptation to advance muscle tissue regeneration strategies. *Cells Tissues Organs* 202, 2016.

102. **Martin KS**, **Virgilio KM**, **Peirce SM**, **Blemker SS**. Computational modeling of muscle regeneration and adaptation to advance muscle tissue regeneration strategies. *Cells Tissues Organs* 202, 2016.

103. **McDonald a. a.**, **Hebert SL**, **Kunz MD**, **Ralles SJ**, **McLoon LK**. Disease course in mdx:utrophin+/- mice: comparison of three mouse models of Duchenne muscular dystrophy. *Physiol Rep* 3: e12391–e12391, 2015.

104. **Mendell JR**, **Rodino-Klapac LR**, **Sahenk Z**, **Roush K**, **Bird L**, **Lowes LP**, **Alfano L**, **Gomez AM**, **Lewis S**, **Kota J**, **Malik V**, **Shontz K**, **Walker CM**, **Flanigan KM**, **Corridore M**, **Kean JR**, **Allen HD**, **Shilling C**, **Melia KR**, **Sazani P**, **Saoud JB**, **Kaye EM**. Eteplirsen

for the treatment of Duchenne muscular dystrophy. *Ann Neurol* 74: 637–647, 2013.

105. **Menetrey J**, **Kasemkijwattana C**, **Day CS**, **Bosch P**, **Vogt M**, **Fu FH**, **Moreland MS**, **Huard J**. Growth factors improve muscle healing in vivo. *J Bone Jt Surg - Ser B* 82: 131–137, 2000.

106. **Meyer G a**, **Lieber RL**. Elucidation of Extracellular Matrix Mechanics from Muscle Fibers and Fiber Bundles. *J Biomech* 44: 771–773, 2011.

107. **Miller KJ**, **Thaloor D**, **Matteson S**, **Pavlath GK**. Hepatocyte growth factor affects satellite cell activation and differentiation in regenerating skeletal muscle. *Am J Physiol Cell Physiol* 278: C174–C181, 2000.

108. **Monaco AP**, **Neve RL**, **Colletti-Feener C**, **Bertelson CJ**, **Kurnit DM**, **Kunkel LM**. Isolation of candidate cDNAs for portions of the Duchenne muscular dystrophy gene. *Nature* 323: 646–650, 1986.

109. **Muir LA**, **Chamberlain JS**. Emerging strategies for cell and gene therapy of the muscular dystrophies. *Expert Rev Mol Med* 11, 2009.

110. **Muntoni F**. Cardiomyopathy in muscular dystrophies. *Curr Opin Neurol* 16: 577–83, 2003.

111. **Muntoni F**, **Mateddu A**, **Marchei F**, **Clerk A**, **Serra G**. Muscular weakness in the mdx mouse. *J Neurol Sci* 120: 71–77, 1993.

112. **Murphy MM**, **Lawson JA**, **Mathew SJ**, **Hutcheson DA**, **Kardon G**. Satellite cells, connective tissue fibroblasts and their interactions are crucial for muscle regeneration. *Development* 138: 3625–3637, 2011.

113. **Nishimura T**. The role of intramuscular connective tissue in meat texture. *Anim Sci J* 81: 21–7, 2010.

114. **Pan Z**, **Ghosh K**, **Hung V**, **Macri LK**, **Einhorn J**, **Bhatnagar D**, **Simon M**, **Clark R a F**, **Rafailovich MH**. Deformation gradients imprint the direction and speed of en masse fibroblast migration for fast healing. *J Invest Dermatol* 133: 2471–9, 2013.

115. **Pelosi L**, **Berardinelli MG**, **Forcina L**, **Spelta E**, **Rizzuto E**, **Nicoletti C**, **Camilli C**, **Testa E**, **Catizone A**, **De Benedetti F**, **Musarò A**. Increased levels of interleukin-6 exacerbate the dystrophic phenotype in mdx mice. *Hum Mol Genet* 24: 6041–6053, 2015.

116. **Pelosi L**, **Berardinelli MG**, **De Pasquale L**, **Nicoletti C**, **D'Amico A**, **Carvello F**, **Moneta GM**, **Catizone A**, **Bertini E**, **De Benedetti F**, **Musarò A**. Functional and Morphological Improvement of Dystrophic Muscle by Interleukin 6 Receptor Blockade. *EBioMedicine* 2: 285–293, 2015.

117. **Perrone CE**, **Fenwick-Smith D**, **Vandenburgh HH**. Collagen and stretch modulate autocrine secretion of insulin-like growth factor-1 and insulin-like growth factor binding proteins from differentiated skeletal muscle cells. *J Biol Chem* 270: 2099–2106, 1995.

118. **Pessina P**, **Cabrera D**, **Morales MG**, **Riquelme C a**, **Gutiérrez J**, **Serrano AL**, **Brandan E**, **Muñoz-Cánoves P**. Novel and optimized strategies for inducing fibrosis in vivo: focus on Duchenne Muscular Dystrophy. *Skelet Muscle* 4: 7, 2014.

119. **Petrof BJ**, **Shrager JB**, **Stedman HH**, **Kelly AM**, **Sweeney HL**. Dystrophin protects the sarcolemma from stresses developed during muscle contraction. *Proc Natl Acad Sci U S A* 90: 3710–3714, 1993.

120. **Petrov V V**, **Fagard RH**, **Lijnen PJ**. Stimulation of collagen production by transforming growth factor-beta1 during differentiation of cardiac fibroblasts to myofibroblasts. *Hypertension* 39: 258–263, 2002.

121. **Porter JD**, **Khanna S**, **Kaminski HJ**, **Rao JS**, **Merriam AP**, **Richmonds CR**, **Leahy P**,

Li J, **Guo W**, **Andrade FH**. A Chronic Inflammatory Response Dominates the Skeletal Muscle Molecular Signature in Dystrophin-Deficient Mdx Mice. *Hum Mol Genet* 11: 263–272, 2002.

122. **Pratt SJ**, **Xu S**, **Mullins RJ**, **Lovering RM**. Temporal changes in magnetic resonance imaging in the mdx mouse. *BMC Res Notes* 6: 262, 2013.

123. **Pratt SJP**, **Shah SB**, **Ward CW**, **Kerr JP**, **Stains JP**, **Lovering RM**. Recovery of altered neuromuscular junction morphology and muscle function in mdx mice after injury. *Cell Mol Life Sci* 72: 153–164, 2014.

124. **Purslow PP**. The structure and functional significance of variations in the connective tissue within muscle. *Comp Biochem Physiol* 133: 947–966, 2002.

125. **Purslow PP**. Muscle fascia and force transmission. *J Bodyw Mov Ther* 14: 411–7, 2010.

126. **Puso MA**. NIKE3D: A Nonlinear, Implicit, Three-Dimensional Finite Element Code for Solid and Structural Mechanics- User's Manual. .

127. **Rahimov F**, **Kunkel LM**. The cell biology of disease: cellular and molecular mechanisms underlying muscular dystrophy. *J Cell Biol* 201: 499–510, 2013.

128. **Rathbone CR**, **Wenke JC**, **Warren GL**, **Armstrong RB**. Importance of satellite cells in the strength recovery after eccentric contraction-induced muscle injury. *Am J Physiol Regul Integr Comp Physiol* 285: R1490-5, 2003.

129. **Rehorn MR**, **Blemker SS**. The effects of aponeurosis geometry on strain injury susceptibility explored with a 3D muscle model. *J Biomech* 43: 2574–2581, 2010.

130. **Reimann J**, **Irintchev A**, **Wernig A**. Regenerative capacity and the number of satellite cells in soleus muscles of normal and mdx mice. *Neuromuscul Disord* 10: 276–282, 2000.

131. **Rocheteau P**, **Gayraud-Morel B**, **Siegl-Cachedenier I**, **Blasco MA**, **Tajbakhsh S**. A subpopulation of adult skeletal muscle stem cells retains all template DNA strands after cell division. *Cell* 148: 112–125, 2012.

132. **Rosenberg AS**, **Nagaraju K**, **Hoffman EP**, **Villalta SA**, **Rao VA**, **Wakefield LM**, **Woodcock J**. Immune-mediated pathology in Duchenne muscular dystrophy. *Sci Transl Med* 7: 1–13, 2015.

133. **Rossi M De**, **Bernasconi P**, **Baggi F**, **Malefyt DW**. Cytokines and chemokines are both expressed by human myoblasts : possible relevance for the immune pathogenesis of muscle inflammation . *Int Immunol* 12: 1329–1335, 2000.

134. **Rouillard AD**, **Holmes JW**, **Rouillard AD**, **Holmes JW**. Mechanical regulation of fibroblast migration and collagen remodelling in healing myocardial infarcts. *J Physiol* 59018: 4585–460218, 2012.

135. **Sacco A**, **Mourkioti F**, **Tran R**, **Choi J**, **Llewellyn M**, **Kraft P**, **Shkreli M**, **Delp S**, **Pomerantz JH**, **Artandi SE**, **Blau HM**. Short telomeres and stem cell exhaustion model duchenne muscular dystrophy in mdx/mTR mice. *Cell* 143: 1059–1071, 2010.

136. **Saclier M**, **Yacoub-Youssef H**, **Mackey AL**, **Arnold L**, **Ardjoune H**, **Magnan M**, **Sailhan F**, **Chelly J**, **Pavlath GK**, **Mounier R**, **Kjaer M**, **Chazaud B**. Differentially activated macrophages orchestrate myogenic precursor cell fate during human skeletal muscle regeneration. *Stem Cells* 31: 384–396, 2013.

137. **Sanderson RD**, **Fitch JM**, **Linsenmayer TR**, **Mayne R**. Fibroblasts promote the formation of a continuous basal lamina during myogenesis in vitro. *J Cell Biol* 102: 740–747, 1986.

138. **Sato K**, **Li Y**, **Foster W**, **Fukushima K**, **Badlani N**, **Adachi N**, **Usas A**, **Fu FH**, **Huard J**.

Improvement of muscle healing through enhancement of muscle regeneration and prevention of fibrosis. *Muscle and Nerve* 28: 365–372, 2003.

139. **Schäfer R**, **Zweyer M**, **Knauf U**, **Mundegar RR**, **Wernig a.** The ontogeny of soleus muscles in mdx and wild type mice. *Neuromuscul Disord* 15: 57–64, 2005.

140. **Segawa M**, **Fukada S**, **Yamamoto Y**, **Yahagi H**, **Kanematsu M**, **Sato M**, **Ito T**, **Uezumi A**, **Hayashi S**, **Miyagoe-Suzuki Y**, **Takeda S**, **Tsujikawa K**, **Yamamoto H**. Suppression of macrophage functions impairs skeletal muscle regeneration with severe fibrosis. *Exp Cell Res* 314: 3232–44, 2008.

141. **Sharafi B**, **Blemker SS**. A micromechanical model of skeletal muscle to explore the effects of fiber and fascicle geometry. *J Biomech* 43: 3207–13, 2010.

142. **Sharafi B**, **Blemker SS**. A mathematical model of force transmission from intrafascicularly terminating muscle fibers. *J Biomech* 44: 2031–2039, 2011.

143. **Shireman PK**, **Contreras-Shannon V**, **Ochoa O**, **Karia BP**, **Michalek JE**, **McManus LM**. MCP-1 deficiency causes altered inflammation with impaired skeletal muscle regeneration. *J Leukoc Biol* 81: 775–785, 2007.

144. **Siegel AL**, **Atchison K**, **Fisher KE**, **Davis GE**, **Cornelison DDW**. 3D timelapse analysis of muscle satellite cell motility. *Stem Cells* 27: 2527–2538, 2009.

145. **Siegel AL**, **Kuhlmann PK**, **Cornelison DDW**. Muscle satellite cell proliferation and association: new insights from myofiber time-lapse imaging. *Skelet Muscle* 1: 7, 2011.

146. **Skutek M**, **van Griensven M**, **Zeichen J**, **Brauer N**, **Bosch U**, **Zeichen GJ**. Cyclic mechanical stretching modulates secretion pattern of growth factors in human tendon fibroblasts. *Eur J Appl Physiol* 86: 48–52, 2001.

147. **Smith C**, **Kruger MJ**, **Smith RM**, **Myburgh KH**. The Inflammatory Response to Skeletal

Muscle Injury. *Sport Med* 38: 947–969, 2008.

148. **Smith LR**, **Barton ER**. Collagen content does not alter the passive mechanical properties of fibrotic skeletal muscle in mdx mice. *Am J Physiol Cell Physiol* 306: C889-98, 2014.

149. **Sonnet C**. Human macrophages rescue myoblasts and myotubes from apoptosis through a set of adhesion molecular systems. *J Cell Sci* 119: 2497–2507, 2006.

150. **Spencer MJ**, **Tidball JG**. Do immune cells promote the pathology of dystrophin-deficient myopathies? *Neuromuscul Disord* 11: 556–564, 2001.

151. **Spurney CF**, **Gordish-Dressman H**, **Guerron AD**, **Sali A**, **Pandey GS**, **Rawat R**, **Van Der Meulen JH**, **Cha HJ**, **Pistilli EE**, **Partridge T a.**, **Hoffman EP**, **Nagaraju K**. Preclinical drug trials in the mdx mouse: Assessment of reliable and sensitive outcome measures. *Muscle and Nerve* 39: 591–602, 2009.

152. **Stratos I**, **Rotter R**, **Eipel C**, **Mittlmeier T**, **Vollmar B**. Granulocyte-colony stimulating factor enhances muscle proliferation and strength following skeletal muscle injury in rats. *J Appl Physiol* 103: 1857–1863, 2007.

153. **Straub V**, **Rafael JA**, **Chamberlain JS**, **Campbell KP**. Animal Models for Muscular Dystrophy Show Different Patterns of Sarcolemmal Disruption. *J Cell Biol* 139: 375–385, 1997.

154. **Summan M**, **Warren GL**, **Mercer RR**, **Chapman R**, **Hulderman T**, **Van Rooijen N**, **Simeonova PP**. Macrophages and skeletal muscle regeneration: a clodronate-containing liposome depletion study. *Am J Physiol Regul Integr Comp Physiol* 290: R1488-95, 2006.

155. **Tang J**, **Ley KF**, **Hunt CA**. Dynamics of in silico leukocyte rolling, activation, and adhesion. *BMC Syst Biol* 1: 1–25, 2007.

156. **Tatsumi R**, **Anderson JE**, **Nevoret CJ**, **Halevy O**, **Allen RE**. HGF/SF is present in

normal adult skeletal muscle and is capable of activating satellite cells. *Dev Biol* 194: 114–128, 1998.

157. **Tedesco FS**, **Hoshiya H**, **D'Antona G**, **Gerli MFM**, **Messina G**, **Antonini S**, **Tonlorenzi R**, **Benedetti S**, **Berghella L**, **Torrente Y**, **Kazuki Y**, **Bottinelli R**, **Oshimura M**, **Cossu G**. Stem cell-mediated transfer of a human artificial chromosome ameliorates muscular dystrophy. *Sci Transl Med* 3: 96ra78, 2011.

158. **Thorne BC**, **Hayenga HN**, **Humphrey JD**, **Peirce SM**. Toward a multi-scale computational model of arterial adaptation in hypertension: Verification of a multi-cell agent-based model. *Front Physiol* MAY: 1–12, 2011.

159. **Tidball JG**, **Dorshkind K**, **Wehling-Henricks M**. Shared signaling systems in myeloid cell-mediated muscle regeneration. *Development* 141: 1184–96, 2014.

160. **Tidball JG**, **Villalta SA**. Regulatory interactions between muscle and the immune system during muscle regeneration. *Am J Physiol Regul Integr Comp Physiol* 298: R1173-87, 2010.

161. **Turgeman T**, **Hagai Y**, **Huebner K**, **Jassal DS**, **Anderson JE**, **Genin O**, **Nagler A**, **Halevy O**, **Pines M**. Prevention of muscle fibrosis and improvement in muscle performance in the mdx mouse by halofuginone. *Neuromuscul Disord* 18: 857–868, 2008.

162. **Uezumi A**, **Fukada S**, **Yamamoto N**, **Takeda S**, **Tsuchida K**. Mesenchymal progenitors distinct from satellite cells contribute to ectopic fat cell formation in skeletal muscle. *Nat Cell Biol* 12: 143–152, 2010.

163. **Uezumi A**, **Ito T**, **Morikawa D**, **Shimizu N**, **Yoneda T**, **Segawa M**, **Yamaguchi M**, **Ogawa R**, **Matev MM**, **Miyagoe-Suzuki Y**, **Takeda S**, **Tsujikawa K**, **Tsuchida K**, **Yamamoto H**, **Fukada S**. Fibrosis and adipogenesis originate from a common

mesenchymal progenitor in skeletal muscle. *J Cell Sci* 124: 3654–64, 2011.

164. **Valentine BA**, **Cooper BJ**, **de Lahunta A**, **Quinn RO**, **Blue JT**. Canine X-linked muscular dystrophy An animal model of Duchenne muscular dystrophy : clinical studies. *J Neurol Sci* 88: 69–81, 1988.

165. **Villalta SA**, **Deng B**, **Rinaldi C**, **Wehling-Henricks M**, **Tidball JG**. IFNgamma promotes muscle damage in the mdx mouse model of Duchenne muscular dystrophy by suppressing M2 macrophage activation and inhibiting muscle cell proliferation. *J Imm* 187: 997–1003, 2011.

166. **Villalta SA**, **Nguyen HX**, **Deng B**, **Gotoh T**, **Tidbal JG**. Shifts in macrophage phenotypes and macrophage competition for arginine metabolism affect the severity of muscle pathology in muscular dystrophy. *Hum Mol Genet* 18: 482–496, 2009.

167. **Villalta SA**, **Rinaldi C**, **Deng B**, **Liu G**, **Fedor B**, **Tidball JG**. Interleukin-10 reduces the pathology of mdx muscular dystrophy by deactivating M1 macrophages and modulating macrophage phenotype. *Hum Mol Genet* 20: 790–805, 2011.

168. **Villalta SA**, **Rosenberg AS**, **Bluestone JA**. The immune system in Duchenne muscular dystrophy: Friend or foe. *Rare Dis (Austin, Tex)* 3: e1010966, 2015.

169. **Virgilio KM**, **Martin KS**, **Peirce SM**, **Blemker SS**. Multiscale models of skeletal muscle reveal the complex effects of muscular dystrophy on tissue mechanics and damage susceptibility. *Interface Focus* 5, 2015.

170. **Virgilio KM**, **Martin KS**, **Peirce SM**, **Blemker SS**. Multiscale models of skeletal muscle reveal the complex effects of muscular dystrophy on tissue mechanics and damage susceptibility. *Interface Focus* 5, 2015.

171. **Wakelam MJ**. The fusion of myoblasts. *Biochem J* 228: 1–12, 1985.

172. **Wang W**, **Pan H**, **Murray K**, **Jefferson BS**, **Li Y**. Matrix metalloproteinase-1 promotes muscle cell migration and differentiation. *Am J Pathol* 174: 541–9, 2009.

173. **Wang YX**, **Dumont N a**, **Rudnicki M a**. Muscle stem cells at a glance. *J Cell Sci* 127: 4543–8, 2014.

174. **Warren GL**, **Hulderman T**, **Jensen N**, **Mckinstry M**, **Mishra M**, **Luster MI**, **Simeonova PP**, **Branch MB**, **Effects H**, **Safety O**, **Virginia W**. Physiological role of tumor necrosis factor α in traumatic muscle injury. *FASEB J* , 2002.

175. **Warren GL**, **Hulderman T**, **Mishra D**, **Gao X**, **Millecchia L**, **Farrell LO**, **Kuziel WA**, **Simeonova PP**. Chemokine receptor CCR2 involvement in skeletal muscle regeneration. *FASEB J.* .

176. **Wehling M**, **Spencer MJ**, **Tidball JG**. A nitric oxide synthase transgene ameliorates muscular dystrophy in mdx mice. *J Cell Biol* 155: 123–131, 2001.

177. **Williams MW**, **Bloch RJ**. Extensive but Coordinated Reorganization of the Membrane Skeleton in Myofibers of Dystrophic (mdx) Mice. *J Cell Biol* 144: 1259–1270, 1999.

178. **Willmann R**, **De Luca A**, **Benatar M**, **Grounds M**, **Dubach J**, **Raymackers JM**, **Nagaraju K**. Enhancing translation: Guidelines for standard pre-clinical experiments in mdx mice. *Neuromuscul Disord* 22: 43–49, 2012.

179. **Wipff PJ**, **Rifkin DB**, **Meister JJ**, **Hinz B**. Myofibroblast contraction activates latent TGF-B1 from the extracellular matrix. *J Cell Biol* 179: 1311–1323, 2007.

180. **Wolff A V.**, **Niday AK**, **Voelker K a.**, **Call J a.**, **Evans NP**, **Granata KP**, **Grange RW**. Passive mechanical properties of maturing extensor digitorum longus are not affected by lack of dystrophin. *Muscle Nerve* 34: 304–12, 2006.

181. **Yablonka-Reuveni Z**. Development and postnatal regulation of adult myoblasts. *Microsc*

Res Tech 30: 366–380, 1995.

182. **Yennek S**, **Burute M**, **Thery M**, **Tajbakhsh S**. Cell adhesion geometry regulates non-random DNA segregation and asymmetric cell fates in mouse skeletal muscle stem cells. *Cell Rep* 7: 961–970, 2014.

183. **Yin H**, **Price F**, **Rudnicki MA**. Satellite Cells and the Muscle Stem Cell Niche. *Physiol Rev* 93: 23–67, 2013.

184. **Zajac FE**. Muscle and Tendon: Properties, models, scaling, and application to biomechanics and motor control. *Crit Rev Biomed Eng* 17: 359–411, 1989.

185. **Zanotti S**, **Gibertini S**, **Mora M**. Altered production of extra-cellular matrix components by muscle-derived Duchenne muscular dystrophy fibroblasts before and after TGF-B1 treatment. *Cell Tissue Res* 339: 397–410, 2010.

186. **Zhang C**, **Gao Y**. The role of transmembrane proteins on force transmission in skeletal muscle. *J Biomech* 47: 3232–6, 2014.

187. **Zhou L**, **Lu H**. Targeting Fibrosis in Duchenne Muscular Dystrophy. *J neuropathol Exp Neurol* 69: 771–776, 2010.

188. **Zou Y**, **Zhang R-Z**, **Sabatelli P**, **Chu M-L**, **Bönnemann CG**. Muscle interstitial fibroblasts are the main source of collagen VI synthesis in skeletal muscle: implications for congenital muscular dystrophy types Ullrich and Bethlem. *J Neuropathol Exp Neurol* 67: 144–154, 2008.